Dynamics of sleep and feeding homeostasis in *Drosophila* glia and neurons

Andres Flores-Valle[1, 2] **and Johannes D. Seelig**[1, *]

[1]Max Planck Institute for Neurobiology of Behavior – caesar (MPINB), Bonn, Germany
[2]International Max Planck Research School for Brain and Behavior, Bonn, Germany
[*]johannes.seelig@mpinb.mpg.de

Summary

In the brain, a homeostatic signal is thought to represent sleep need, steadily increasing during wakefulness and gradually decreasing during sleep. Here, we find that ensheathing glia of Drosophila show the dynamics expected of a sleep homeostat. Calcium levels in these cells – monitored in central brain areas such as the central complex and mushroom bodies – integrate different kinds of behavioral effort across time and reset during sleep. Ensheathing glia track sleep-wake behavior more reliably than other sleep related neurons. Interestingly, sleep-related dFB neurons integrate hunger and are modulated by walking, suggesting a role in feeding homeostasis. Ensheathing glia act as a system for tracking sleep need distributed across brain areas, establishing an interaction between sleep homeostasis and behavior at the level of identified cells and circuits in the fly brain.

Introduction

Sleep is important for multiple dynamic processes in the brain, such as those underlying learning and memory[1,2] Sleep homeostasis, that is, how sleep need is measured and controlled, is however little understood at the circuits level[1,3]. Recent experiments in mice that take advantage of calcium imaging during behavior point to the importance of glia for sleep homeostasis[4–10].

Glia are also important for sleep regulation in *Drosophila*[11,12]. Glia constitute about 10 percent of the cells in the fly brain and about a third of these are ensheathing glia[13]. Removal of the excitatory amino acid transporter 2 (Eaat2) from ensheathing glia increases sleep[14,15]. However, little is known about the dynamics of glia in behaving flies.

A circuit for sleep regulation has been investigated in the *Drosophila* ellipsoid body (EB) and fan-shaped body (FB) of the central complex[16–19], an area in the center of the fly brain important for memory and navigation[20]. Sleep depriving flies for several hours led to an increase of activity in calcium or electrophysiology recordings in neurons and astroglia recorded in brain explants[16,18,21].

However, sleep processes in *Drosophila* occur at the timescale of minutes[22,23] and many short bouts of sleep are distributed throughout the day and night with a mean duration of around 20 minutes[24–26]. A frequently used definition of sleep assumes at least 5 minutes of immobility[27,28], and already shorter periods of rest lead to reduced responsiveness to sensori stimulation[22,26]. Whether the sleep homeostatic signals that are measured in the central complex after many hours of sleep deprivation[16,18] allow keeping track of such much shorter intervals critical for naturally occurring wake and sleep[24–26] is not known.

This motivates experiments in behaving animals where neural activity and behavior are recorded at the same time and which therefore do not have to rely on extended periods of sleep deprivation. While recordings during behavior are a common approach for investigating sleep in mammals, this has not been the case for flies. We therefore developed methods for two-photon[29] calcium imaging in head-fixed walking flies[30,31], that allow combined neural and behavior recordings over multiple days during wakefulness and sleep while the fly is maintained in a virtual reality setup.

Using this method we find that ensheathing glia activity in multiple brain areas can be well described with the

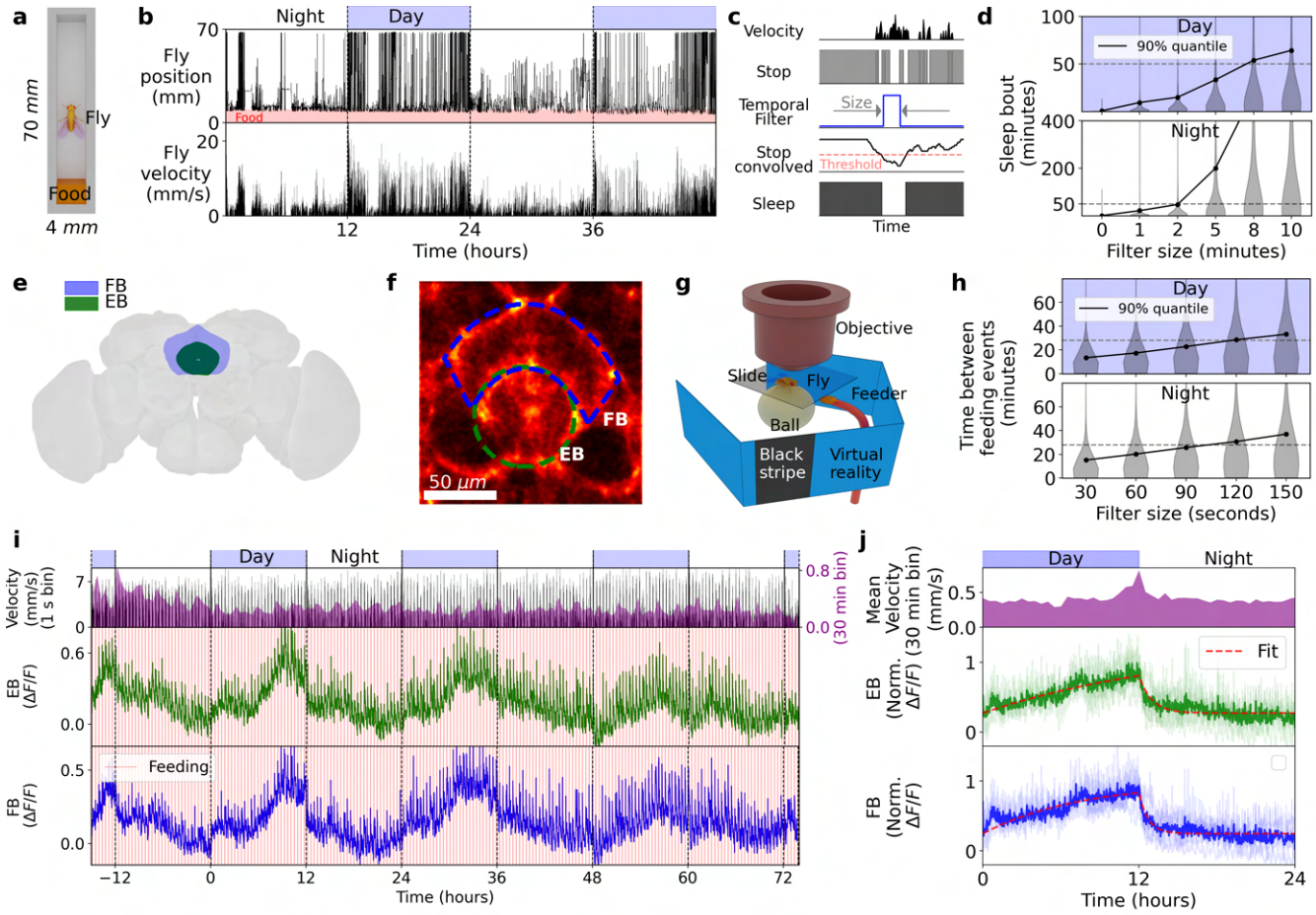

Figure 1. Sleep and feeding behavior in freely moving flies and long-term calcium imaging in ensheathing glia. **a** The position of flies walking in a rectangular chamber with food is tracked from the top with a camera. **b** Position along the rectangular chamber and velocity over two days for a single fly. **c** Velocity (first row) is thresholded to find bouts of immobility ('stop', second row). A temporal filter (third row) is convolved with the stop state of the fly (fourth row) and a threshold is used to characterize sleep (fifth row). **d** Distribution of sleep bouts for a total of 15 flies during the day and night as a function of filter size. **e** EB and FB in the *Drosophila* brain. **f** Ensheathing glia express jGCaMP8m and regions of interest (ROIs) for analyzing fluorescence in EB (green) and FB (blue). **g** Setup for long-term imaging: a fly is glued to a cover slide and navigates on an air supported ball in VR under the microscope objective. **h** Distribution of time between feeding events in freely moving flies as a function of filter size (see Methods). **i** Long-term calcium imaging in a fly walking in VR over 89 hours. Top row: day and night cycle in VR. Second row from top: absolute ball velocity in 1 second bins. Third and fourth rows: calcium activity (100 hours high-pass-filtered, see Methods) in EB and FB. Red lines indicate time of feeding (every 26 minutes). **j** Average of 5 flies over 24 hours (see Methods). Top row shows day and night cycle. Mean velocity binned over 30 minutes is shown in the second row. The third and fourth rows show average calcium activity in the EB and FB.

exponential dynamics of a sleep homeostat[32]. Interestingly, ensheathing glia monitor sleep and wakefulness more reliably than previously identified sleep related neurons in the central complex. Activity of sleep-related neurons in the fan-shaped body can be explained by taking into account feeding and walking behavior, emphasizing the importance of monitoring neural circuits in central brain areas during behavior[20].

Time scales of sleep homeostasis

A sleep homeostat needs to keep track of time spent awake and sleeping, which can be achieved by continuously integrating time[32,33]. The time constants of such a homeostat must therefore lie in the range of the naturally occurring sleep bouts.

Walking flies show a distribution of bouts of rest or sleep of different lengths during the day and night[24,25,27,34] with a mean bout duration of around 20 minutes[24,25]. To confirm that this sleep duration is not the result of minor fly movements that could only briefly interrupt overall longer sleep bouts, we quantified the distribution of sleep in flies walking in a rectangular chamber by tracking them with a camera (Fig. 1a and b, Supplementary Fig. S1a and b, see Methods). We removed shorter periods of movement of varying lengths between consecutive bouts of immobility (Fig. 1c) and computed the resulting distribution of sleep bouts. Even when filtering out movement periods of 2 minutes, 90% of sleep bouts were still shorter than 50 minutes during the day and night (Fig. 1 d), with even shorter sleep bouts in constant darkness (Supplementary Fig. S1c), consistent with previous results[24,25]. Thus, based on behavior the dynamics of the sleep homeostat responsible for such naturally occurring sleep bouts is expected to lie in the tens of minutes.

Glia activity varies across the day

To monitor the dynamics of ensheathing glia during sleep and wakefulness, we expressed the calcium indicator jGCaMP8m[35] using the GAL4 line R56F03[13,36] and imaged in the EB and FB (Fig. 1e and f) of the central complex. In these experiments, flies walked on an air supported ball in a virtual reality setup in closed-loop with a single dark stripe on a bright background during the day and in darkness during the night (12 hours light/dark cycle, Fig. 1g)[30].

We fed the flies every 26 (Fig 1i, j, and Supplementary Fig. S2) or 16 minutes (Supplementary Fig. S3), respectively, at a similar rate at which freely walking flies approached food (Fig. 1h), for 2 minutes without interrupting the experiments using an automated feeder (Fig. 1g)[30]. In these experiments, the approaching feeder led to brief bouts of walking behavior around the time of feeding and correlated spikes of calcium activity (Fig 1i, Supplementary Fig. S2, and S3), but little walking activity between feeding events. Under these conditions, calcium activity in individual flies as well as averaged across flies slowly increased across the day and reset during the night with a circadian pattern independent of behavior (Fig. 1j, Supplementary Fig. S3d).

Glia activity monitors active and rest states

To disentangle the factors that contribute to such calcium dynamics, in a second experiment we fed flies in the imaging setup only every four hours, which induced epochs of continuous walking activity (often before feeding) or rest and sleep (often after feeding). Under these conditions, ensheathing glia in different brain areas including the EB, FB (Fig. 1e and f), the lateral accessory lobe (LAL, Supplementary Fig. S29a and b), mushroom bodies (MB), and commissure (Supplementary Fig. S29c), showed pronounced calcium fluctuations (Fig. 2a, Supplementary Figs. S4a-e and S6a-e, S8a-e, and Supplementary Videos S1-S6 for EB and FB). To determine whether the overall trend of these fluctuations was consistent with the dynamics of a sleep homeostat, we subdivided the fly's behavior approximately into active and rest epochs (a higher-resolution analysis is performed in the next sections). We first distinguished only two behavioral states based on the fly's walking activity: 'walk' (fly is walking) and 'stop' (fly is standing still as assessed based on ball velocity, second row in Fig. 2a and Methods). We then selected epochs of at least 10 minutes during which the fly was walking most of the time (active, third row in Fig. 2a) or immobile most of the time (rest, third row in Fig. 2a) by thresholding the 'walk density', obtained by low-pass filtering of 'walk' (see Methods).

Fluorescence traces were averaged over the selected active and rest epochs (Figs. 2b and c, and Supplementary Figs. S5, S7 and S9). The averaged fluorescence could be fitted with exponentials (see Methods), a common model for homeostatic activity[37,38] (red line in Figs. 2b and c, and Supplementary Figs. S5, S7 and S9). The resulting rise and decay rates of the exponentials, defined by their time constants, are shown in Fig. 2d for 6 flies for EB and FB, 5 flies for LAL, and 5 flies for MB and commissure, respectively. Thus, consistent with the behavior of a sleep homeostat, activity levels changed exponentially on the minutes timescale during epochs where the animals were predominantly active or inactive, respectively. Dynamics in the EB, FB, and LAL were similar, whereas the MB and

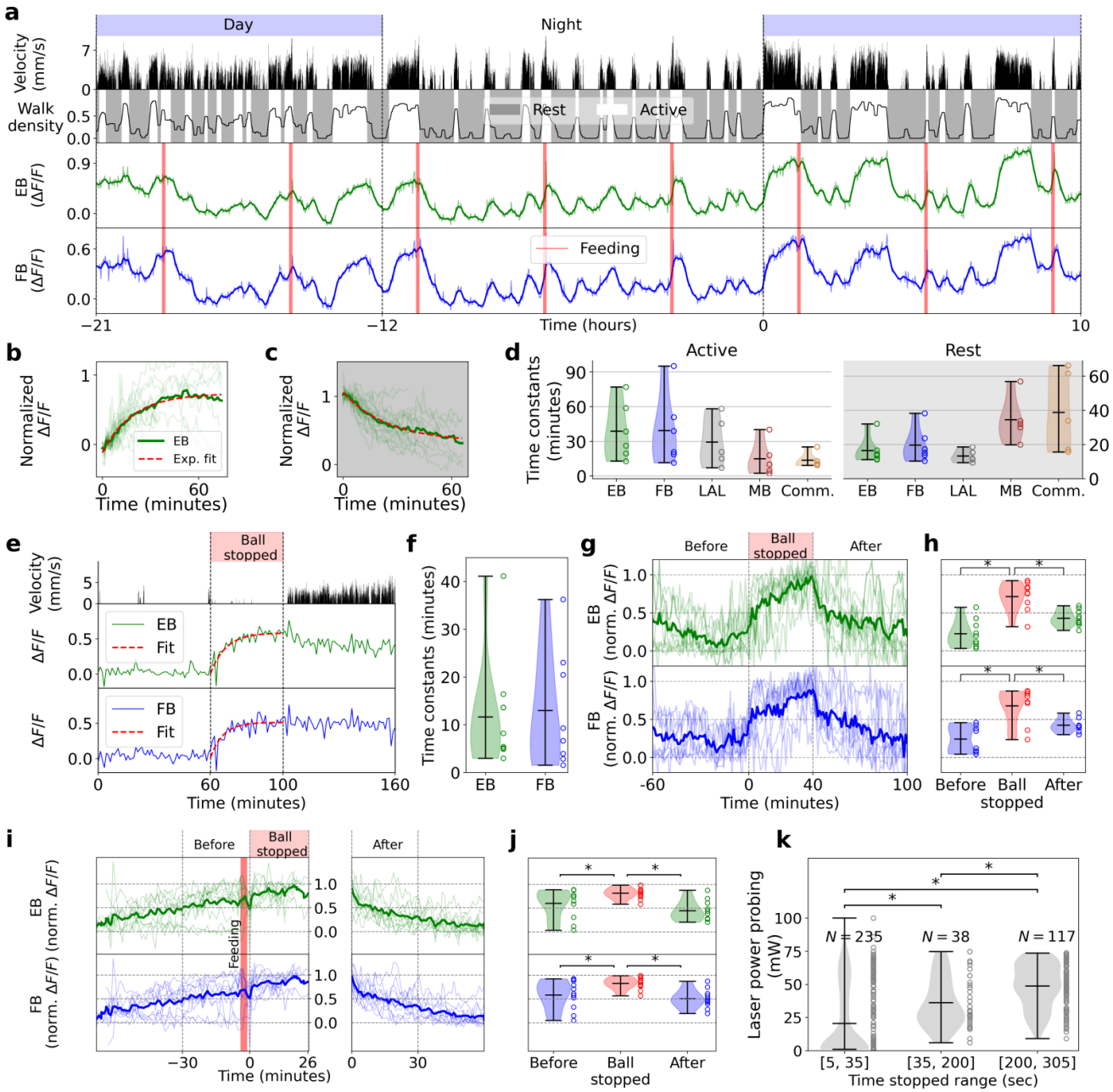

Figure 2

commissure showed slower dynamics during rest epochs (Fig. 2d).

Glia activity in the MB and commissure showed in some cases weaker correlations with walking activity (Extended Fig. S21a and Methods than the central complex. However, intermittently opening and closing the air stream supporting the ball with a valve every second, which induced fast walking activity, reliably induced increased calcium activity in MB and commissure similar to the central complex (Extended Figs. S12 and S13). That activity in the EB, FB, and LAL was better correlated with walking activity compared to activity in the MB and commissure (see Methods and Extended Fig. S21a, likely due to neurons in EB, FB and LAL being important for visual navigation, the behavioral paradigm used in these experiments.

Figure 2. Calcium dynamics in ensheathing glia increases due to effortful behavior and decreases during rest. **a** Long-term recording of a single fly over 31 hours. Top row: day and night cycle in VR. Second row from top: absolute ball velocity. Third row: walk density obtained by low-pass filtering (cut-off period of 6 minutes) of 'walk' (walk: 1 if the fly has non-zero velocity in 1 second bins, 0 otherwise). Active and rest states were defined when the walk density was above or below a threshold (see Methods). Fourth and fifth row: calcium activity (24 hours high-pass-filtered, see Methods) in EB and FB ensheathing glia over time, respectively. Red lines indicate time of feeding. **b** Single traces of increasing normalized calcium activity (see Methods) during active states (thin lines), average (thick line), and exponential fit (red) for EB. **c** Same as b but during rest state, fitted with exponentials (red). **d** Time constants for exponential fitting during active (white region) and rest states (grey region) for EB, FB, LAL, MB, and commissure (comm.). Violin plots represent the distribution of time constants for 6 flies in the EB and FB, 5 flies in the LAL, and 5 flies in the MB and commissure (circles). Short horizontal black lines show maximum, mean, and minimum values in descending order. **e** Calcium activity during effort with blocked treadmill ball. Second row: velocity of fly over time (zero while stopping the ball). Third and fourth row: ensheathing glia activity and exponential fit (red) in EB and FB, respectively. **f** Time constants of exponential fits while ball was stopped for $N = 10$ trials in 5 flies. **g** Normalized fluorescence traces of activity in EB and FB before, during, and after ball was stopped (top row). Second and third row: single trials (thin lines) and average (thick lines) in EB and FB, respectively. **h** Normalized fluorescence levels (y-axis shared with panel g) before, during, and after ball stopping (60, 40, and 60 minutes average), respectively. Statistical significance was assessed using t-test. **i** Calcium activity during effortful behavior after feeding. Normalized fluorescence traces of glia activity in EB and FB before feeding, after feeding while the ball was stopped, and after releasing the ball (for $N = 11$ trials in 5 flies). Normalized fluorescence levels (y-axis shared with panel j) before feeding, after feeding while stopping the ball, and after releasing the ball (30, 26, and 30 minutes average); asterisks represent statistical significance for p-values less than 0.05 using t-test. **k** Laser power required to awaken the fly based on the previous durations of immobility during calcium imaging. Durations of immobility are arranged in three different time ranges; the number of probing trials is indicated at the top (for a total of 6 flies). Statistical significance was assessed with Kolmogorov–Smirnov test. Asterisks in all the panels indicate p-values less than 0.05.

Glia monitor behavioral effort

Sleep behavior was often (but not always) correlated with feeding (red lines in Fig. 2a and Supplementary Fig. S4a-e), with flies increasingly walking more with time elapsed since feeding and sleeping more after feeding (as observed in freely walking flies[39,40]). We therefore first asked whether the increase in calcium in ensheathing glia was specifically due to walking, or whether other effortful behaviors could also cause similar activity changes. To address this question, we immobilized the ball for epochs of 40 minutes while the fly was in the VR setup, and recorded behavior and glia activity in the EB and FB as before (Fig. 2e and Supplementary Fig. S10). Movement of the ball was blocked by pushing it against the ball holder with the tip of a brush, positioned close to the fly with a motorized remote controlled micromanipulator. This induced the fly to continually push or pull the ball; if the fly stopped moving, the brush was slightly repositioned and due to the induced perturbation the fly resumed active behavior. As seen in the resulting fluorescence traces in Fig. 2g, this led to a steady increase in or saturation of calcium levels similar to the dynamics observed due to walking activity (Fig. 2b) with slightly faster time constants (Fig. 2f). This shows that glia calcium activity increases (Fig. 2h) not only due to coordinated walking but also due to other effortful behaviors, as similarly observed in zebrafish[41].

We then verified that feeding was not the cause for the decay of calcium activity in those instance where flies were immobile or sleeping after feeding. We sleep deprived flies immediately after feeding by inhibiting ball movement as above (Fig. 2i and Supplementary Fig. S11). This not only suppressed resetting of calcium levels, but slightly increased calcium signals after feeding (Fig. 2j), demonstrating that rest or sleep, and not feeding, are responsible for the decay of calcium levels after feeding.

Flies sleep during imaging

To determine whether epochs of immobility observed during long-term imaging experiments correspond to sleep, we tested whether the arousal threshold, the required stimulus strength to induce a behavioral response in resting flies, increased with the duration of immobility, as expected for sleep[22,42]. As a stimulus we used an infrared laser beam pointed at the fly's abdomen. At the start of each trial of probing of the arousal threshold, we ensured that the fly was first awake by closing and opening the air stream to the air supported ball every second for 3 seconds (see Methods), which stimulated the fly to walk. Then, using an automated control loop for monitoring ball velocity, we detected bouts of immobility. After either 30 seconds or 5 minutes of immobility, the power of the heating laser was gradually ramped up until the fly started to walk (see Methods). To ensure that flies were completely still during the detected epochs of immobility, we classified behavior recorded with a camera using machine learning in post-processing (see Methods and Supplementary Fig. S28). Removing those sections where the fly was grooming resulted in the final bouts of immobility between 5 seconds and 5 minutes. A representative trial of threshold probing is shown in Supplementary Fig. S14a. Fig. 2k shows that longer periods of immobility required higher laser powers for a behavioral response, showing that the arousal threshold increases with the duration of immobility, a feature of sleep also observed in freely walking flies[22,27,34] (see Supplementary Fig. S14b-g for individual flies).

Sleep deprivation saturates glia activity

A signature of a sleep homeostat is that it saturates and plateaus under sleep deprivation[32,43]. Sleep deprivation for extended periods of time leads to rebound sleep in flies[27,34,40]. The amount of rebound sleep however depends on the method of sleep deprivation. Sleep deprivation which avoids strong mechanical perturbation resulted in less than one hour of mean rebound sleep after 12 hours of sleep deprivation[44], consistent with the dynamics of a sleep homeostat in the order of minutes.

To sleep deprive flies during long-term imaging, we periodically opened and closed the air stream supporting the ball at 1 second intervals for 6 seconds every 20 seconds, similar to sleep deprivation in freely walking flies[16,18,44], which induced short bouts of fast walking (at least every 20 seconds). Calcium activity saturated in EB, FB (Fig. 3a and b, and Supplementary Fig. S15a) within 2 hours and plateaued (Fig. 3c), with occasional fluctuations around the saturation level (indicated by an exponential fit, red line in Fig. 3a). This experiment additionally again confirmed that behavioral activity, here walking, prevents resetting of after feeding, similar to Fig. 2i and j (see Fig. 3a and Supplementary Fig. S15a for feeding events during sleep deprivation).

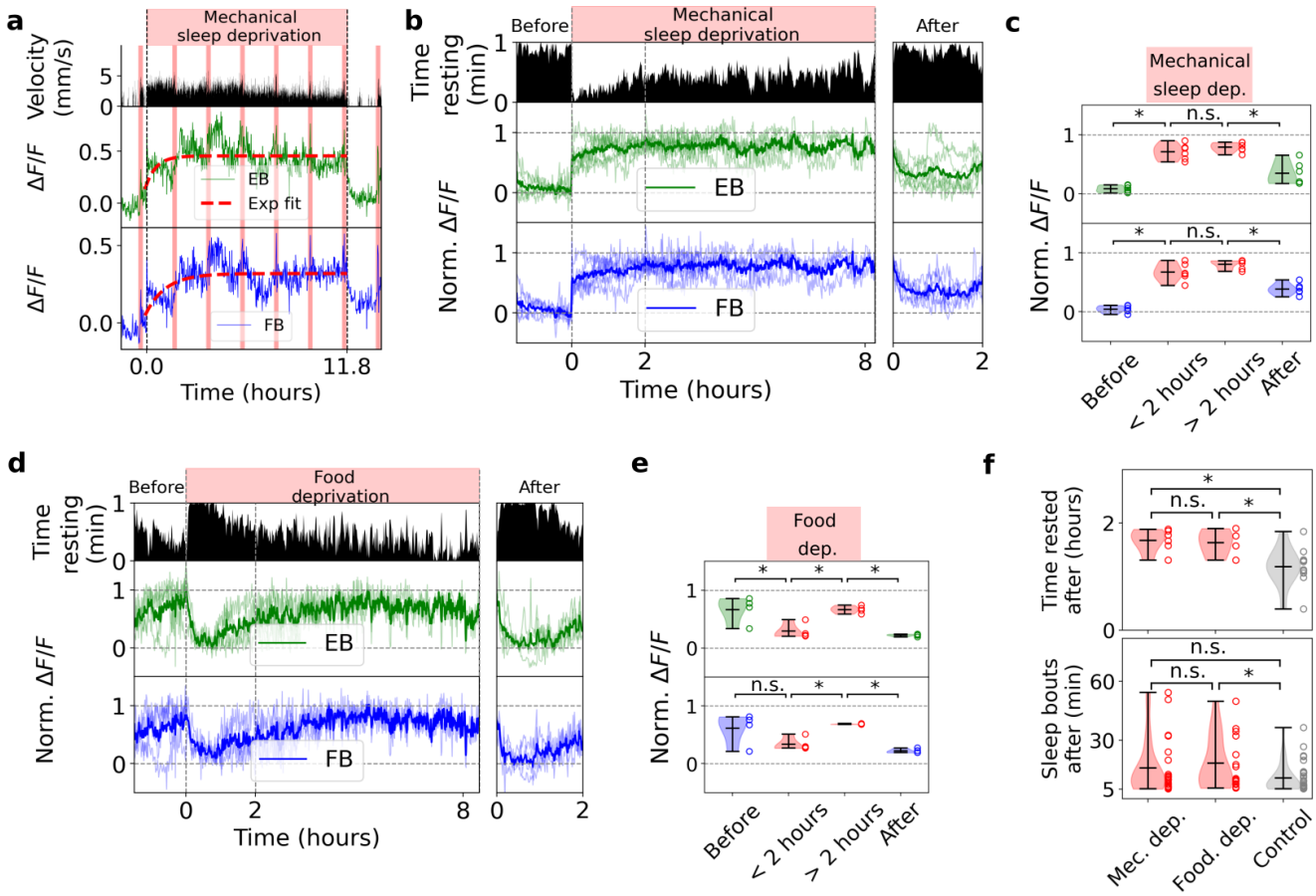

Figure 3. Glia activity due to sleep deprivation and effort. **a** Behavior and calcium activity in EB and FB ensheathing glia under mechanically induced sleep deprivation. Top row: time interval where sleep deprivation was applied. Second row: fly velocity. Third and fourth row: activity of glia with exponential fit for visualization of plateau level (red) during mechanical sleep deprivation for EB and FB, respectively. Vertical red lines indicate feeding events. **b** Mechanical sleep deprivation for $N = 6$ trials in 5 flies (including fly in a). Top row as in a. Second row: averaged time resting over time, calculated in bins of 1 minute. Third and fourth row: normalized fluorescence traces of ensheathing glia activity in each fly (thin lines) and average (thick line, at least 2 flies) in EB (green) and FB (blue), respectively, shown during up to 8 hours of mechanical sleep deprivation. Times of mechanical sleep deprivation varied between flies and flies were fed during these experiments (see Supplementary Fig. S15). **c** Average fluorescence distributions before (over 1.5 hours), during the first 2 hours of sleep deprivation, between 2 and 8 hours of sleep deprivation, and after (2 hours). **d** Same as b but during food deprivation for $N = 4$ trials in different flies. Top row shows the time interval (in red) between two consecutive feeding events. Times of food deprivation varied between flies (see Supplementary Fig. S15b). **e** Same as c but for food deprivation. **f** Top row: time rested over 2 hours for each trial after mechanical sleep deprivation, food deprivation, and for control trials ($N = 10$ in 6 flies). Bottom row: distribution of sleep bouts (longer than 5 minutes) over the 2 hours after mechanical sleep deprivation, starvation induced sleep deprivation, and in control flies. Asterisks in all panels indicate statistical significance ($p < 0.05$) using t-test (panels c,e and the top row of f) and Kolmogorov–Smirnov test in the bottom row of f.

For comparison, we also used food deprivation to sleep deprive flies. Absence of food and starvation induce hyperactivity or foraging behavior and prevent sleep[40,45–47] and in some flies resulted in long epochs of continued fast walking. Single trials and average activity of 4 flies that were continuously walking for at least 3 hours following

food deprivation with fluorescence traces normalized for comparison, are shown in Fig. 3d (see Supplementary Fig. S15b for individual trials). Starvation-induced walking produced a slow increase of glia calcium activity (Fig. 3d), and, similar to mechanical sleep deprivation, calcium activity saturated after 2 hours (Fig. 3e).

After the offset of mechanically or food induced sleep deprivation, flies became less active (right side of Fig. 3b and d), and glia activity returned to lower levels. Flies displayed rebound sleep and showed an average of 1.68 and 1.64 hours of immobility in the two hours after the offset of mechanical and starvation induced sleep deprivation, respectively, compared to 1.19 hours in control flies (top row in Fig. 3f, see Methods). The difference between sleep-deprived and control flies (around 30 minutes more in sleep-deprived flies on average) is consistent with the time that it takes to reset glia activity to baseline levels (Fig. 2d). Additionally, mechanical sleep deprivation resulted in more sleep bouts with a duration of more than 5 minutes (Fig. 3f).

Glutamate changes faster than calcium

Ensheathing glia are important for glutamatergic signaling[15] and glutamatergic neurons show activity correlated with walking[48]. We therefore tested whether the slow calcium dynamics observed in glia corresponded to the accumulation of extracellular glutamate. The glutamate sensor iGluSnFR was expressed in ensheathing glia and we performed long-term imaging experiments as before[49,50].

Glutamate activity was correlated with walking (Fig. 4a and Supplementary Figs. S16 and S21b) and we again defined active and rest epochs based on the velocity of the fly and fitted exponential curves for EB and FB fluorescence traces (Fig. 4b and Supplementary Fig. S17). Extracellular glutamate increased during active epochs and decreased during rest (Fig. 4b). However, time constants were faster than those obtained for calcium (compare Fig. 4c and Fig. 2d, and Extended Fig. S21a and b), indicating that ensheathing glia calcium levels do not simply reflect extracellular glutamate concentration.

Homeostat model describes glia activity

Homeostatic activity can be modeled as exponentially decaying during sleep and exponentially approaching a saturation level during wakefulness[37,38,43]. We therefore quantified whether ensheathing glia calcium levels integrate behavioral history, that is, wake and sleep, according to such homeostatic dynamics across timescales. We fitted a differential equation with two time constants for charging and resetting of the homeostat, respectively, to glia calcium activity dependent on behavioral state (see Methods). As illustrated in Fig. 4d, the behavioral states, here 'walk' and 'stop', are passed to the model which represents homeostat activity and differentially increases or decreases with time constants characterizing the exponential dynamics. After fitting (see Methods), the homeostat model[33,51] describes ensheathing glia activity over the time course of the experiments based on behavior (31 hours in Fig. 4e, see also Supplementary Figs. S18, S19, and S20).

The resulting rise and decay time constants for 6 flies in EB and FB, respectively, are shown in Fig. 4f (see Supplementary Fig. S21c for the LAL, MB, and commissure). The homeostat model fitted activity in the EB, FB, and LAL regions better than activity in the MB and commissure, as shown by a lower fitting error (Supplementary Fig. S21d). Time constants in Fig. 2d were more similar between rise and decay than those obtained by model fitting (Fig. 4f and Supplementary Fig. S21c). This is due to the fact that active and rest states in Fig. 2b and c were determined using low-pass filtering of the animal's walking activity (Fig. 2a), thus resulting in rest states that still contained a fraction of walking activity, and *vice versa* for active states.

Models for the EB and FB assuming two different rest states, distinguishing between epochs with less and more than 5 minutes of immobility (defining sleep[28]), did not result in significantly different time constants between the two rest state, even when defining a second state as starting only 5 minutes after the onset of immobility (see Supplementary Figs. S23, S24 and Methods). This shows that the homeostat resets similarly in short and long bouts of immobility, consistent with the observation that already short bouts of immobility show features of sleep[22,26].

Ensheathing glia integrate activity over long timescales (tens of minutes) as indicated by the time constants resulting from model fitting (Fig. 2f and Extended Fig. S21c). Modulations of fluorescence signals were however already observed at the timescale of 1 minute when comparing changes in walking velocity with changes in high-pass filtered calcium signals in the EB and FB ($\Delta F/F$, Fig. 4h, Supplementary Fig. S27 and Methods). Thus, the

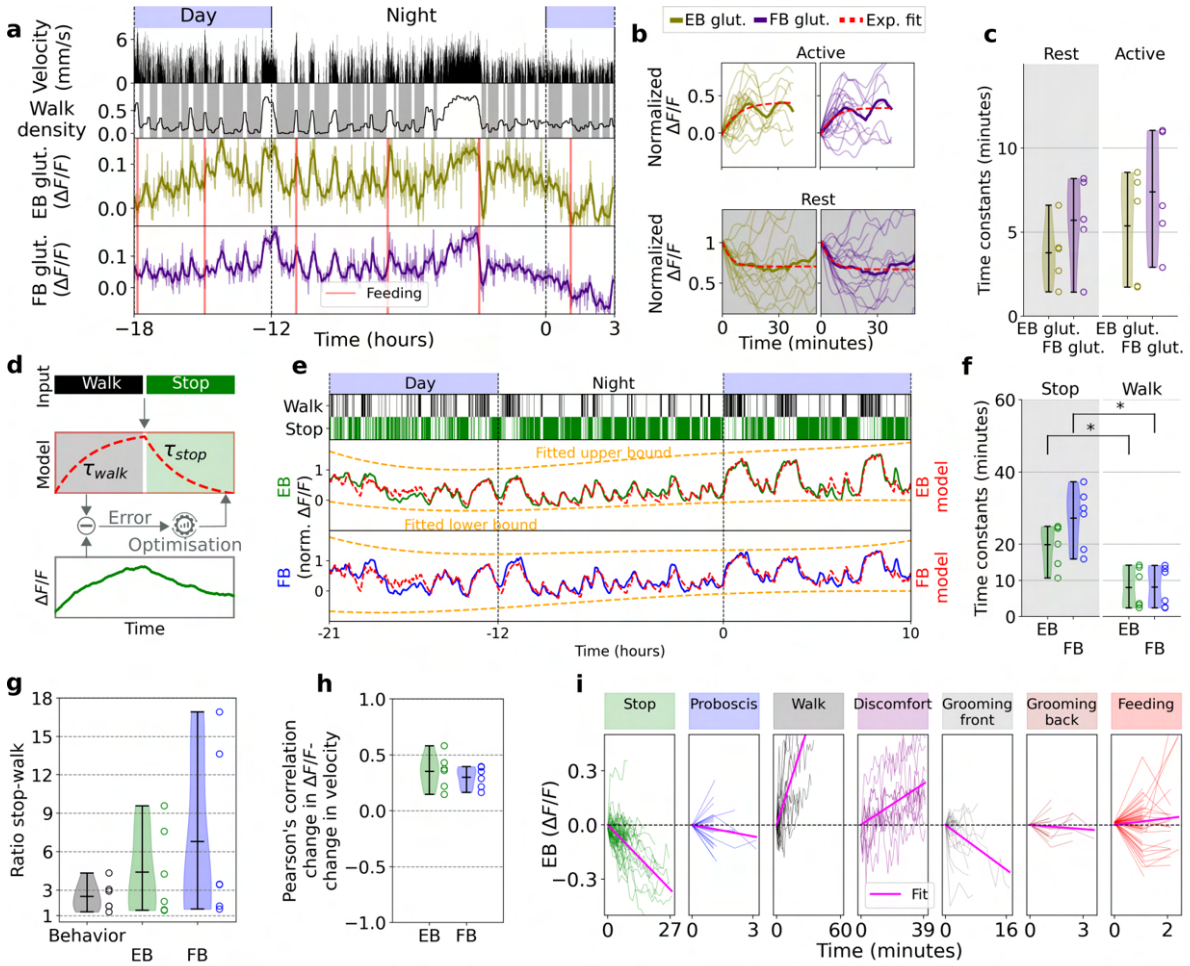

Figure 4. Glia glutamate dynamics and two-state model for calcium dynamics. **a** Glutamate long-term imaging in EB and FB. Similar to Fig. 2a for glutamate. Top row: day and night cycle in VR. Second row: fly velocity. Third row: walk density with rest (grey region) and active (white region). Fourth and fifth row: extracellular glutamate activity in EB and FB, respectively. Thick lines indicate band-pass filtered signal (0.1 hours). **b** Single traces of increasing normalized glutamate activity (see Methods) during active state (thin lines), with average (thick line) and exponential fit (red) for EB and FB. **c** Time constants for exponential fit during active (white region) and rest (grey region) for extracellular glutamate in EB and FB in $N = 5$ flies. **d** Schematic of model fitting approach for calcium imaging: behavior (walk, stop) is integrated as model input with corresponding time constants and fitted to glia calcium activity using optimization. **e** Band-pass filtered (0.5 to 12 hours) calcium activity in EB and FB over time. Top row: 'walk' state (velocity larger than zero in 1 second bins). Second and third row: activity in EB and FB. Red line: fitted homeostat model (two-state model); orange lines: fitted corrections for fluorescence levels (see Methods). **f** Distributions of time constants for 'stop' and 'walk' states from model fitting for $N = 6$ flies in EB (green) and FB (blue). Asterisks represent statistical significance with p-values lower than 0.05 using t-test. **g** Ratios of time in 'stop' and 'walk' states (black) and ratio of time constants between 'stop' and 'walk' states in EB (green) and FB (blue) for each fly ($N = 6$). Ratios were not significantly different, p-values were above 0.05 using t-test. **h** Correlation coefficients as in e for $N = 6$ flies. All flies had p-values lower than 0.05 (see Supplementary Fig. S27 and Table S5). **i** Fluorescence traces from EB and linear fit (pink line) over time intervals of seven behaviors which were classified using machine learning (see Supplementary Fig. S28 and Methods).

accumulation of such faster fluctuations could lead to the integrated activity observed over longer timescales.

Homeostat integrates multiple behaviors

Different behaviors contribute differently to sleep need and are therefore expected to charge the sleep homeostat with different time constants[1,40,52]. We therefore tested whether a more detailed analysis, distinguishing multiple behaviors, could improve model fitting. Behavior on the ball, which was monitored with a camera throughout the experiments, was classified into the following 7 categories using machine learning with 1 second time resolution (similar to[53], Supplementary Fig. S28): immobility (stop), proboscis extension, walking, discomfort (where the fly was pushing or pulling the ball), grooming of the front, grooming of the back, and feeding (see Methods and Supplementary Video S7).

We used the intervals where flies performed one of the defined behaviors continuously over consecutive imaging epochs to assess whether they contributed to an increase or decrease of calcium activity. As expected, glia activity in the EB and FB decreased when flies were stopped, but also during proboscis extension and grooming. Glia activity increased with walking, feeding (during which flies were often walking), and discomfort (Fig. 4i and Supplementary Fig. S25a).

We next fitted a model to activity in EB and FB to obtain the time constants for each of the seven behaviors (Supplementary Fig. S25b). This model predicts that resetting of the homeostat occurs faster during proboscis extension and back-grooming than during immobility, and also resets during front-grooming, although more slowly than during immobility. Proboscis extension and back-grooming was only observed in short bouts, and rarely over more than two consecutive imaging epochs (Supplementary Fig. S26a). Consistent with these observations, proboscis extension has been described to occur during a deep sleep state, and other brief movements have also been observed during sleep[24,26,34].

Glia and neuron dynamics

We next asked whether the observed dynamics in glia could result from activity of previously described homeostatic sleep circuit in the same brain compartments. In the EB, ring neurons (R5) increase calcium activity after extended sleep deprivation consistent with a sleep homeostat[16–19], an effect which also depends on the circadian rhythm[54]. A second component of this circuit, the dFB neurons (Supplementary Fig. S29f), innervate the FB and are frequently used as a 'sleep switch' to induce sleep[55–57].

We recorded calcium activity of R5 neurons in the EB (with Gal4 lines R58H05 and R88F06, Supplementary Fig. S29d and e), and in dFB neurons (Gal4 line 23E10), using multiple calcium indicators (GCaMP7f, GCaMP8f, and GCaMP8m), as well as imaging protocols (Fig. 5a, b, Supplementary Figs. S30, S33 S37, S38, S39, see Methods).

To determine whether these neurons encode sleep homeostasis similar to ensheathing glia in the respective neuropils, we first again determined active and rest epochs based on behavior (Fig. 5c,d and Supplementary Figs. S31, S35 and S40). We then computed the correlation between active (Fig. 5e) or rest epochs (Fig. 5f) and the normalized calcium activity of neurons and glia (to avoid saturation we limited this analysis to traces of 30 minutes, Fig. 5e). For a sleep homeostat, the correlation should be positive during active epochs (increasing activity over time) and negative during rest epochs (decreasing activity over time). This was on average the case for both neurons and glia, with however considerably higher correlations for glia than for R5 neurons (Fig. 5e and f, left side). dFB neurons displayed high correlations during active epochs, while the slope of decreasing activity in dFB neurons was close to zero during rest epochs (Supplementary Fig. S48, see Methods).

We further analyzed whether a homeostat model as used for glia could fit activity of R5 and dFB neurons (Supplementary Fig. S32, S36, S37, S44, S45, and Methods). However, Fig. 5g shows that the L2 error between the fitted model and normalized activity was larger for both neural populations than for glia.

Finally, we computed the convolution between walking activity with a triangular-shaped temporal filter, which produces an exponential increase during 'walk' bouts and a (symmetric) exponential decrease during 'stop' bouts at a rate defined by the filter size (Fig. 5h, see Methods). We calculated the correlation between activity in neurons and glia with the corresponding signal resulting from the convolution of different temporal filter sizes with 'walk' (Fig. 5i). The correlation with glia activity was high and peaked at a filter size of 24 minutes, similar to the dynamics obtained with previous methods (Figs. 2d and 4f). The correlation for R5 and dFB neurons was positive but lower compared to glia activity (Fig. 5i, see Methods).

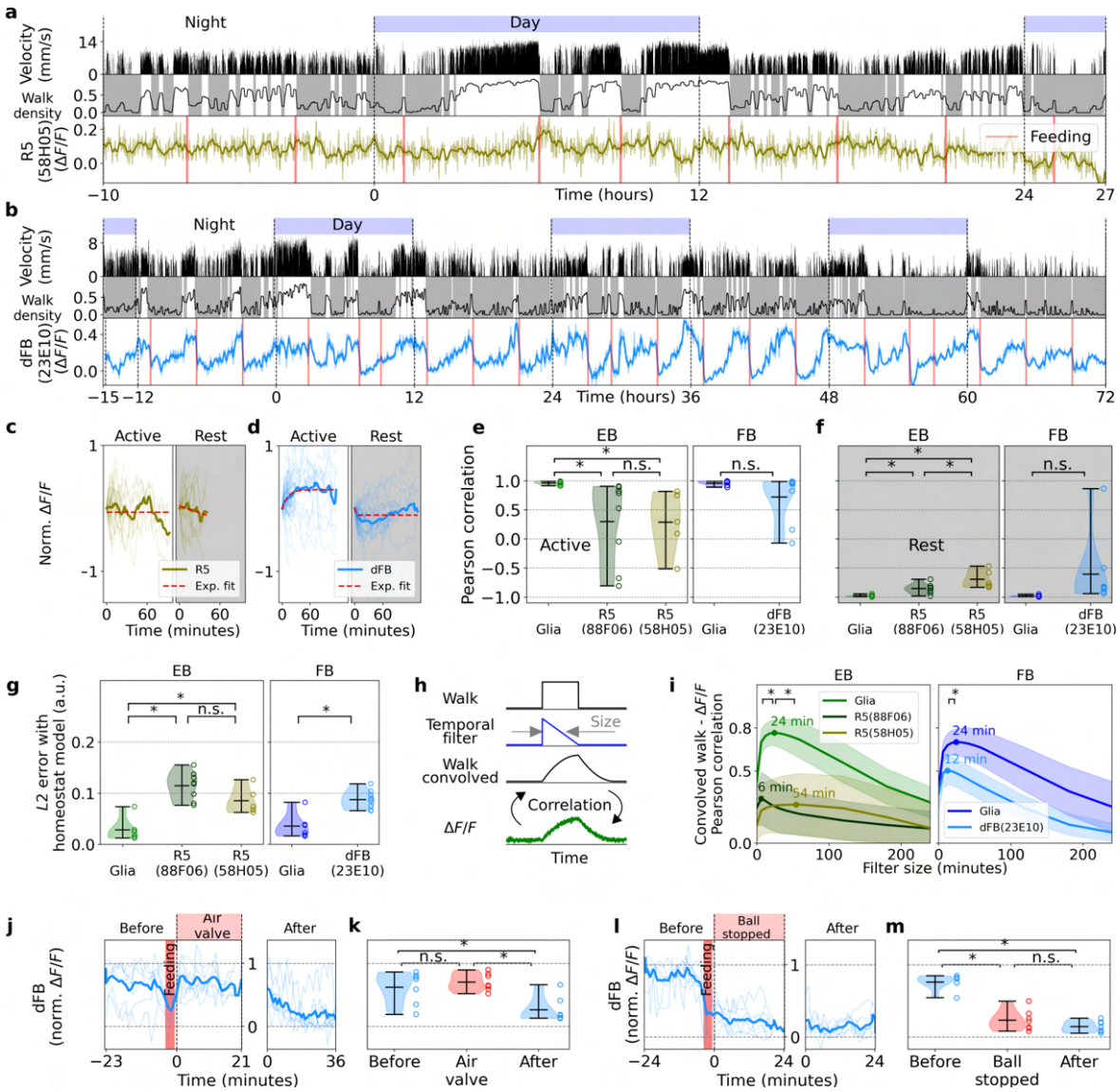

Figure 5

Taken together, activity observed in ensheathing glia is not a simple reflection of activity of homeostatic circuits in the underlying compartments. Additionally, as the above analysis shows, ensheathing glia better represent sleep homeostasis for the naturally occurring sleep and wake bouts than either R5 or dFB neuron activity recorded in the EB and FB, respectively.

Hunger and walking state encoded in dFB neurons

While activity in dFB neurons was often correlated with walking activity and rapidly reset during feeding, resetting additionally depended on the behavioral state. If the fly was sleep deprived immediately after feeding by opening and closing the valve that controlled the air stream to the ball (mostly inducing quick bouts of fast walking), fluorescence activity increased again (Fig. 5j, k, and Supplementary Fig. S43). If the fly was sleep deprived by blocking the ball (which resulted in the fly pushing and pulling on the ball but not coordinated walking), fluorescence reset (Fig. 5l, m, and Supplementary Fig. S42) indicating that dFB neurons monitor feeding as well as walking state.

Activity of dFB neurons additionally increased with time since the last feeding, without a strong correlation with walking activity. We therefore averaged fluorescence traces of dFB neurons during hungry and fed epochs, defined

Figure 5. Calcium dynamics in sleep-related neurons and comparison with ensheathing glia **a** Long-term imaging in R5 neurons (labeled by R58H05). Top row: day and night cycle in the VR. Second row: fly velocity. Third row: 'walk' density, rest (grey region), and active epochs (white region). Fourth row: calcium activity in R5 neurons. Thick line is low-pass filtered (0.1 hours cut off period). **b** Same as a, but imaging in dFB neurons (labeled by R23E10). **c** Normalized individual (thin lines) and average (thick lines) fluorescence traces, as well as exponential fits (red lines, see Methods), during active and rest epochs for R5 neurons shown in a. **d** Same as c, but for dFB neurons shown in b. **e** Left side: Pearson correlation between the time flies are active and the average fluorescence traces for glia (in the EB, $N = 6$), as well as R5 neurons labeled by R88F06 ($N = 8$) and R58H05 ($N = 5$)). Right side: same as left side, but for glia (in the FB, $N = 6$) and dFB neurons ($N = 8$). **f** Pearson correlation between time resting and average fluorescence traces from glia and neurons, as in e. **g** $L2$ error between fitted homeostat model and calcium activity of glia and neurons in EB (left) and FB (right). **h** Approach followed to compute correlation between calcium activity and convolved 'walk'. First, walk is obtained from the behavior of the fly (first row). Then, 'walk' is convolved with a triangular temporal filter with a defined size (second row) to obtain 'convolved walk'. Finally, the correlation between calcium activity and 'convolved walk' is obtained. **i** Pearson correlation between 'convolved walk' and calcium activity for different filter sizes (x-axis) for glia and neurons in EB (left) and FB (right). **j** Calcium activity in dFB neurons during sleep deprivation by perturbing the ball-supporting air stream after feeding. Normalized fluorescence traces of dFB activity (thin lines) and average (thick lines) before feeding, after feeding while the air valve was perturbing the ball, and after offset of the perturbation. **k** Normalized fluorescence levels (y-axis shared with panel j) before feeding, after feeding during sleep deprivation, and after offset of sleep deprivation. Sleep deprivation was performed by periodically interrupting air stream to ball. **l**, **m** Same as j and k, respectively, but with sleep deprivation by blocking the ball to induce effortful behaviors. Asterisks in all panels indicate statistical significance using t-test ($p < 0.05$).

as periods of 3.5 hours before and 0.5 hours after feeding events, respectively (Fig. 5a, see below and Methods for a more detailed model). Activity of dFB neurons exponentially increased during hungry epochs, with time constants in the order of hours, and exponentially decreased during fed epochs, with time constants in the minutes range (Fig. 5b, c, and Supplementary Fig. S41), indicating that dFB neurons could encode hunger, as has also been suggested for other FB neurons[58].

Using a dynamic model, activity of dFB neurons could be well described with a hunger component, which increases and decreases with respect to feeding events (Fig. 6f), and a walking component (Fig. 4d, see Methods), which were fitted together to the normalized fluorescence of dFB neurons ('hunger-walk' model, Fig. 6g, Supplementary Figs. S46, and S47, see Methods for details). Fig. 6h shows the resulting model time constants, with slow calcium dynamics during the stop state (in the order of minutes), and feeding related time constants close to zero, indicating that dFB activity resets immediately at feeding. Flies stayed satiated (with the hunger component not increasing) on average for around 40 minutes, although this varied between flies (Fig. 6h). The fitted 'hunger-walk' model (Fig. 6g, Supplementary Figs. S46, and S47) produced a lower error with dFB activity (Fig. 6i) and statistically significant better fits (see Table S4 and Methods) than a homeostat model (Supplementary Figs. S44 and S45).

Additionally, the decay amplitude during fed epochs was correlated with the amount of food ingested by the fly. The correlation between the relative change in abdomen size before feeding and after feeding events (as a proxy for the amount of food ingested, see Methods) with the change in fluorescence is shown in Fig. 6d and e. This correlation was stronger for small changes in body size (red line in Fig. 6e), suggesting that resetting of dFB neurons saturates after a certain increase in the volume of the abdomen (see Methods).

Discussion

Ensheathing glia show the characteristics expected of a sleep homeostat[32,43]: calcium levels increase with behavioral activity or effort during wakefulness, decay when the fly is sleeping, resting, extending its proboscis, or grooming

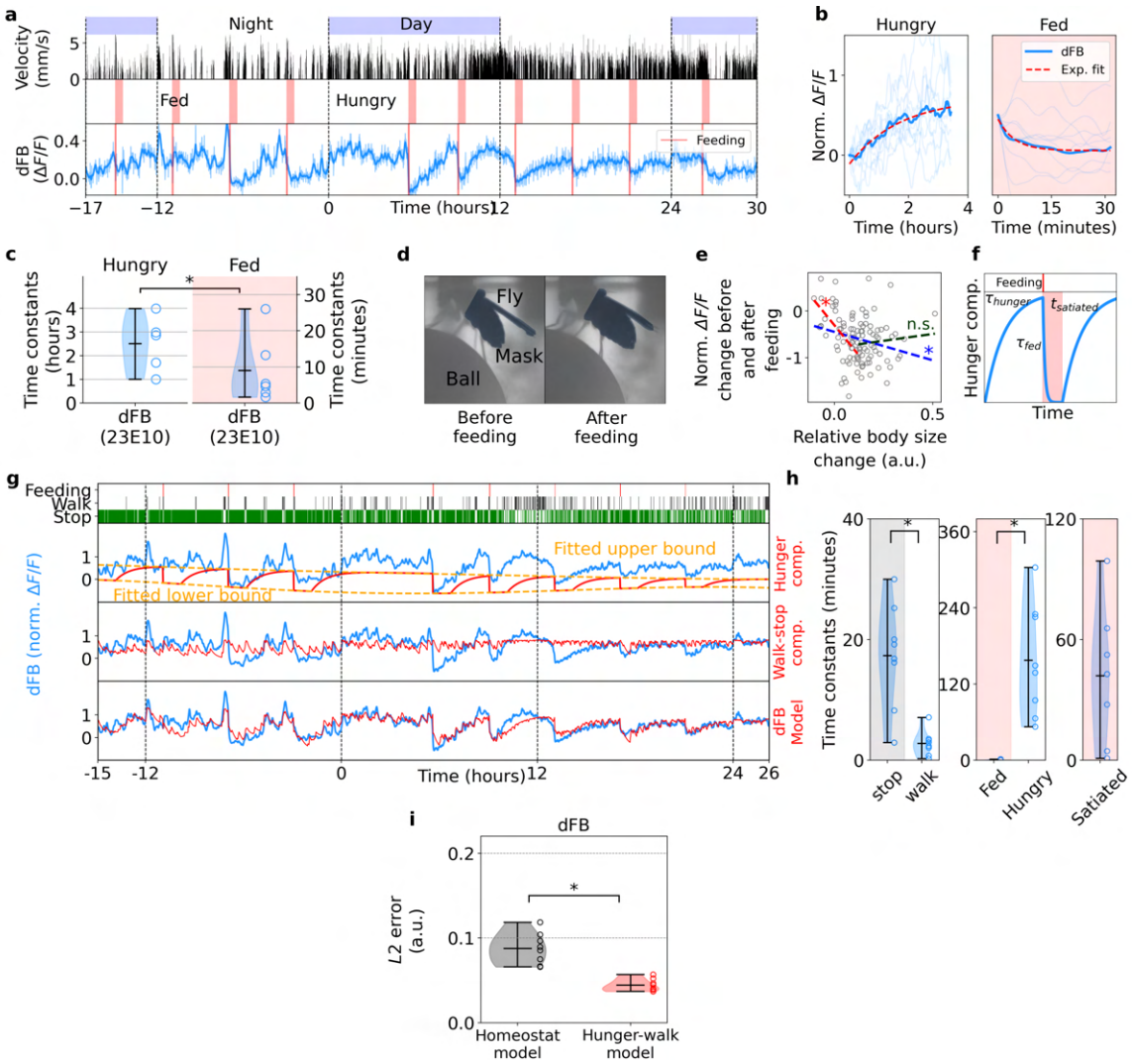

Figure 6

(Fig. 2a-d, and Supplementary Figs. S4, S5, S18, and Supplementary Videos S1-S6), and saturate during sleep deprivation (Fig. 3), all with an exponential time course. For example resetting of the homeostat to below 2% from baseline occurs over about 4 time constants or 60 to 120 minutes for the CX, or 80 to 200 minutes in the MB, a time span that covers a large fraction of the sleep bouts observed in freely walking flies[24,25,34] (Figs. 1d, 2d and 4f).

The time constants were faster for charging than for resetting of the homeostat (Fig. 4f and Supplementary Fig. S26a), consistent with the observation that flies sleep more than they are awake over a 24 hour period[24,25]. Reaching the upper or lower thresholds of the sleep homeostat did not automatically trigger awakening or sleep; however, long bouts of activity with a saturated homeostat were only observed under mechanically or hunger induced sleep deprivation (Fig. 3b and d).

Glia activity describes wake and sleep bouts more reliably than the investigated neurons in the corresponding brain compartments (Fig. 5e-i). Ring neuron activity in the EB[16,18] was not well described with a homeostatic model. Activity of dFB neurons in the FB[55] could be described more accurately by taking into account walking activity and hunger[58–60], than with a sleep homeostat (Fig. 6g-i and Supplementary Figs. S44, S45, S46 and S47). The rapid reset of activity after feeding in dFB neurons depended on the behavioral state of the fly, which is not the case for ensheathing glia. Glia activity remained high during sleep deprivation after feeding (Figs. 2i, j, 3a, Supplementary Figs. S15a, and S11), whereas in dFB neurons only walking activity, and not other effortful behaviors, could suppress

Figure 6. Feeding-related modulation in dFB neurons. **a** Long-term imaging in dFB neurons. Top row: day and night cycle in VR. Second row: fly velocity. Third row: 'hungry' epochs before feeding (white region) and 'fed' epochs after feeding (red region). Fourth row: calcium activity in dFB neurons. Thick line indicates low-pass filtering (with 0.1 hours cut-off period). **b** Normalized individual (thin lines) and average (thick lines) fluorescence traces and exponential fits (red lines, see Methods) during hungry and fed epochs from the recording in dFB neurons shown in a. **c** Time constants of fitted exponentials during hungry and fed epochs ($N = 8$ flies). Asterisk indicates statistical significance using t-test ($p < 0.05$). **d** Side view of a fly during a long-term imaging recording before feeding (hungry, left side) and after feeding (fed, right side). Mask of the abdomen (highlighted in dark color) for computing change in size. **e** Normalized fluorescence change against relative change in body size (see Methods) between 10 minutes before and 10 minutes after feeding. The blue line represents a linear fit over all points, while the red and green lines represent a linear fit over the first half and second half of relative body size change, respectively. Asterisks indicate the statistical significance of each fit using Pearson correlation ($p < 0.05$). **f** Parametrization (three parameters, τ_{hunger}, τ_{fed} and $t_{satiated}$) of the hunger component of the 'hunger-walk' model. Before a feeding event (top row in red) the hunger component increases with the time constant τ_{hunger} and resets after feeding with the time constant τ_{fed} for a given time $t_{satiated}$. **g** Fitting of the hunger-walk model to activity of dFB neurons. Top row: events of feeding as well as walking and stopping bouts of the fly. Second, third and fourth row: normalized fluorescence (blue) and the fitted hunger component, 'walk-stop' component, and the 'hunger-walk' model (obtained from the two previous combined components), respectively (red). **h** Time constants ($N = 8$ flies) of stop and walk (left, from the stop-walk component), and time constants of 'fed', 'hungry', and 'satiated' (center and right, from the hunger component). Asterisks indicate statistical significance using t-test ($p < 0.05$). $L2$ error between the fitted homeostat and 'hunger-walk' models and the normalized activity of dFB neurons. Asterisk indicates statistical significance using paired t-test.

resetting of calcium levels (Fig. 5j-m, Supplementary Figs. S42, and S43). These findings are also consistent with recent observations that dFB neurons might not have the previously thought role for sleep control[61].

Homeostatic sleep signals were observed across brain areas, such as the CX and MBs, but also in areas that have not been previously implicated in sleep, such as the LAL or the commissure. Ensheathing glia form barriers around all these brain compartments[13,62] and could therefore integrate activity of the underlying circuits, for example by sensing glutamate. Consistent with this idea, we observed an increase or respectively a decrease of extracellular glutamate at ensheathing glia in the CX during active and inactive, or wake and sleep states (Fig. 4a-c, Supplementary Figs. S16, and S17).

That glia around different brain compartments show different calcium dynamics could be due to locally different activity and resulting sleep needs in different brain compartments[63–65]. Integration of local neural activity was performed based on electrical recordings in the cortex of mice and allowed the computational reconstruction of a sleep homeostat[65]. Glia could perform a similar local integration of neural activity for each brain compartment of the fly.

The action of ensheathing glia could include the regulation of glutamate in the enclosed circuits[15,66]. Fly glia are also important for supplying energy to neurons and the underlying mechanism could also rely on glutamate[12,67].

Calcium levels in glia have been suggested as a mechanism for integrating neural activity and providing feedback to underlying neural circuits by modulating their environment in other animals as well[68]. Modulation of sleep circuits by glia has for example been described in C. elegans[69,70]. In mice, microglia generate inhibitory feedback and suppress activity of glutamatergic neurons[71], a mechanism which could also play a role in sleep regulation in an adenosine-dependent manner[72]. Recent evidence suggests that ensheathing glia could also release adenosine with increasing calcium levels[73]. Adenosine seems however not to be important for sleep control in the fly[74]. An alternative gliotransmitter could be taurine which promotes sleep in flies and is also regulated by ensheathing glia[14].

Overall, ensheathing glia offer a homeostatic sleep signal distributed across different brain areas. Combining imaging in behaving flies over long timescales with a range of behavior paradigms, including learning, as well as the genetic tools available in the fly will enable the brain-wide investigation of the interplay between behavior, sleep

homeostasis, and sleep function.

Funding

Max Planck Society, Max Planck Institute for Neurobiology of Behavior – caesar (MPINB). Netzwerke 2021, Ministry of Culture and Science of the State of Northrhine Westphalia.

Acknowledgements

We thank Marcelo Cintra, Christoph Geisen, Omar Valerio Minero, and Sercan Yegin for help with the MPINB cluster, Ivan Vishniakou for technical support, Jasmin Beinert, Tim Krause, Tolga Ates and Anne Buecker for maintaining flies, and Vivek Jayaraman for Chrimson flies. We thank Kevin Briggman and Jason Kerr for comments on the manuscript.

Author contributions

Both authors designed the study, performed experiments, and wrote the manuscript. AFV performed data analysis.

Competing interests

The authors declare that there are no conflicts of interest related to this article.

References

1. Duhart, J. M., Inami, S. & Koh, K. Many faces of sleep regulation: beyond the time of day and prior wake time. *The FEBS journal* (2021).
2. Sulaman, B. A., Wang, S., Tyan, J. & Eban-Rothschild, A. Neuro-orchestration of sleep and wakefulness. *Nat. Neurosci.* 1–17 (2022).
3. Heller, C. The regulation of sleep. In *Oxford Research Encyclopedia of Neuroscience* (2021).
4. Bojarskaite, L. *et al.* Astrocytic ca 2+ signaling is reduced during sleep and is involved in the regulation of slow wave sleep. *Nat. communications* **11**, 1–16 (2020).
5. Ingiosi, A. M. *et al.* A role for astroglial calcium in mammalian sleep and sleep regulation. *Curr. Biol.* **30**, 4373–4383 (2020).
6. Tsunematsu, T., Sakata, S., Sanagi, T., Tanaka, K. F. & Matsui, K. Region-specific and state-dependent astrocyte ca2+ dynamics during the sleep-wake cycle in mice. *J. Neurosci.* **41**, 5440–5452 (2021).
7. Vaidyanathan, T. V., Collard, M., Yokoyama, S., Reitman, M. E. & Poskanzer, K. E. Cortical astrocytes independently regulate sleep depth and duration via separate gpcr pathways. *Elife* **10**, e63329 (2021).
8. Peng, W. *et al.* Adenosine-independent regulation of the sleep–wake cycle by astrocyte activity. *Cell Discov.* **9**, 16 (2023).
9. Hastings, M. H., Brancaccio, M., Gonzalez-Aponte, M. F. & Herzog, E. D. Circadian rhythms and astrocytes: The good, the bad, and the ugly. *Annu. Rev. Neurosci.* **46** (2022).
10. Ingiosi, A. M. & Frank, M. G. Goodnight, astrocyte: Waking up to astroglial mechanisms in sleep. *The FEBS J.* (2022).
11. Artiushin, G. & Sehgal, A. The glial perspective on sleep and circadian rhythms. *Annu. review neuroscience* **43**, 119–140 (2020).
12. De Backer, J.-F. & Kadow, I. C. G. A role for glia in cellular and systemic metabolism: insights from the fly. *Curr. Opin. Insect Sci.* 100947 (2022).

13. Kremer, M. C., Jung, C., Batelli, S., Rubin, G. M. & Gaul, U. The glia of the adult drosophila nervous system. *Glia* **65**, 606–638 (2017).

14. Stahl, B. A. *et al.* The taurine transporter eaat2 functions in ensheathing glia to modulate sleep and metabolic rate. *Curr. Biol.* **28**, 3700–3708 (2018).

15. Bittern, J. *et al.* Neuron–glia interaction in the drosophila nervous system. *Dev. neurobiology* **81**, 438–452 (2021).

16. Liu, S., Liu, Q., Tabuchi, M. & Wu, M. N. Sleep drive is encoded by neural plastic changes in a dedicated circuit. *Cell* **165**, 1347–1360 (2016).

17. Donlea, J. M. *et al.* Recurrent circuitry for balancing sleep need and sleep. *Neuron* **97**, 378–389 (2018).

18. Raccuglia, D. *et al.* Network-specific synchronization of electrical slow-wave oscillations regulates sleep drive in drosophila. *Curr. Biol.* **29**, 3611–3621 (2019).

19. Flores-Valle, A., Gonçalves, P. J. & Seelig, J. D. Integration of sleep homeostasis and navigation in drosophila. *PLoS Comput. Biol.* **17**, e1009088 (2021).

20. Hulse, B. K. & Jayaraman, V. Mechanisms underlying the neural computation of head direction. *Annu. review neuroscience* **43**, 31–54 (2020).

21. Blum, I. D. *et al.* Astroglial calcium signaling encodes sleep need in drosophila. *Curr. Biol.* **31**, 150–162 (2021).

22. Van Alphen, B., Yap, M. H., Kirszenblat, L., Kottler, B. & van Swinderen, B. A dynamic deep sleep stage in drosophila. *J. Neurosci.* **33**, 6917–6927 (2013).

23. Tainton-Heap, L. A. *et al.* A paradoxical kind of sleep in drosophila melanogaster. *Curr. Biol.* **31**, 578–590 (2021).

24. Zimmerman, J. E., Raizen, D. M., Maycock, M. H., Maislin, G. & Pack, A. I. A video method to study drosophila sleep. *Sleep* **31**, 1587–1598 (2008).

25. Donelson, N. *et al.* High-resolution positional tracking for long-term analysis of drosophila sleep and locomotion using the "tracker" program. *PloS one* **7**, e37250 (2012).

26. Van Alphen, B., Semenza, E. R., Yap, M., Van Swinderen, B. & Allada, R. A deep sleep stage in drosophila with a functional role in waste clearance. *Sci. advances* **7**, eabc2999 (2021).

27. Shaw, P. J., Cirelli, C., Greenspan, R. J. & Tononi, G. Correlates of sleep and waking in drosophila melanogaster. *Science* **287**, 1834–1837 (2000).

28. Huber, R. *et al.* Sleep homeostasis in drosophila melanogaster. *Sleep* **27**, 628–639 (2004).

29. Denk, W., Strickler, J. H. & Webb, W. W. Two-photon laser scanning fluorescence microscopy. *Science* **248**, 73–76 (1990).

30. Flores-Valle, A., Honnef, R. & Seelig, J. D. Automated long-term two-photon imaging in head-fixed walking drosophila. *J. neuroscience methods* **368**, 109432 (2022).

31. Flores-Valle, A. & Seelig, J. D. Axial motion estimation and correction for simultaneous multi-plane two-photon calcium imaging. *Biomed. optics express* **13**, 2035–2049 (2022).

32. Borbély, A. A., Daan, S., Wirz-Justice, A. & Deboer, T. The two-process model of sleep regulation: a reappraisal. *J. sleep research* **25**, 131–143 (2016).

33. Skeldon, A. C., Dijk, D.-J. & Derks, G. Mathematical models for sleep-wake dynamics: comparison of the two-process model and a mutual inhibition neuronal model. *PloS one* **9**, e103877 (2014).

34. Hendricks, J. C. *et al.* Rest in drosophila is a sleep-like state. *Neuron* **25**, 129–138 (2000).

35. Zhang, Y. *et al.* jgcamp8 fast genetically encoded calcium indicators. *Janelia Res. Campus* **10**, 13148243 (2020).

36. Jenett, A. *et al.* A gal4-driver line resource for drosophila neurobiology. *Cell reports* **2**, 991–1001 (2012).

37. Daan, S., Beersma, D. & Borbély, A. A. Timing of human sleep: recovery process gated by a circadian pacemaker. *Am. J. Physiol. Integr. Comp. Physiol.* **246**, R161–R183 (1984).

38. Borbély, A. A. & Achermann, P. Concepts and models of sleep regulation: an overview. *J. sleep research* **1**, 63–79 (1992).

39. Beckwith, E. J. & French, A. S. Sleep in drosophila and its context. *Front. physiology* 1167 (2019).

40. Shafer, O. T. & Keene, A. C. The regulation of drosophila sleep. *Curr. Biol.* **31**, R38–R49 (2021).

41. Mu, Y. *et al.* Glia accumulate evidence that actions are futile and suppress unsuccessful behavior. *Cell* **178**, 27–43 (2019).

42. Yap, M. H. *et al.* Oscillatory brain activity in spontaneous and induced sleep stages in flies. *Nat. communications* **8**, 1–15 (2017).

43. Borbély, A. A. A two process model of sleep regulation. *Hum neurobiol* **1**, 195–204 (1982).

44. Geissmann, Q., Beckwith, E. J. & Gilestro, G. F. Most sleep does not serve a vital function: Evidence from drosophila melanogaster. *Sci. advances* **5**, eaau9253 (2019).

45. Lee, G. & Park, J. H. Hemolymph sugar homeostasis and starvation-induced hyperactivity affected by genetic manipulations of the adipokinetic hormone-encoding gene in drosophila melanogaster. *Genetics* **167**, 311–323 (2004).

46. Isabel, G., Martin, J.-R., Chidami, S., Veenstra, J. A. & Rosay, P. Akh-producing neuroendocrine cell ablation decreases trehalose and induces behavioral changes in drosophila. *Am. J. Physiol. Integr. Comp. Physiol.* **288**, R531–R538 (2005).

47. Pool, A.-H. & Scott, K. Feeding regulation in drosophila. *Curr. opinion neurobiology* **29**, 57–63 (2014).

48. Aimon, S., Cheng, K. Y., Gjorgjieva, J. & Grunwald Kadow, I. C. Global change in brain state during spontaneous and forced walk in drosophila is composed of combined activity patterns of different neuron classes. *eLife* **12**, e85202 (2023).

49. Richter, F. G., Fendl, S., Haag, J., Drews, M. S. & Borst, A. Glutamate signaling in the fly visual system. *Iscience* **7**, 85–95 (2018).

50. Marvin, J. S. *et al.* An optimized fluorescent probe for visualizing glutamate neurotransmission. *Nat. methods* **10**, 162–170 (2013).

51. Borb, A. A. & Achermann, P. Sleep homeostasis and models of sleep regulation. *J. biological rhythms* **14**, 559–570 (1999).

52. Kirszenblat, L. & van Swinderen, B. Sleep in drosophila. In *Handbook of Behavioral Neuroscience*, vol. 30, 333–347 (Elsevier, 2019).

53. Bohnslav, J. P. *et al.* Deepethogram, a machine learning pipeline for supervised behavior classification from raw pixels. *Elife* **10**, e63377 (2021).

54. Andreani, T. *et al.* Circadian programming of the ellipsoid body sleep homeostat in drosophila. *Elife* **11**, e74327 (2022).

55. Donlea, J. M., Thimgan, M. S., Suzuki, Y., Gottschalk, L. & Shaw, P. J. Inducing sleep by remote control facilitates memory consolidation in drosophila. *Science* **332**, 1571–1576 (2011).

56. Dissel, S. *et al.* Sleep restores behavioral plasticity to drosophila mutants. *Curr. Biol.* **25**, 1270–1281 (2015).

57. Dag, U. *et al.* Neuronal reactivation during post-learning sleep consolidates long-term memory in drosophila. *Elife* **8**, e42786 (2019).

58. Sareen, P. F., McCurdy, L. Y. & Nitabach, M. N. A neuronal ensemble encoding adaptive choice during sensory conflict in drosophila. *Nat. communications* **12**, 1–13 (2021).

59. Liu, Q. *et al.* Branch-specific plasticity of a bifunctional dopamine circuit encodes protein hunger. *Science* **356**, 534–539 (2017).

60. Dissel, S. *et al.* Sleep-promoting neurons remodel their response properties to calibrate sleep drive with environmental demands. *PLoS biology* **20**, e3001797 (2022).

61. De, J., Wu, M., Lambatan, V., Hua, Y. & Joiner, W. J. Re-examining the role of the dorsal fan-shaped body in promoting sleep in drosophila. *Curr. Biol.* (2023).

62. Pogodalla, N. *et al.* Drosophila ßheavy-spectrin is required in polarized ensheathing glia that form a diffusion-barrier around the neuropil. *Nat. communications* **12**, 1–18 (2021).

63. Rector, D. M., Schei, J. L., Van Dongen, H. P., Belenky, G. & Krueger, J. M. Physiological markers of local sleep. *Eur. J. Neurosci.* **29**, 1771–1778 (2009).

64. Krueger, J. M., Nguyen, J. T., Dykstra-Aiello, C. J. & Taishi, P. Local sleep. *Sleep medicine reviews* **43**, 14–21 (2019).

65. Thomas, C. W., Guillaumin, M. C., McKillop, L. E., Achermann, P. & Vyazovskiy, V. V. Global sleep homeostasis reflects temporally and spatially integrated local cortical neuronal activity. *Elife* **9**, e54148 (2020).

66. Otto, N. *et al.* The sulfite oxidase shopper controls neuronal activity by regulating glutamate homeostasis in drosophila ensheathing glia. *Nat. communications* **9**, 1–12 (2018).

67. DiNuzzo, M. & Nedergaard, M. Brain energetics during the sleep–wake cycle. *Curr. opinion neurobiology* **47**, 65–72 (2017).

68. Araque, A. *et al.* Gliotransmitters travel in time and space. *Neuron* **81**, 728–739 (2014).

69. Katz, M., Corson, F., Iwanir, S., Biron, D. & Shaham, S. Glia modulate a neuronal circuit for locomotion suppression during sleep in c. elegans. *Cell reports* **22**, 2575–2583 (2018).

70. Nagai, J. *et al.* Behaviorally consequential astrocytic regulation of neural circuits. *Neuron* **109**, 576–596 (2021).

71. Badimon, A. *et al.* Negative feedback control of neuronal activity by microglia. *Nature* **586**, 417–423 (2020).

72. Pfeiffer, T. & Attwell, D. Brain's immune cells put the brakes on neurons (2020).

73. Wang, F. *et al.* Gliotransmission orchestrates neuronal type-specific axon regeneration. *bioRxiv* 799635 (2022).

74. Wu, M. N. *et al.* The effects of caffeine on sleep in drosophila require pka activity, but not the adenosine receptor. *J. Neurosci.* **29**, 11029–11037 (2009).

75. Huang, C. *et al.* Long-term optical brain imaging in live adult fruit flies. *Nat. communications* **9**, 1–10 (2018).

76. Vishniakou, I., Plöger, P. G. & Seelig, J. D. Virtual reality for animal navigation with camera-based optical flow tracking. *J. neuroscience methods* **327**, 108403 (2019).

77. Bushey, D., Tononi, G. & Cirelli, C. Sleep-and wake-dependent changes in neuronal activity and reactivity demonstrated in fly neurons using in vivo calcium imaging. *Proc. Natl. Acad. Sci.* **112**, 4785–4790 (2015).

78. Berry, J. A., Cervantes-Sandoval, I., Chakraborty, M. & Davis, R. L. Sleep facilitates memory by blocking dopamine neuron-mediated forgetting. *Cell* **161**, 1656–1667 (2015).

79. Virtanen, P. *et al.* SciPy 1.0: Fundamental Algorithms for Scientific Computing in Python. *Nat. Methods* **17**, 261–272, DOI: 10.1038/s41592-019-0686-2 (2020).

80. Zwietering, M., Jongenburger, I., Rombouts, F. & Van't Riet, K. Modeling of the bacterial growth curve. *Appl. environmental microbiology* **56**, 1875–1881 (1990).

1 Methods

Drosophila preparation

All flies were reared in an incubator at 25 degrees with a 12 hour light/dark cycle. For experiments with freely moving flies, we used 7 days old females expressing jGCaMP8m in ensheathing glia (UAS-jGCaMP8m;56F03-GAL4). Flies were anesthetized on ice and placed individually in rectangular chambers with food (Fig. 1a).

The same 12 hour light/dark cycle as in the incubator was used in VR during imaging experiments. All imaging experiments were performed with female flies between 3 and 8 days old at the beginning of the experiment. To record calcium activity of ensheathing glia, we expressed jGCaMP8m using the Gal4 line 56F03 (UAS-jGCaMP8m;56F03-GAL4). Experiments for monitoring extracellular glutamate were performed by expressing the glutamate sensor iGluSnFR in ensheathing glia (UAS-iGluSnFR;56F03-GAL4). To monitor activity of R5 ring neurons we used two different GAL4 lines: 58H05-GAL4 expressing jGCaMP8m (UAS-jGCaMP8m;58H05-GAL4), and 88F06-GAL4 expressing jGCaMP8m, 8f or 7f (UAS-jGCaMP8m;88F06-GAL4, UAS-jGCaMP8f;88F06-GAL4 and UAS-jGCaMP7f;88F06-GAL4), respectively. Activity of dFB neurons was monitored by expressing jGCaMP8m or jGCaMP8f in 23E10-GAL4 (UAS-jGCaMP8m;23E10-GAL4, UAS-jGCaMP8f;23E10-GAL4).

For imaging, flies were dissected using laser surgery as described[30] to insert a transparent window into the cuticle[30,75]. The cut cuticle and air sacks were removed under a dissection microscope using forceps, either manually or with a microrobotic arm[30]. The opening was sealed with a drop of transparent UV glue (Freeform, UV fixgel composite). Between 2 and 5 flies were dissected at a time and were left to recover in vials with food for 1 to 3 days before imaging. Flies were then glued to a glass slide using UV glue and transferred to the long-term imaging setup. Flies were selected for imaging based on the optical access to the structures of interest which varied dependent on dissections. Only data recorded at least 48 hours after surgery were included in the analysis.

Setup for experiments with freely walking flies

Flies were placed in transparent chambers of 70×4 mm (Fig. 1a) and activity was recorded in 15 chambers using a camera from above with a resolution of 1920×1080 pixels at 30 Hz. A rectangular grid of IR LEDs illuminated the chambers from below through a diffuser. A high-pass filter (Thorlabs FGL780S) in front of the camera rejected white light from LEDs which generated the same 12 hour light /dark cycle as in the incubator. Since flies needed to adapt to the new environment, the first day of the experiment was discarded, and we only considered the subsequent two days for the following analysis.

Tracking of fly positions was done offline, using color segmentation in OpenCV and Python, by extracting the dark color of the flies from the bright background (Supplementary Video S8). The position and velocity of each fly were smoothed using a Kalman filter. Fig. 1b shows examples of the position along the chamber and the velocity of one fly. Supplementary Figs. S1a and b show the mean velocity of 15 flies with a light/dark cycle and in darkness over 48 hours, respectively. Under both conditions flies displayed circadian activity.

To find epochs of immobility, we set the velocity of each fly to zero if a fly did not move for at least 0.25 body lengths in a second (a body length was defined as 2.5 mm) (Fig. 1c, first row). We then computed each fly's 'stop' binary profile over time from the velocity (Fig. 1c, second row). To compute sleep bouts, we used different temporal filters with a size of 1, 2, 5, 8, and 10 minutes (Fig. 1c, third row) and convolved them with the binary 'stop' signal (Fig. 1c, third row). These temporal filters removed small bouts of movement of the fly (depending on the filter size) between stop epochs. Sleep was then obtained by thresholding the convolved 'walk' signal at the value of 0.5 (Fig. 1c, fourth row). The distribution of continuous sleep bouts was computed for each filter size during the day and night (Fig. 1d), and during darkness (Supplementary Fig. S1c), and the 90% quantile of the distribution is highlighted. A filter size of 2 minutes, which already removes up to 1 minute of walking in between stop epochs, produces a distribution where 90% of sleep bouts are below 50 minutes (Fig. 1d). Sleep bouts were even shorter in dark conditions, where even using a filter size of 10 minutes, which removes 5 minutes of walking in between stop bouts, led to a distribution where 90% of sleep bouts were below 40 minutes (Supplementary Fig. S1c).

To compute how frequently flies ate in these behavior experiments, we determined all occasions where the fly was close to the food (at around 7 *mm* in the chamber, see Fig. 1b). As before, we used temporal filters with different sizes (30, 60, 90, 120, and 150 seconds) to filter out small movements of the fly entering and leaving the

food. We then obtained the distribution of time intervals between consecutive feeding events during the day and night depending on filter size (Fig. 1h). Using a filter size of 120 seconds, 90 % of the times between consecutive feeding events were around 26 minutes during both day and night. Similar rates of feeding were used in some of the imaging experiments, where flies were fed every 26 minutes (Fig. 1i and j, and Supplementary Fig. S2) or every 16 minutes (Supplementary Fig. S3).

Imaging setup

The setup for long-term imaging was as described in[30]. For recording volumetric calcium activity and to reduce brain motion artifacts, two axially offset focal planes were recorded at the same time with beams with an extended focal length, with temporally multiplexed acquisition[30]. This setup allowed motion correction at high time resolution in all three dimensions as described in[31]. Virtual reality projection and closed loop behavior were implemented as previously described[30,76].

Data acquisition

At the start of each long-term imaging experiment, a z-stack of 100 μm depth with an axial step size of 0.25 μm was recorded, which was used for z-motion correction in post-processing[31] (see next section). Additionally, an automated robotic feeder was configured at the beginning of the experiment, for example to feed flies every 4 hours for 2 minutes[30]. Imaging data was recorded at a resolution of 256×256 pixels at 60 Hz. In most of the experiments, we recorded for 1 second with a wait time of 60 seconds between consecutive recordings, resulting in a total imaging time of 1.6% of the duration of the experiment, which helped to reduce photobleaching and phototoxicity. However, we additionally used a different protocol in four other flies, where we recorded in trials of 30 seconds with a wait time of 5 minutes between trials, which resulted in a total imaging time of 11% of the duration of the experiment (Supplementary Figs. S39g and S34f-h).

The VR, implemented as described[19,76] displayed a dark stripe on a bright background using a blue laser (488 nm), which was switched off during the night for 12 hours. The VR night and day cycle was the same as the one used in the incubator. Ball movement was tracked at 200 Hz and a calibration factor was determined for calculating ball velocities. The water temperature at the objective was maintained at 22 degrees with a perfusion system[30].

Flies were left to recover for at least 2 days after surgery and before imaging started. In some flies, imaging started after 1 day of recovery and the first day was excluded from data analysis. Recordings of calcium activity in ensheathing glia are shown in Figs. 1i, 2a and e and Supplementary Figs. S2, S3, S4, and S10 for EB and FB, Supplementary Fig. S6 for LAL, and Supplementary Figs. S8 and S12 for MB and commissure. Recordings of glutamate activity in ensheathing glia are shown in Fig. 4a and Supplementary Fig. S16. Recordings of calcium activity in R5 neurons using 58H05-GAL4 are shown in Fig. 5a and Supplementary Fig. S30, and recordings using 88F06-GAL4 are shown in Supplementary Figs. S33 and S34. Finally, recordings of calcium activity in dFB neurons are shown in Fig. 5b and Supplementary Figs. S38, S38, S43 and S42.

Data post-processing

Imaging data was corrected for lateral motion by alignment with respect to a template (average of the first 60 frames) using cross-correlation (Fig. 2f). The z-stack was also aligned with respect to this template. Then, 24 regions of interest (ROIs) were defined for recordings in ensheathing glia in different brain areas (the 24 ROIs merged into a single one are shown in Fig. 2f for EB and FB, Supplementary Fig. S29b for LAL and Supplementary Fig. S29c for MB and commissure). ROIs were also defined for the case of R5 and dFB neurons (the combined 24 ROIs are shown in Supplementary Fig. S29d,e for R5 neurons, and f for dFB neurons). The intensity of each ROI was computed by summing all pixel values within each ROI per frame as well as in each frame in the z-stack. The intensity of the ROIs was then used to estimate the z-motion of the sample for each imaging frame as described[31]. The resulting z-motion over the time of the experiment was filtered using a median filter with 1000 points to discard high-frequency motion, and maximum displacements of around 10*um* along the z-axis were detected. The filtered z-motion was used to estimate the fluorescence of each ROI corrected for z-motion[31]. Differences between corrected and uncorrected fluorescence was generally low, with maximum differences of 0.1 $\Delta F/F$ due to the extended focal

volume used for imaging[31].

The 200 Hz used to track ball motion underestimated ball displacements in the 3 axes by a factor of 0.50 compared to using 500 Hz tracking as in[76]. This factor was experimentally measured by rotating the ball by 3600 degrees. Ball displacements during long-term imaging were corrected with this calibration factor in post-processing and used to compute the absolute velocity of the fly in bins of 1 second using the ball radius ($3mm$).

For fitting models to fluorescence traces (see sections below), we first smoothed the fluorescence signal using a low-pass filter with a cut-off period of 15 minutes (thick lines Figs. 2a, 4a, 5a,b and Supplementary Figs. S4, S6, S8 S16, S30, S33, S34, S38, S39). Then, we normalized the filtered fluorescence, $F(t)$, by remapping the 10% and 90% quantiles of $F(t)$ ($Q_{10\%}$ and $Q_{90\%}$, respectively) to the values 0 and 1, respectively, with the following equation:

$$\text{Normalized } F(t) = \frac{F(t) - Q_{10\%}}{Q_{90\%} - Q_{10\%}}. \tag{1}$$

This was done to reliably compare glia and neurons in Fig. 5e-i, since different recordings have different fluorescence dynamic ranges and different noise levels. By smoothing and normalizing fluorescence traces from all experiments, we ensured that correlations (Fig. 5e, f and i) and errors from model fittings (Fig. 5g and Fig. 6i) were correctly compared across recordings.

Behavior classification

Fly behavior was monitored during the entire experiment using a camera (Supplementary Fig. S28a) under IR illumination at 10 frames per second (fps). Based on blocks of 10 consecutive frames (1 second time resolution), we classified the following 7 behaviors (rows in Supplementary Fig. S28A). Stop: the fly does not move. Proboscis: the fly does not move but extends and retracts the proboscis. Walk: the fly walks on the ball. Discomfort: the fly pushes or pulls the ball. Grooming front: grooming of head and proboscis with front legs. Grooming back: grooming of the abdomen and wings with hind legs. Feeding: fly is fed with the feeding robot.

We used a 3D convolutional neural network (3D CNN) to classify behavior based on 10 frames at a time. The field of view of the camera (with resolution 640×480 pixels) was cropped around the fly and was resized to a resolution of $256x256$ pixels. The architecture of the 3D CNN is shown in Supplementary Fig. S28b, where each convolutional block consisted of a 3D convolutional layer with a $3x3x3$ kernel size and rectified linear unit activation function (ReLU), a dropout layer with a rate of 0.2 to prevent overfitting, and 3D max pooling with size $2x2x1$. The filters of the convolutional layer increased by a factor of 2 in each consecutive convolutional block. Finally, a dense layer with a softmax activation function assigned a value to each class. The 3D CNN had a total of around 6.5M trainable parameters.

A total of 45610 manually labeled frames from 10 different flies were used for training. The dataset was normalized to train the network with the same number of samples for each class. We further increased this dataset with data augmentation that randomly transformed the input frames by changing illumination, translation, rotation, and/or scale during training. To train the network we used TensorFlow with a binary cross-entropy loss function and Adam as optimizer. After 150 epochs with a batch size of 50 samples, the loss function reached a minimum saturation value in about 2 hours, using 4 QUADRO GPUs.

To test the performance of the network, we used 2410 labeled frames, which were augmented to a total of 20000 with the previously described augmentation transformations. The accuracy of the network to predict the right class of behavior was 98.6%, and the normalized confusion matrix for each class is shown in Supplementary Fig. S28c. An example of behavior classification is shown in Supplementary Video S7.

Probing of arousal threshold

For probing the arousal threshold of the fly during long-term imaging, we used a total of 6 flies where we recorded calcium activity (data not included) from ensheathing glia using the same protocol as before. We recorded multiple trials of probing the arousal threshold in each fly. Trials were initiated automatically using custom software (see number of trials, N, for each fly in Extended Fig. S14b-g). At the beginning of each trial, the amount of expected sleep time for probing the arousal threshold was selected randomly, either 30 seconds or 5 minutes. Then the fly

was stimulated to walk by closing and opening the valve controlling the air stream supporting the treadmill ball repeatedly 3 times during 6 seconds (1 second closed and 1 second open). This ensured that the fly was awake at the beginning of each trial. After this, the velocity of the fly on the ball (thresholded to remove tracking noise) was monitored in real-time to detect epochs of walking or immobility. A timer was used to measure the time the fly was not walking since the end of the last walking bout (non-zero velocity). If this time reached the previously selected duration (30 seconds or 5 minutes), probing of the arousal threshold started. Probing was performed with an IR laser focused on the abdomen (Toptica, ibeam-smart-785-S-HP with pulse option, 785 nm) by ramping the power from 0 to $100mW$ in steps $1mW$ every second. When the fly started to walk due to the heating effect of the IR laser, the trial finished and the IR laser was turned off. During probing with the IR laser, the shutter of the two-photon laser was closed and imaging data was not recorded, since the combined power of the two-photon and heating lasers would distort the detection of the threshold. After a trial had finished, the next trial started after 10 minutes of waiting. Experiments for each fly were performed for at least 1 day, resulting in several hundreds of probing trials in each fly.

We used the 3D CNN to classify the behavior in post-processing. For each trial, we computed the actual elapsed time that the fly was immobile (either in the 'stop' state or 'proboscis' state) prior to the arousal threshold probing, in order to remove grooming events. Only trials with prior times of complete immobility larger than 5 seconds were considered, therefore the resulting times of immobility ranged from 5 seconds to 5 minutes. During the probing period in each trial, we obtained the required laser power to awake the fly. The fly was considered awake when it showed walking, discomfort, or grooming behaviors (obtained from the 3D CNN classification). An example of a trial for arousal threshold probing is shown in Supplementary Fig. S14a.

We computed the distribution of IR laser powers required to awake the fly prior to three different time intervals of immobility: [5, 35], [35, 200], and [200, 305] seconds. These distributions are shown in Supplementary Fig. S14b-g for individual flies, and in Fig. 2k for all flies. Asterisks indicate statistical significance using t-test (p-value < 0.05). As shown for individual flies as well as for all flies (Fig. 2k and Supplementary Fig. S14b-g), longer times of immobility required higher IR laser powers to awake the flies, confirming that the arousal threshold increases with time of immobility during our long-term recordings.

Fitting of fluorescence traces during 'active' and 'rest' states

Sleep is commonly identified in flies as bouts of immobility that last at least 5 minutes[27,28], a threshold that has also been used for assessing sleep in tethered walking flies[77,78]. However, shorter bouts of quiescence already show many of the characteristics of sleep[23]. The distribution of time bouts that the flies did not walk during the recordings in ensheathing glia is shown in Supplementary Fig. S22 for 6 flies. We compare the amount of sleep according to a 5 minutes threshold, according to only distinguishing between walking and stopping, and according to the 'rest' and 'active' states (used in Fig. 2a) in Table S1.

To find epochs of at least 10 minutes during which the fly was walking most of the time (active) or sleeping most of the time (rest), first, walking velocity on the ball (with a diameter of 3 mm) was averaged over one second. Then, velocities below a threshold of 0.25 body lengths per second (body length defined again as 2.5 mm) were set to zero to remove tracking noise, and we defined a binary walk state of the fly, $w(t)$, when the thresholded velocity was non-zero ($w(t) = 1$). We defined active and rest states where the fly was walking or standing still most of the time. To calculate these states, we used a walk density, which was obtained by low-pass filtering of the walk state with a period of 0.1 hours (6 minutes). Active and rest states were defined based on the walk density being above or below a threshold of 0.5, respectively (Fig. 2a and Supplementary Figs. S4, S6, S8, S16, S30, S33, S34, S38, S39). We subdivided the normalized fluorescence of each recording (equation (1)) into N_a traces of at least 10 minutes of continuous active epochs, $F^i_{active}(t)$ for $i = 1, \ldots N_a$. At least 4 trace traces were used from each fly to obtain the normalized averaged fluorescence over active epochs, which was fitted with an exponential (Figs. 2b, 4b, and 5c, and left side in Supplementary Figs. S5a-e, S7a-e, S9a-e, S17a-d, S31a-d, S35a-h and S40a-g). The exponential was defined by the following equation:

$$\hat{F}_{active}(t) = A_{active}(1 - e^{-t/\tau_{active}}) + C_{active}. \tag{2}$$

Here, A_{active} is the saturation level, C_{active} is an offset, and τ_{active} is the time constant.

Fly	Sleep using ball velocity (stop) (% per hour)	Sleep using walk density (rest) (% per hour)	Sleep with 5 minutes threshold (% per hour)
1	50.0	49.1	18.7
2	56.8	51.5	28.8
3	68.1	61.0	33.6
4	70.8	51.6	30.4
5	57.6	46.0	19.1
6	76.4	61.2	31.0

Table S1. Percentage of time sleeping per hour for each fly according to the different definitions used in the paper.

Fluorescence traces for the rest state were similarly selected as epochs of at least 10 minutes. At least 4 normalized fluorescence traces were used to obtain the normalized average fluorescence over rest epochs, which was fitted with an exponential (Figs. 2c, 4b, and 5d, and right side in Supplementary Figs. S5a-e, S7a-e, S9a-e, S17a-d, S31a-d, S35a-h and S40a-g). The exponential was defined by the following equation:

$$\hat{F}_{rest}(t) = A_{rest} e^{-t/\tau_{rest}} + C_{rest}. \tag{3}$$

Here, A_{rest} is the amplitude, C_{rest} is an offset and τ_{rest} is the time constant of the decay. The time constants during active and rest states for activity in glia and in extracellular glutamate are shown in Figs. 2d and 4c.

Correlation between 'convolved walk' and calcium activity

To compare how glia calcium activity, glutamate, and R5 and dFB neurons integrate wake time in the different compartments, we first computed the convolution of the binary 'walk' state of the fly, $w(t)$ (assigned with a value of 1 for velocities higher than the threshold and 0 otherwise), with a temporal filter, $T_f(t)$. The temporal filter had a triangular shape (second row in Fig. 5h) defined by a filter size, s_f, as:

$$T_f(t) = \left[1 - \frac{1}{s_f} t\right]_+ \tag{4}$$

where $[\cdot]_+$ represents a threshold-linear function to ensure only positive values. The convolution between the 'walk' state and the triangular filter produced the 'convolved walk' (third row in Fig. 5h), which exponentially increased when the 'walk' state was 1 and exponentially decreased otherwise. The rate of increase and decrease was the same, defined by the filter size s_f. The 'convolved walk' can therefore be used to compute the Pearson correlation with the normalized fluorescence (as previously described, see equation (1)) for different filter sizes s_f. We used a total of 34 temporal filters, ranging from 0 to 60 minutes in steps of 6 minutes, and from 1 hour to 25 hours in steps of 1 hour. The average correlation for ensheathing glia in EB, FB, LAL, MB, and commissure is shown with colored lines in Fig. S21a, while the standard deviation of the correlation from each group is represented by semi-transparent colored regions around the average in Fig. S21a. Only filter sizes lower than 240 minutes were considered, as larger filter sizes produced close to zero correlation. We obtained the maximum value of the averaged correlation and its corresponding filter size (colored numbers in Fig. S21a) and assessed the statistical difference between these maxima using t-test. Statistical significance was indicated by asterisks in Fig. S21a (p-values < 0.05 represented by one asterisk, and p-values < 0.005 represented by two asterisks). The same analysis was performed for glutamate recordings, shown in Supplementary Fig. 5b, as well as for R5 and dFB neurons to compare with glia activity in the EB and FB (Fig. 5i).

Sleep deprivation

Sleep deprivation was performed for recordings in ensheathing glia in the EB and FB. Mechanical sleep deprivation was performed in a total of 5 flies between 3.6 and 8.2 hours, by opening and closing the air stream of the ball repeatedly 3 times for 6 seconds (alternating between 1 second closed and 1 second open) every 20 seconds. This

stimulated flies to walk and prevented sleep. Food deprivation was performed for a total of 4 flies between 4 and 16 hours. Individual recordings for both conditions are shown in Supplementary Fig. S15a and b, respectively, where exponentials were fitted for visualization (equation (2)).

For each fly, we computed the 'stop' state of the fly (zero velocity) in 1 second bins. We then averaged the 'stop' time for all flies over 1.5 hours before sleep deprivation and over 8 hours of sleep deprivation (left side, first row in Fig. 3b and d). We computed the average of the fluorescence in the EB and FB, which were first normalized through equation (1) (left side, second and third row in Fig. 3b and d, respectively). At least two flies were considered for the average over the sleep deprivation period. The average 'stop' time and fluorescence were also computed over 2 hours after sleep deprivation (right side in Fig. 3b and d). We then computed the distribution of the mean values of the normalized fluorescence in each fly over 1.5 hours before sleep deprivation, over the first 2 hours of sleep deprivation, after the first 2 hours of sleep deprivation, and over 2 hours after sleep deprivation (Fig. 3c and e). Statistical significance between these distributions was assessed using t-test (p-value < 0.05).

We also calculated the distribution of 'stop' time after 2 hours of sleep deprivation from the 'stop' state of each fly, as well as the duration of bouts of immobility that were larger than 5 minutes (Fig. 3f). For control flies, we used the recordings from Supplementary Fig. S4, which had identical conditions as sleep-deprived flies except for sleep deprivation. We then computed the distribution of 'stop' time over 2 hours at the time of the day when sleep deprivation finished for the sleep-deprived flies, as well as the distribution of sleep bout duration for all flies (Fig. 3f). Statistical difference between distributions was assessed again using t-test (p-value < 0.05).

Homeostat model

The homeostat model was fitted to activity of glia in the EB, FB, LAL, MB, and commissure, as well as activity of R5 neurons, and dFB neurons. For model fitting, fluorescence was filtered and normalized as described before (equation (1)). In the homeostat model we did not distinguish between immobility and sleep, but distinguished two behavioral states based on the fly's walking activity for charging and resetting of the homeostat, respectively: 'walk' and 'stop'. The homeostat model was fitted over the time range of each experiment, defined by $[T_{min}, T_{max}]$ for 'stop' and 'walk' periods of the fly. The 'stop' behavior of the fly, $s(t)$, was set to 1 when the velocity of the fly was below a threshold of (0.25 body lengths per second, to remove tracking noise level) and a value of 0 otherwise. Conversely, the 'walk' state of the fly, $w(t)$, was assigned a value of 1 for velocities higher than the threshold and 0 otherwise (top rows in Fig. 4e, Supplementary Figs. S18, S19, S20, S32, S33, S34, S44 and S45). The time resolution for distinguishing between 'stop' and 'walk' was 1 second. The following model was used for fitting:

$$\dot{h}_v(t) = s(t)\frac{1}{\tau_s}\Big(-h_v(t)+L(t)\Big) + w(t)\frac{1}{\tau_w}\Big(-h_v(t)+U(t)\Big). \tag{5}$$

Here, $h_v(t)$ describes the fluorescence signal ($\Delta F/F$) or homeostat, while $s(t)$ and $w(t)$ act as binary weights for each behavior. Therefore only one behavioral state contributes to the homeostat at any given time. τ_s and τ_w are the time constants for the stop and walk states, and $L(t)$ and $U(t)$ are functions that describe the lower and upper bounds of the homeostat, respectively (yellow lines in Fig. 4e, Supplementary Figs. S18, S19, S20, S32, S33, S34, S44 and S45). These bounds were allowed to vary with time to take into account slow modulations in fluorescence that are unavoidable during long-term imaging recordings, such as photobleaching, circadian modulation, or slow changes in calcium levels potentially due to phototoxicity. These changes affect both baseline levels as well as the dynamic range of fluorescence signals over time. Therefore these upper and lower bounds allowed to correct for dynamic range and baseline changes, and were defined as Bezier curves:

$$\begin{cases} U(t) = \sum_k^K C_k u_k \\ L(t) = \sum_k^K C_k l_k, \end{cases} \qquad \text{where} \quad C_k = \binom{K}{k}\left(\frac{T_{max}-t}{T_{max}-T_{min}}\right)^{K-k}\left(\frac{t-T_{min}}{T_{max}-T_{min}}\right)^{k} \tag{6}$$

These curves were fitted at the same time as the parameters of the model. The Bezier curves were parameterized by points separated by at least 6 hours, which defined the number of parameters K for each experiment as

$$K = \lfloor \frac{T_{max}-T_{min}}{6\,\text{hours}} \rfloor, \tag{7}$$

where $\lfloor \cdot \rfloor$ indicates the floor division operation. For each experiment we fitted the 2 time constants τ_s and τ_w, and the K upper and lower bound parameters, u_k and l_k:

$$\{\tau_s, \tau_w, u_1, ..., u_K, l_1, ..., l_k\}. \tag{8}$$

The fitting procedure is described in the next section. The fitted homeostat model for glia activity is shown in Fig. 4e and Supplementary Fig. S18 for EB and FB, S19 for LAL, and S20 for MB and commissure; for R5 neurons in Supplementary Figs. S32, S33 and S34; and for dFB neurons in Supplementary Figs. S44 and S45. All the fitted time constants for stop and walk and their estimated errors are shown on the left side of all the previous Supplementary Figs., and the combined time constants for glia are shown in Fig. 4f for EB and FB and Supplementary Fig. S21c for EB, FB, LAL, MB, and commissure, where asterisks show statistical significance (p-values lower than 0.05) between the walk and stop states in the EB (green) and FB (blue) using t-test.

Three-state homeostat model

This model was only fitted for glia activity in the EB and FB, where fluorescence was filtered and normalized as described before (equation (1)). In this model, we distinguished two states for resetting the homeostat: a 'stop' state where the fly was at rest (as assessed by ball velocity) for less than 5 minutes, and a sleep state, where the fly was at rest for epochs lasting more than 5 minutes.

$$f(t) = \{\text{Stop}(t), \text{Sleep}(t), \text{Walk}(t)\} \tag{9}$$

The following model was used for fitting:

$$\dot{h_s}(t) = \sum_i^{N_s} f_i(t) \frac{1}{\tau_i} \Big(-h_s(t) + F(w_i, t) \Big). \tag{10}$$

Here, $h_s(t)$ describes the fluorescence signal ($\Delta F/F$) or homeostat, and $f_i(t)$ acts as a mask for each state, and therefore only the assigned behavior contributes to the homeostat at any given time (similar to the 2-state model). τ_i is a time constant for each behavior i, and w_i is the weight with which each behavior contributes to the homeostat, -1 for 'stop' and 'sleep' states and +1 for 'wake'. F is a function that describes the upper and lower bounds of the homeostat,

$$F[w_i, t] = \begin{cases} U(t) & \text{if } w_i = 1 \\ L(t) & \text{if } w_i = -1, \end{cases} \tag{11}$$

where functions $U(t)$ and $L(t)$ are the upper and lower bounds defined in equation (6), similarly to the previous homeostat model.

For each model we fitted the N_s time constants τ_i and the K upper and lower bound parameters, u_k and l_k:

$$\{\tau_1, ..., \tau_{N_s}, u_1, ..., u_K, l_1, ..., l_k\} \tag{12}$$

An example of model fitting for glia activity in the EB and FB is shown in Supplementary Fig. S23a. The fitted time constants for each of the states, as well as their estimated errors in EB and FB, are shown in Supplementary Fig. S23b. The distribution of time constants for each state in the EB and FB is shown in Supplementary Fig. S23c. Only time constants with an estimated error lower than 0.2 times its fitted value were included to discard estimated time constants with high error. Asterisks in Supplementary Fig. S23c indicate statistical significance (p-values lower than 0.05) between different behaviors in EB (green) and FB (blue) using t-test.

We also asked if the homeostat would reset differently after 5 minutes of immobility. For this purpose, we defined a sleep state only after the fly was stopped for 5 minutes and fitted again equation 10. Supplementary Fig. S24a shows an example for glia activity in the EB and FB, together with the fitted time constants in Supplementary Fig. S24b. The distribution for time constants with an estimated error lower than 0.2 times its value are shown in Supplementary Fig. S24c for EB and FB. We did not find statistical significance between the time constants of the 'sleep' and 'stop' states using t-test.

Seven-state homeostat model

Activity of glia in the EB and FB, which was filtered and normalized as described before (equation (1)), was fitted to a homeostat model using the classified behaviors (an example is shown in the top row of Supplementary Fig. S25b. We fitted the dynamics of the homeostat with a model taking into account the $N_b = 7$ classified behaviors from the 3D CNN:

$$b(t) = \{\text{Stop}(t), \text{Proboscis}(t), \text{Walk}(t), \text{Discomfort}(t), \text{Grooming front}(t), \text{Grooming back}(t), \text{Feeding}(t)\}. \quad (13)$$

Each behavior, $b_i(t)$, was assigned a binary value, $b_i(t) \in \{0,1\}$, and only one behavior had value 1 at any given time, corresponding to the maximum class value predicted by the 3D CNN. The time resolution for the classification of behavior was 1 second.

We used the following model to fit the data:

$$\dot{h_b}(t) = \sum_{i}^{N_b} b_i(t) \frac{1}{\tau_i} \Big(-h_b(t) + F(w_i, t) \Big). \quad (14)$$

Here, $h_b(t)$ describes the fluorescence signal ($\Delta F/F$) or homeostat, and $b_i(t)$ acts as a mask for each behavior, and therefore only the assigned behavior contributes to the homeostat at any given time (similar to the 2-state model). τ_i is a time constant for each behavior i, and w_i is the weight with which each behavior contributes to the homeostat, which can take only two values: $w_i \in \{-1, 1\}$. When a weight is $w_i = -1$, the homeostat decreases while the fly performs the behavior, while with $w_i = 1$, the homeostat increases. F is a function that describes the upper and lower bounds of the homeostat, given by equation (11), similar to the previous 2- and 3-states model.

Fitting this differential equation requires determining for each behavior whether it charges or resets the homeostat, that is, contributes with a negative or positive weight to the model. To determine the weight of each behavior in the model, we used fluorescence traces from flies that performed one of the 7 behaviors for at least two consecutive imaging epochs (120 seconds). For 'discomfort' we used fluorescence traces recorded when the ball was stopped (Fig. 2e and Supplementary Fig. S10), since this behavior was not observed continuously for 120 seconds when the ball was free to rotate. For the rest of the behaviors, we used fluorescence traces from the recordings of ensheathing glia in 6 flies. For each behavior, all traces were aligned at the origin (thin lines in Fig. 4i for the EB and Supplementary Fig. S25a for the FB) and linear regression was used to determine the slope. If the slope was positive for a behavior, the weight was set to 1 and otherwise to -1 (negative slope, magenta lines in Fig. 4i). We repeated the same procedure for FB and found the same weights as in EB (Supplementary Fig. S25a). For each model we fitted the N_b time constants τ_i and the K upper and lower bound parameters, u_k and l_k:

$$\{\tau_1, ..., \tau_{N_b}, u_1, ..., u_K, l_1, ..., l_k\}. \quad (15)$$

Models were fitted independently to EB and FB data.

The fitting procedure is explained in the next section. Since some behaviors were very rare in some flies, the estimation error for model fitting was large for some of the time constants. Therefore only time constants with an estimated error lower than 0.2 times its fitted value were included in the distribution of the time constants for each behavior in Supplementary Fig. S26a. Asterisks in Supplementary Fig. S26a indicate statistical significance (p-values lower than 0.05) for behaviors in the EB (green) and FB (blue) using t-test.

Hunger-walk model

We analyzed the dynamics of dFB activity with respect to feeding by fitting exponentials (see below for a more detailed model). The average fluorescence traces were divided into two epochs, one where the fly was hungry (defined as 3.5 hours before feeding) and one where the fly was fed (defined as 30 minutes after feeding, see Fig. 6a, b, Supplementary Fig. S41, and Methods). The time constants during epochs where the fly was hungry were in the order of hours (Fig. 6c). The time constants for resetting after feeding were in the range of minutes, but they might not reflect the actual dynamics of dFB neurons after feeding since resetting depended also on the fly behavioral state (Fig. 5j-m).

For a more detailed model-based analysis, fluorescence traces were first filtered and normalized as described before (equation (1)). The model contained two different components that contributed differently: a hunger component, and a walk-stop component. The hunger component was fitted based on the time relative to the feeding events. We defined a "hungry" variable, hungry(t), defined as 0 between a feeding event and a time after feeding, called satiated time $t_{satiated}$, and as 1 after the satiated time and the next feeding event. Another variable, fed(t), was defined as 1 after feeding and before the satiated time, and as 0 otherwise. Therefore fed$(t) = 1 -$ hungry(t). The satiated time, $t_{satiated}$, interpreted as the time during which the hunger component resets and stays low, was fitted as a model parameter. The hunger component, h_{hunger}, was therefore fitted using the following differential equation:

$$\dot{h_{hunger}}(t) = \text{hunger}(t)\frac{1}{\tau_{hunger}}\Big(-h_{hunger}(t)+U(t)\Big)+\text{fed}(t)\frac{1}{\tau_{fed}}\Big(-h_{hunger}(t)+L(t)\Big). \tag{16}$$

Here, hungry(t) and fed(t) act as a mask and therefore only the assigned variable contributes to the hunger component at any given time (similar to the 2-state model). τ_{hungry} and τ_{fed} are the time constants that describe the increase and decrease of the hunger component, respectively. The hunger component and its parameters are shown in Fig. 6f. $U(t)$ and $L(t)$ represent the upper and lower bounds, defined in equation (6), which were fitted together with the parameters. The walk-stop component, $h_v(t)$, was defined as in the homeostat model (equation (5), but the upper and lower bouts were set constant, $U(t) = 1$ and $L(t) = 0$.

Finally, the hunger-walk model was defined as the weighted sum of the hunger and walk-stop components as follows:

$$h_{hunger-stop} = h_{hunger} + w_v h_v(t) \tag{17}$$

where w_v was a weight that indicated the contribution of the walk-stop component, which was also fitted. In summary, for this model we fitted the following 6 parameters,

$$\{\tau_{hungry}, \tau_{fed}, t_{satiated}, \tau_w, \tau_s, w_v\}, \tag{18}$$

as well as the parameters that defined the upper and lower bounds of the hunger component, u_k and l_k from equation (6). The fitting procedure is explained in the next section, and the fitted models are shown in Fig. 6g and Supplementary Figs. S46 and S47. The fitted time constants of all flies are shown in Fig. 6h, where only parameters with an estimated error lower than 0.2 times their fitted value were included. Asterisks in Supplementary Fig. 6h indicate statistical significance (p-values lower than 0.05) for behaviors in the EB (green) and FB (blue) using t-test.

Model fitting

Fitting of models was performed using the function *curve fit* in Scipy[79] in Python. Given a set of initial values of the parameters, we integrated each model with the corresponding equation, for example using equation 5 for the 2-state model, equation 10 for the 3-state model and equation 14 for the 7-state model, from their corresponding behavioral states ('stop', 'walk', ...) over the experiment timeline using Euler integration (with 1 second steps). Since the fluorescence data was not recorded continuously, we then interpolated the values of the model in agreement with the times of the recordings. Finally, we obtained an $L2$-error function between the interpolated model values and fluorescence data. The parameter values were updated iteratively from the Jacobian of the error function, and the minimum was found using the trust region reflective algorithm as optimization method.

To prevent parameters from taking forbidden values during optimization, we used parameter bounds. For the homeostat model, as well as the 3-state and 7-state homeostat models, the allowed range for time constants was $[0,2]$ hours. For the hunger-walk model, time constants in the range of $[0,2]$ hours were allowed, except for the time constant for "hungry", $_tau_{hungry}$, where the allowed range was [0, 6] hours. The allowed range for the weight w_v in the hunger model was [0,1], and the allowed range for the upper and lower bound parameters, u_k and l_k, were $[-1,0]$ and $[0,2]$ normalized $\Delta F/F$, respectively.

We computed the error or variance of each parameter from the covariance matrix between all parameters, which was returned by the function *curve fit*. This error indicated one standard deviation error of the parameter, obtained

Fly	L2 error in 2-state model (EB)	L2 error in 7-state model (EB)	F-statistic (EB)	p-value (EB)
1	3.479988	3.478012	0.32	0.9
2	3.063297	2.696925	70.74	1.1e-16
3	4.955734	4.186857	56.23	1.1e-16
4	4.281183	4.167001	13.01	1.6e-12
5	1.520076	1.658245	-40.54	1.0
6	11.306768	10.176129	61.61	1.1e-16

Table S2. Comparison between 2-state and 7-state models in the EB

as the square root of the corresponding diagonal element in the covariance matrix. In all models, parameters with errors lower than 0.2 times the magnitude of the fitted parameter were considered for distribution analysis (Fig. 4f, 1h and Supplementary Figs. S23, S24 and S26a).

Comparison between models

We asked whether the 7-state homeostat model fitted the glia activity better than the homeostat model. In this case, the homeostat model is a nested model, the 7-state homeostat model, which means that the homeostat model and its parameters are included in the 7-state homeostat model and parameters. We therefore asked if a null hypothesis holds, which establishes that the more complex (7-state homeostat) model does not fit fluorescence data significantly better than the simpler model (homeostat model). For this purpose we used a F-test[80].. Since the more complex model has different numbers of parameters than the simpler model, we can compute the F-statistic of the F-test, as:

$$\text{F-statistic} = \frac{(R_{simple} - R_{complex})/(N_{complex} - N_{simple})}{R_{complex}/(N_F - (N_{compex})}, \tag{19}$$

where R_{simple} and $R_{complex}$ are the residual sum of squares for the simpler and the more complex model, respectively (same as $L2$-error), N_{simple} and $N_{complex}$ are the number of parameters for the simpler and more complex model, respectively (in this case $N_{complex} - N_{homeostat} = 5$) and N_F is the number of fluorescence points that was used for fitting both models. The F-statistic value can then be used to generate a p-value, rejecting the null hypothesis stated above if it is lower than 0.05. If the null hypothesis is rejected, we can conclude that the more complex model fits the data significantly better than the simpler model.

The L2-errors between each pair of models for each fly in EB and FB are shown in Fig. S26b, while the L2-errors, F-statistic values, and p-values comparing each pair of models in EB and FB are shown in Tables S2, S3. This analysis concludes that the 7-state homeostat model provides a better fit for the glia data than the homeostat model.

We performed a similar analysis to compare the homeostat model with the hunger-walk model fitted to dFB neurons. As before, the homeostat model was a nested model of the hunger-walk model. We computed the F-statistic between the two models (being the homeostat model the simpler model, while the hunger-walk model is the more complex model) from equation 19 and obtained the corresponding p-values. The L2-errors between each pair of models fitted for each fly in shown in Fig. 6i, while the L2-errors, F-statistic values, and p-values are shown in Table S4. Since all the p-values were lower than 0.05, we conclude that the hunger-walk model fits the activity of dFB neurons better than the homeostat model.

Velocity modulation of glia activity

To assess the influence of fly velocity at short timescales in calcium activity of glia in the EB and FB, we computed the mean velocity of the fly during each 1 second imaging epoch, and used a high-pass filter to calculate fluorescence oscillations below periods of 0.5 hours. Supplementary Fig. S27a shows the mean velocity of fly 1 in each trial (black) as well as the high-pass filtered fluorescence in EB (green) and FB (blue). Each data point in Supplementary Fig. S27a was separated by the time difference between consecutive imaging recordings of 60 seconds. We computed the change in mean velocity and the change of ΔF/F in EB and FB between consecutive epochs, Supplementary

Fly	L2 error in 2-state model (FB)	L2 error in 7-state model (FB)	F-statistic (FB)	p-value (FB)
1	3.588580	3.246188	59.59	1.1e-16
2	0.784993	0.733569	36.50	1.1e-16
3	3.402890	2.818227	63.52	1.1e-16
4	1.604965	1.512774	28.95	1.1e-16
5	2.616210	2.554074	11.84	2.4e-11
6	5.747171	5.153419	63.90	1.1e-16

Table S3. Comparison between the 2-state and 7-state models in the FB

Fly	L2 error in homeostat model	L2 error in hunger-walk model	F-statistic	p-value
1	0.093624	0.041422	1395.11	1.110223e-16
2	0.131172	0.055818	790.07	1.110223e-16
3	0.084375	0.057946	233.75	1.110223e-16
4	0.075678	0.058143	90.18	1.110223e-16
5	0.101618	0.045378	635.48	1.110223e-16
6	0.065754	0.039686	84.41	1.110223e-16
7	0.066197	0.037298	498.03	1.110223e-16
8	0.101609	0.043907	1574.07	1.110223e-16

Table S4. Comparison between the homeostat model and hunger-walk model for dFB neurons

Fig. S27b-g. We fitted a linear regression (red line in Supplementary Fig. S27b-g) and computed the Pearson's correlation between the change in velocity and change in ΔF/F for the EB and FB, finding a positive correlation for each fly with p-values lower than 0.05 (see Fig. 4h and Table S5).

Comparison between activity of ensheathing glia and neurons

The dynamics of activity in ensheathing glia, R5, and dFB neurons were compared with respect to how well they described a sleep homeostat. For this, we used three different methods. In a first approach, we reasoned that a homeostatic signal should increase over active epochs, producing a positive correlation with the time during which the fly was active, and decrease over epochs of rest or sleep, thus producing a negative correlation with time spent resting or sleeping. We therefore computed the Pearson correlation between the averaged normalized traces over 30 minutes of active and rest epochs (Figs. 2b, c, 5c, d, Supplementary Figs. S5, S31, S35, and S40). We distinguished between the EB and FB neuropils and compared the distributions of correlation values in the EB between glia and R5 neurons and the distribution of correlation values in the FB between glia and dFB neurons (Fig. 5e, f). To assess whether the distributions of correlation values were statistically different we used t-test. Asterisks in Fig. 5e and f represent p-values lower than 0.05.

Alternatively, we compared the normalized average traces to a linear fit (Figs. 2b, c, 5c, d, Supplementary Figs. S5, S31, S35, and S40) during the first 30 minutes of rest and activity. The slope of this fit for each fly, shown in Fig. S48, represents how fast activity increases towards a maximum value during active epochs (Fig. S48, left side) and

Fly	Number of points	Pearson's correlation (EB)	Pearson's correlation (FB)	p-value (EB)	p-value (FB)
1	1664	0.46	0.37	5.3e-86	3.8e-56
2	1543	0.31	0.25	1.7e-35	4.5e-23
3	680	0.12	0.16	1.2e-03	3.8e-04
4	1065	0.61	0.44	2.1e-108	3.6e-51
5	1283	0.37	0.25	2.3e-43	1.0e-19
6	904	0.28	0.28	1.2e-17	2.9e-18

Table S5. Pearson's correlation between the changes in high frequency fluorescence fluctuations (change in ΔF/F) and changes in velocity.

how fast activity decreases during epochs of rest to baseline (Fig. S48, right side). Statistical differences of the slope distributions were again assessed using t-test and are represented by asterisks (p-value < 0.05) in Fig. S48. The slope for a homeostatic signal that increases and decreases linearly over 30 minutes of activity or rest should be 1 and -1, respectively. Glia activity was very close to these values (Fig. S48), while the slope for dFB neurons during rest was close to zero.

As a second approach, we calculated the $L2$-error of the homeostat model fitted for glia and R5 neurons. We again distinguished between neuropils and compared the $L2$-error of glia in the EB and of R5 neurons, as well as glia in the FB and dFB neurons (Fig. 5g). Statistical significance was assessed using t-test, where asterisks indicate that p-values were lower than 0.05.

As a third approach, we computed the Pearson correlation between the normalized fluorescence and the 'convolved walk' (third row in Fig. 5h) for different filter sizes (equation (4), as described previously. A total of 34 temporal filters were used, ranging from 0 to 60 minutes in steps of 6 minutes, and from 1 hour to 25 hours in steps of 1 hour. The average correlation for glia in the EB and R5 neurons, and for glia in the FB and dFB neurons, is shown with colored lines in Fig. 5i, while the standard deviation of the correlation from each group is represented by semi-transparent colored regions around the average in Fig. 5i. Filter sizes larger than 240 minutes are not shown, since they produced close to zero correlation. The maximum value of the averaged correlation was obtained together with its corresponding filter size (colored numbers in Fig. 5i). Statistical significance between these maxima was assessed using t-test, indicated by asterisks in Fig. 5i (p-values < 0.05).

Fitting of fluorescence traces during 'hungry' and 'fed' states

This analysis was only performed for dFB neurons and was similar to the analysis using active and rest epochs. We defined 'hunger' and 'fed' epochs to characterize the trend of activity of dFB neurons. Fed epochs were defined over the first 30 minutes after a feeding event, while hungry epochs were defined as starting 30 minutes after a feeding event and lasting until the next feeding. At least 4 normalized fluorescence traces were used to obtain the normalized average fluorescence over hungry or fed states, which was fitted with a rising exponential (equation (2)) or a resetting exponential (equation (3)), respectively (Fig. 6b and Supplementary Fig. S41). The time constants of the fitted exponentials are shown in Fig. 6c, where the asterisk indicates statistical significance (p-value < 0.05) using t-test.

Change in body size before and after feeding

This analysis was only performed for dFB neurons. We asked whether the reset of activity of dFB neurons was linked with how much food flies were ingesting at each feeding event. We therefore used the side view of the fly in the video recorded during the experiment 10 minutes before feeding and 10 minutes after feeding. Using color segmentation in OpenCV, we obtained a mask of the fly that only included the abdomen and the wings (Fig. 6d). We did not include the legs or the head in this mask, as flies could for example move the legs or extend the proboscis, producing an enlarged body size. We computed the area of the mask before and after feeding, A_{before} and A_{after}, respectively, and calculated the relative body size change between feeding events, ΔA_r, as follows:

$$\Delta A_r = \frac{A_{after} - A_{before}}{A_{before}} \tag{20}$$

The relative body size changes between feeding events were then compared to the corresponding differences in activity of dFB neurons before and after feeding. For this, we averaged the activity of dFB neurons over the last 10 minutes before a feeding event, $< F >_{before}$, and over the next 10 minutes after feeding, $< F >_{after}$, and obtained the difference, $< \Delta F > = < F >_{before} - < F >_{after}$. We obtained a total of 107 pairs of relative body size changes and fluorescence changes from 8 flies, shown in Fig. 6e. We computed the Pearson correlation between all pairs of points, as well as during the first half of the lowest relative body size changes (50% quantile) and the second half, shown in Table S6. While the correlation was positive and statistically significant (p-value < 0.05), this correlation was stronger for lower relative body size changes (Table S6).

	Correlation coefficient	p-value
All pair of points	-0.25	0.011
0% to 50% quantile in relative body size change	-0.56	1.57e-5
50% to 100% quantile in relative body size change	0.09	0.501

Table S6. Pearson correlation and p-values for the relative body size changes and changes in activity of dFB neurons before and after feeding events.

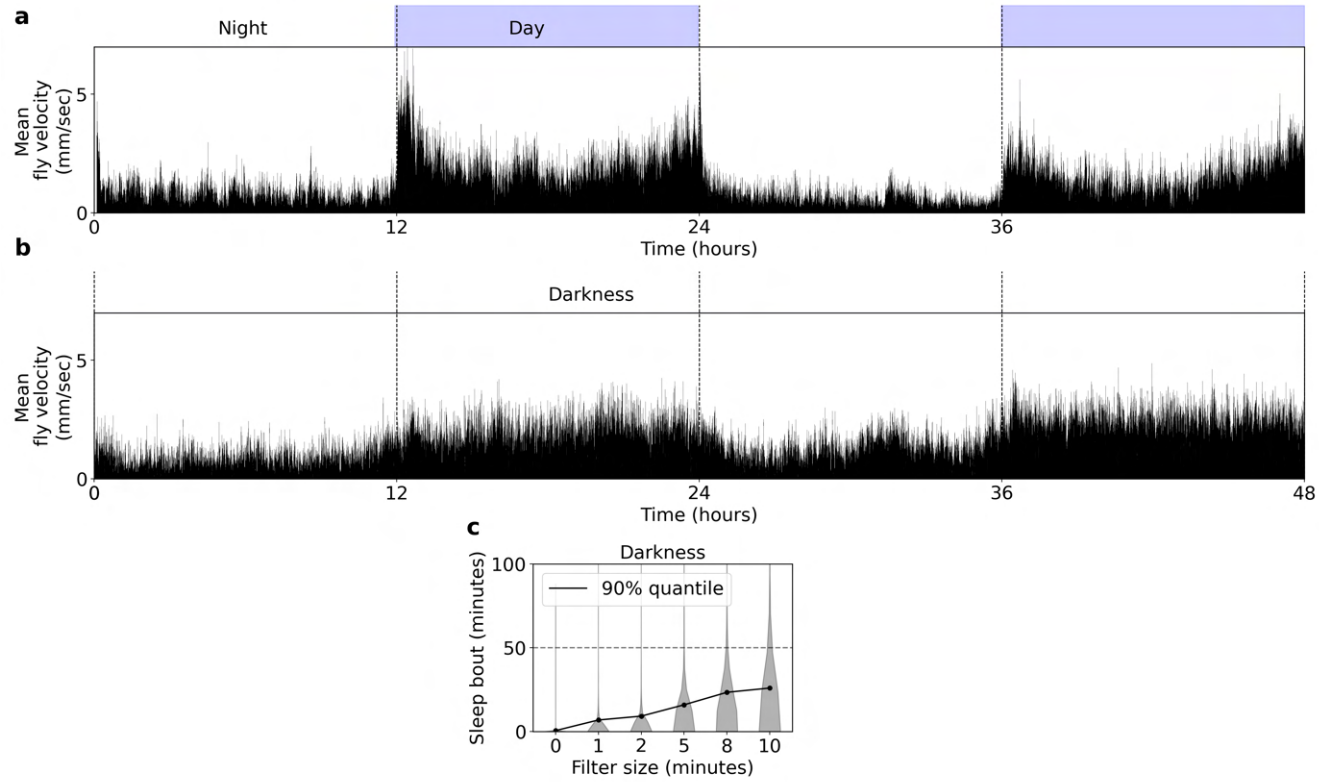

Figure S1. Behavioral activity of freely moving flies. **a** Mean fly velocity in 1 second bins over 48 hours with 12 hours of light (day) and 12 hours of darkness (night). **b** Same as in a, but in constant darkness. **c** Distribution of sleep bouts for a total of 15 flies in complete darkness (from b) as function of filter size.

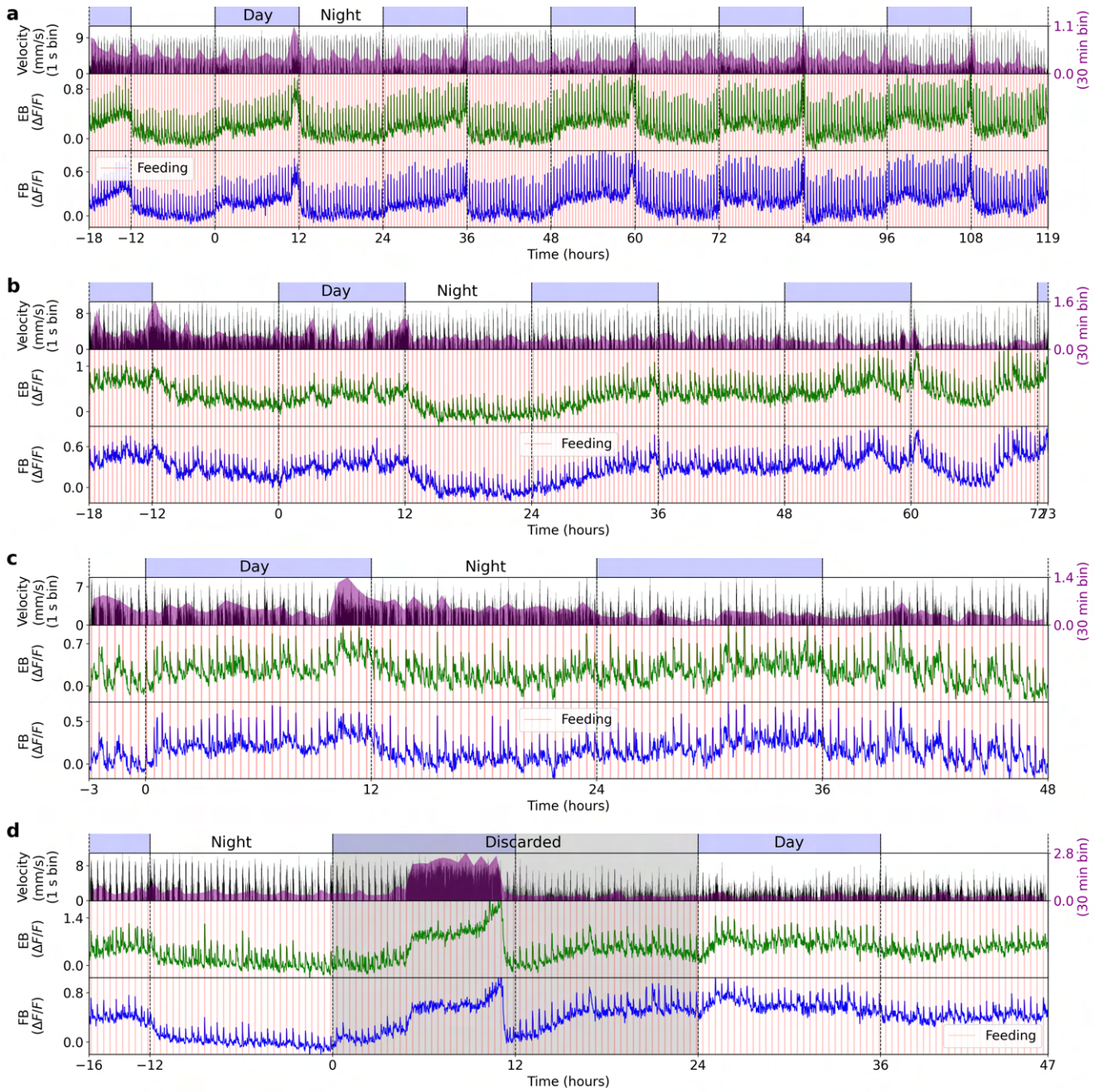

Figure S2. Four different recordings in ensheathing glia where flies are fed every 26 minutes. **a** Top row: day and night cycle in VR. Second row: in black, velocity of the fly in 1 second bins. Purple: velocity of the fly in 30 minutes bins. Third and fourth row: calcium activity of ensheathing glia in the EB (green) and FB (blue). Vertical red lines indicate feeding events. **b-d** Same as a. Each panel shows a different fly. In panel d, the grey area was discarded from the average in Fig. 6j, since there was an epoch of increased walking and calcium activity between hours 5 and 11. The reason for this increase during the recording is unknown but was likely due to an unexpected event during the recording such as a sudden increase in two-photon laser power or temperature. We also discarded the subsequent 12 hours of the experiment.

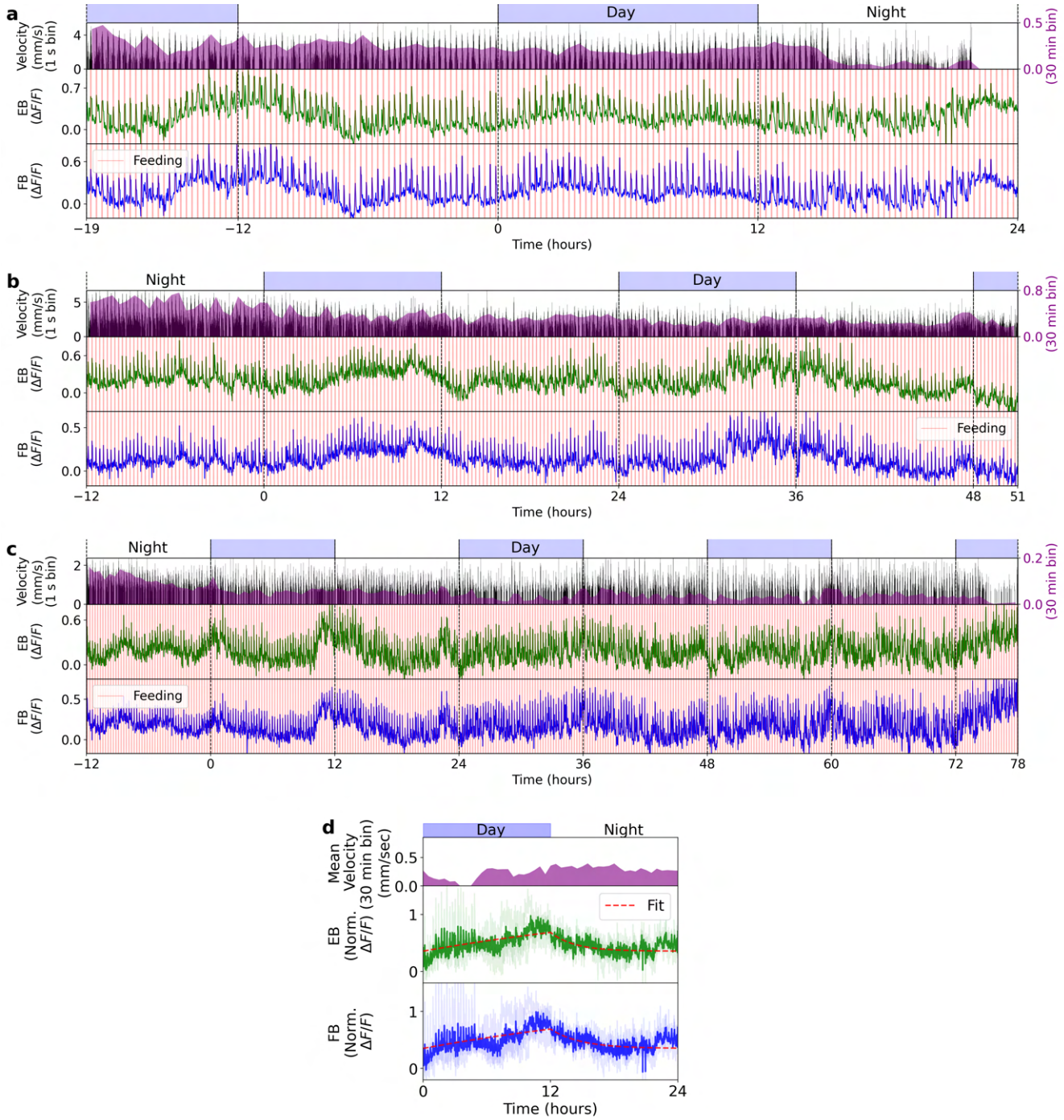

Figure S3. Three different long-term imaging recordings in ensheathing glia where flies are fed every 16 minutes. **a** Top row: day and night cycle in VR. Second row: in black, velocity of the fly in 1 second bins. Purple: velocity of the fly in 30 minutes bins. Third and fourth row: Calcium activity of ensheathing glia in the EB (green) and FB (blue), respectively. Vertical red lines indicate feeding events. **b, c** Same as a, but for different flies. **d** Average of previous recordings (in a, b, and c) with all trials aligned to one 24 hour period. Top row: day and night cycle. Second row: Mean velocity of all flies over 30 minutes bins. Third and fourth row: average glia activity in the EB (green) and FB (blue). Red lines indicate exponential fits during the day and night (see Methods).

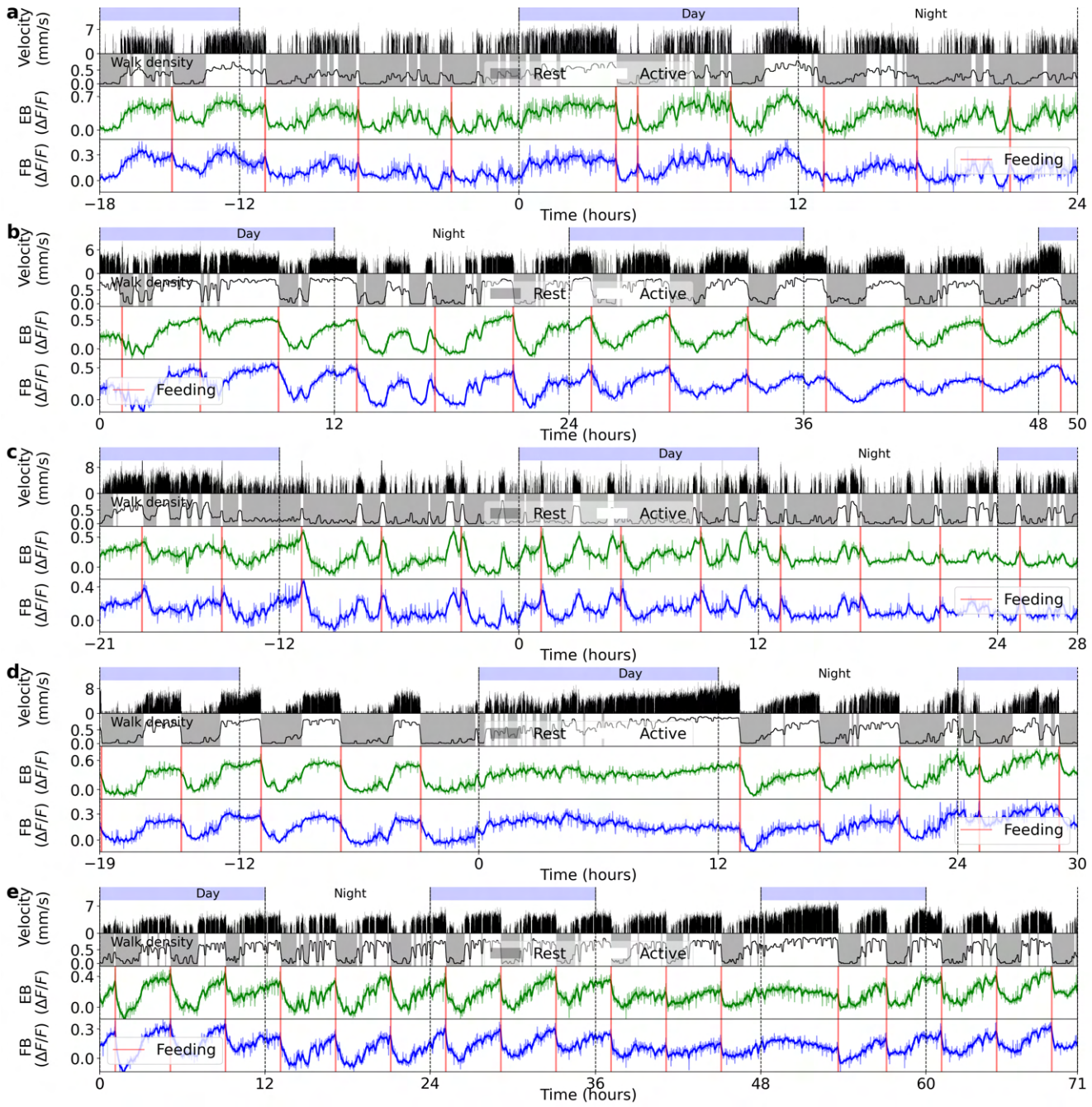

Figure S4. Five different recordings in ensheathing glia where flies are fed every 4 hours. **a** Top row: day and night cycle in VR. Second row: velocity of the fly in 1 second bins. Third row: walk density (see Methods) and rest (grey region) and active (white region) epochs. Fourth and fifth row: Calcium activity of ensheathing glia in the EB (green) and FB (blue), respectively. Thick lines indicate low-pass filter with a 0.1 hours cut-off period, while vertical red lines represent feeding events. **b-e** Same as a. Each panel shows different flies.

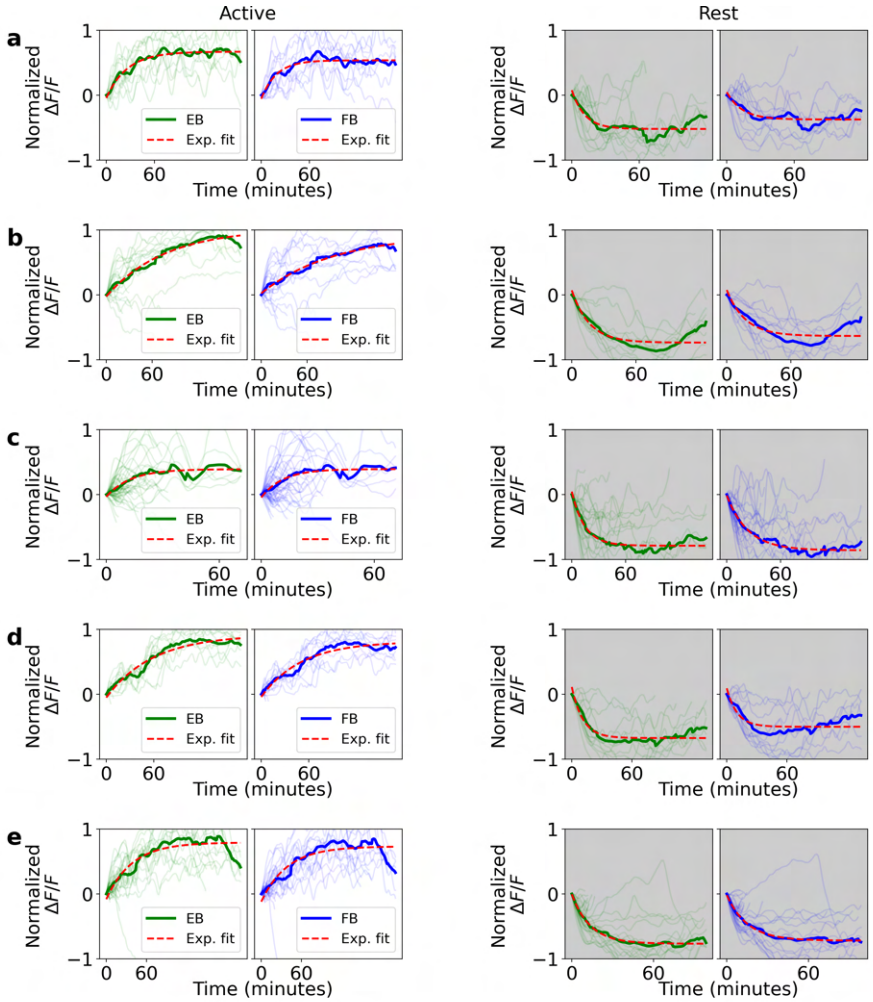

Figure S5. Normalized fluorescence traces during active and rest epochs for 5 flies. **a** Left side: single (thin lines) and average (thick lines) normalized fluorescence traces in the EB (green) and FB (blue) during active epochs. Red lines indicate exponential fit. Right side: same as left side, but during rest epochs. **b-e** Same as a. Each panel is from a different fly.

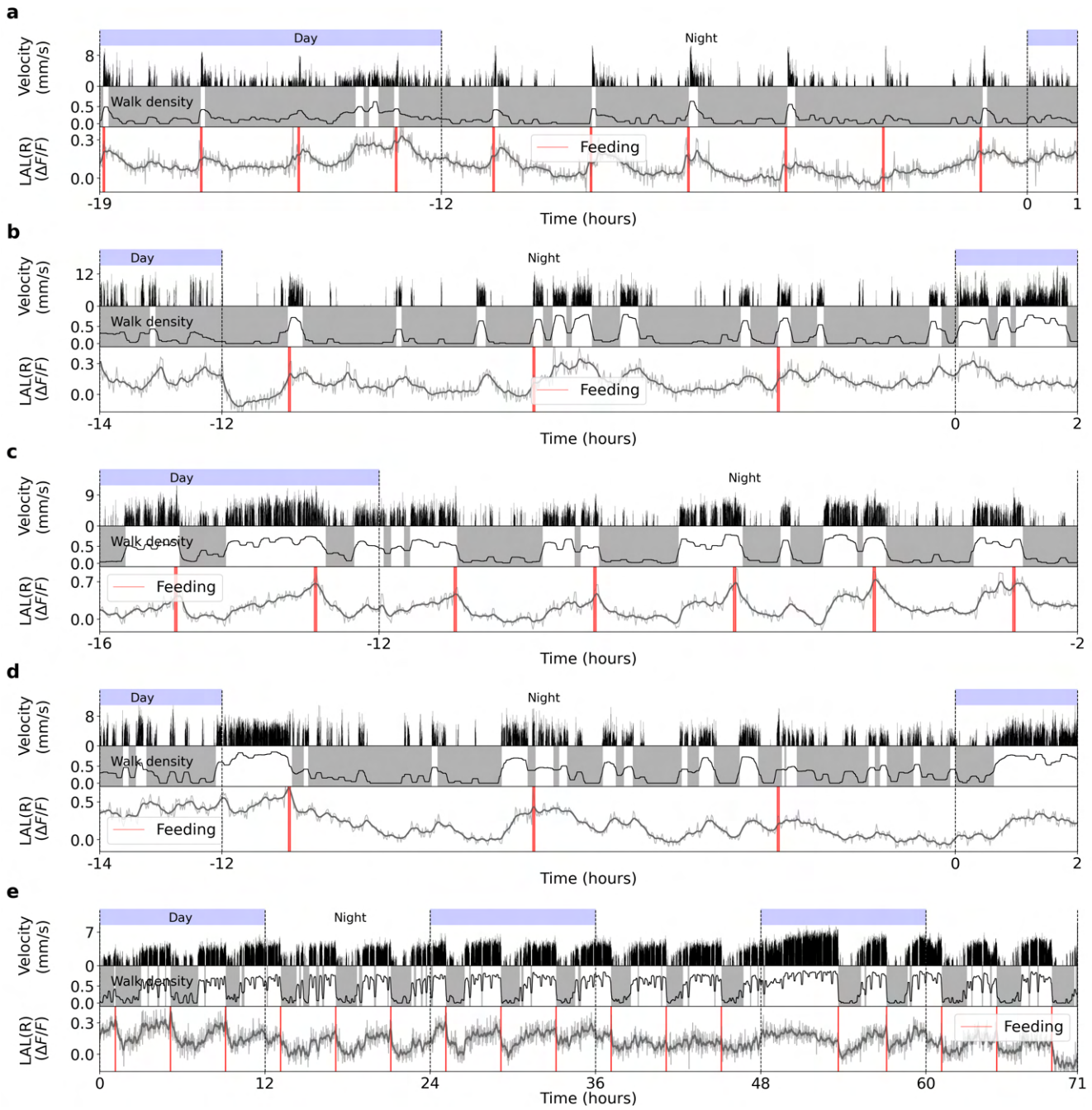

Figure S6. Ensheathing glia calcium activity in the LAL for 5 flies fed every 4 hours. **a** Top row: day and night cycle in VR. Second row: velocity of the fly in 1 second bins. Third row: walk density (see Methods) and rest (grey region) and active (white region) epochs. Fourth row: Calcium activity of ensheathing glia in the LAL (grey). Thick lines indicate a low-pass filter with 0.1 hour cut-off period, while vertical red lines represent feeding events. **b-e** Same as a. Each panel shows a different fly.

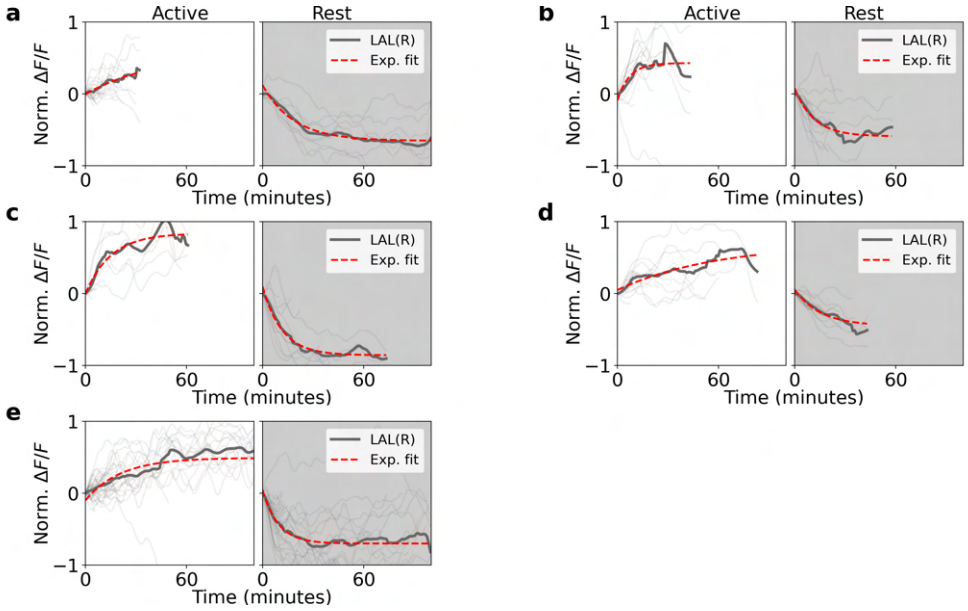

Figure S7. Normalized fluorescence traces during active and rest epochs for 5 flies. **a** Left side: single (thin lines) and average (thick lines) normalized fluorescence traces in the LAL (grey) during active epochs. Red lines indicate exponential fit. Right side: same as left side, but during rest epochs. **b-e** Same as a. Each panel is from a different fly.

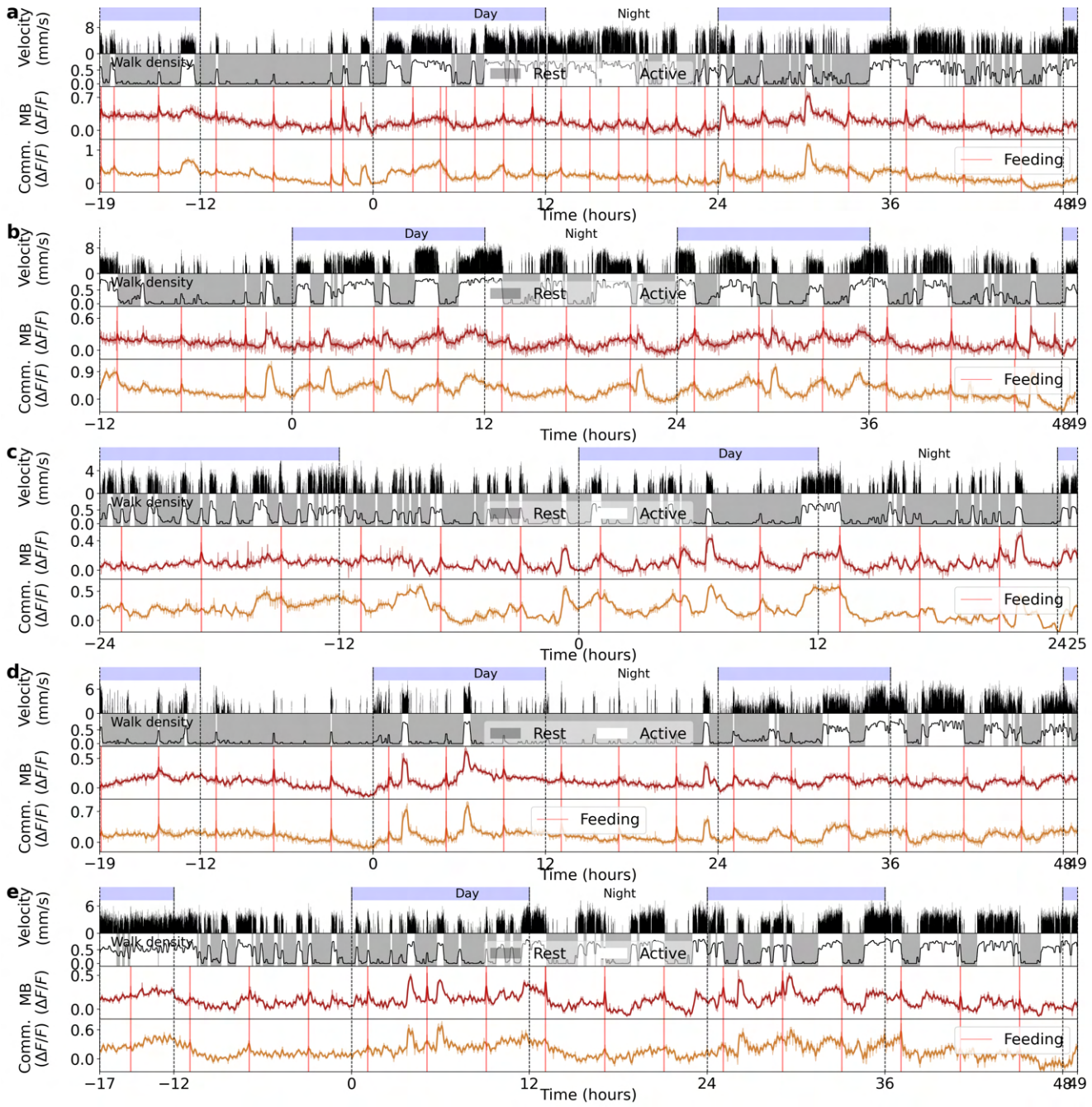

Figure S8. Ensheathing glia calcium activity in the MB and commissure for 5 flies fed every 4 hours. **a** Top row: day and night cycle in VR. Second row: velocity of the fly in 1 second bins. Third row: walk density (see Methods) and rest (grey region) and active (white region) epochs. Fourth and fifth row: Calcium activity of ensheathing glia in the MB (brown) and commissure (dark orange). Thick lines indicate a low-pass filter with 0.1 hour cut-off period, while vertical red lines represent feeding events. **b-e** Same as a. Each panel shows a different fly.

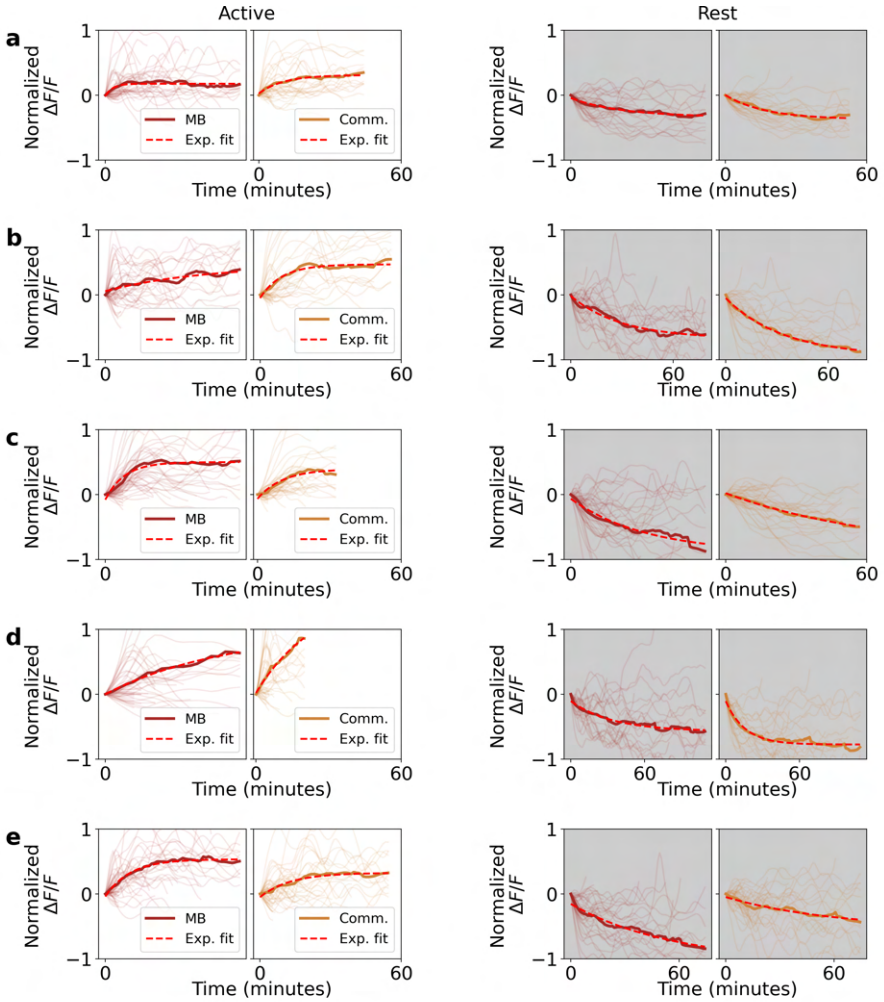

Figure S9. Normalized fluorescence traces during active and rest epochs for 5 flies. **a** Left side: single (thin lines) and average (thick lines) normalized fluorescence traces in the MB (brown) and commissure (dark orange) during active epochs. Red lines indicate exponential fit. Right side: same as left side, but during rest epochs. **b-e** Same as a. Each panel is from a different fly.

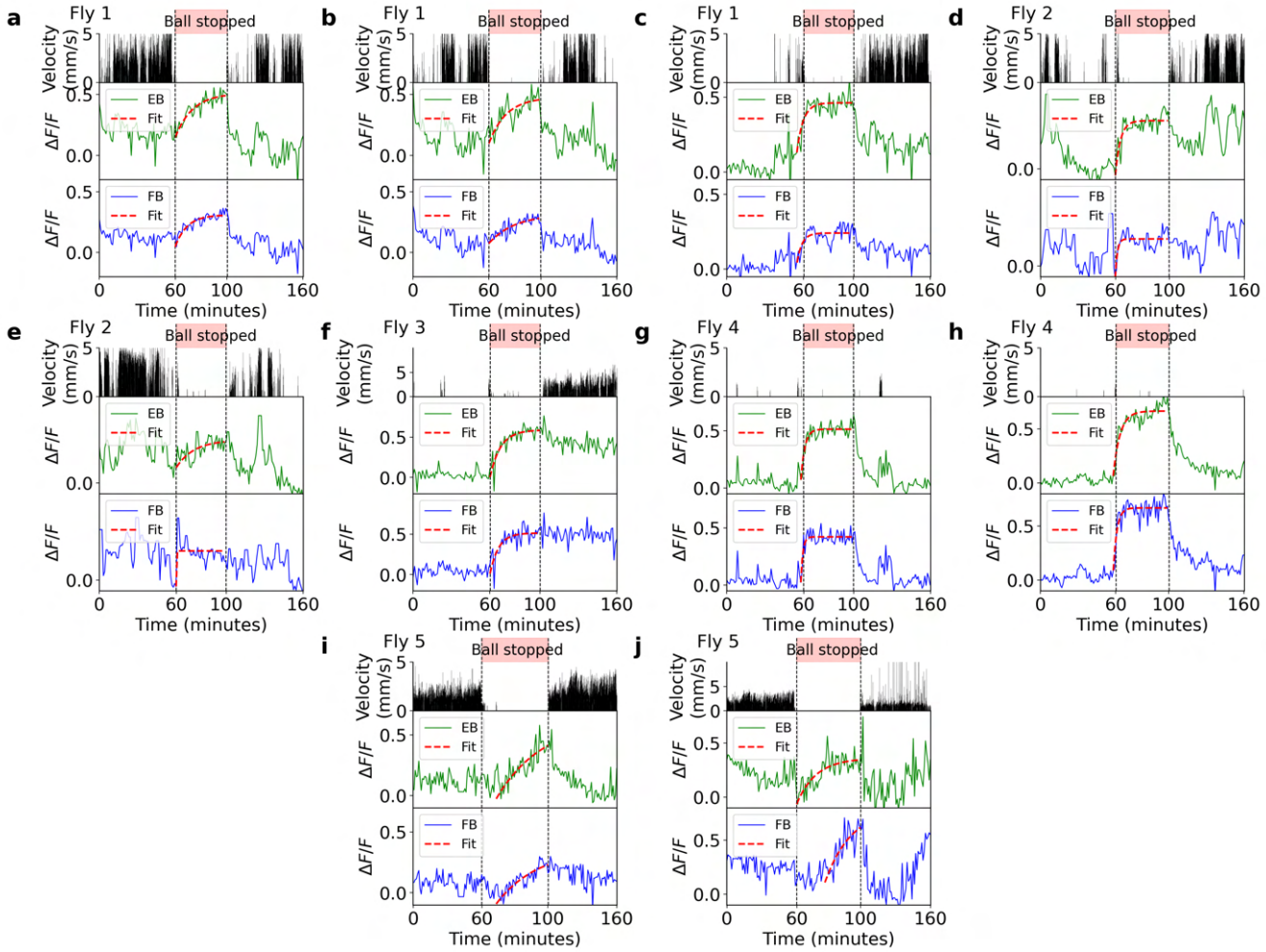

Figure S10. Trials where the ball was blocked during recordings in glia. **a** First row: time where the ball was stopped (red region). Second row: velocity of fly. Third and fourth row: Calcium activity of ensheathing glia in the EB (green) and FB (blue), respectively. Red lines are exponential fits. **b-j** Same as a. Each panel represents a different trial and the fly from which each trial was recorded is shown in the left top corner of each panel.

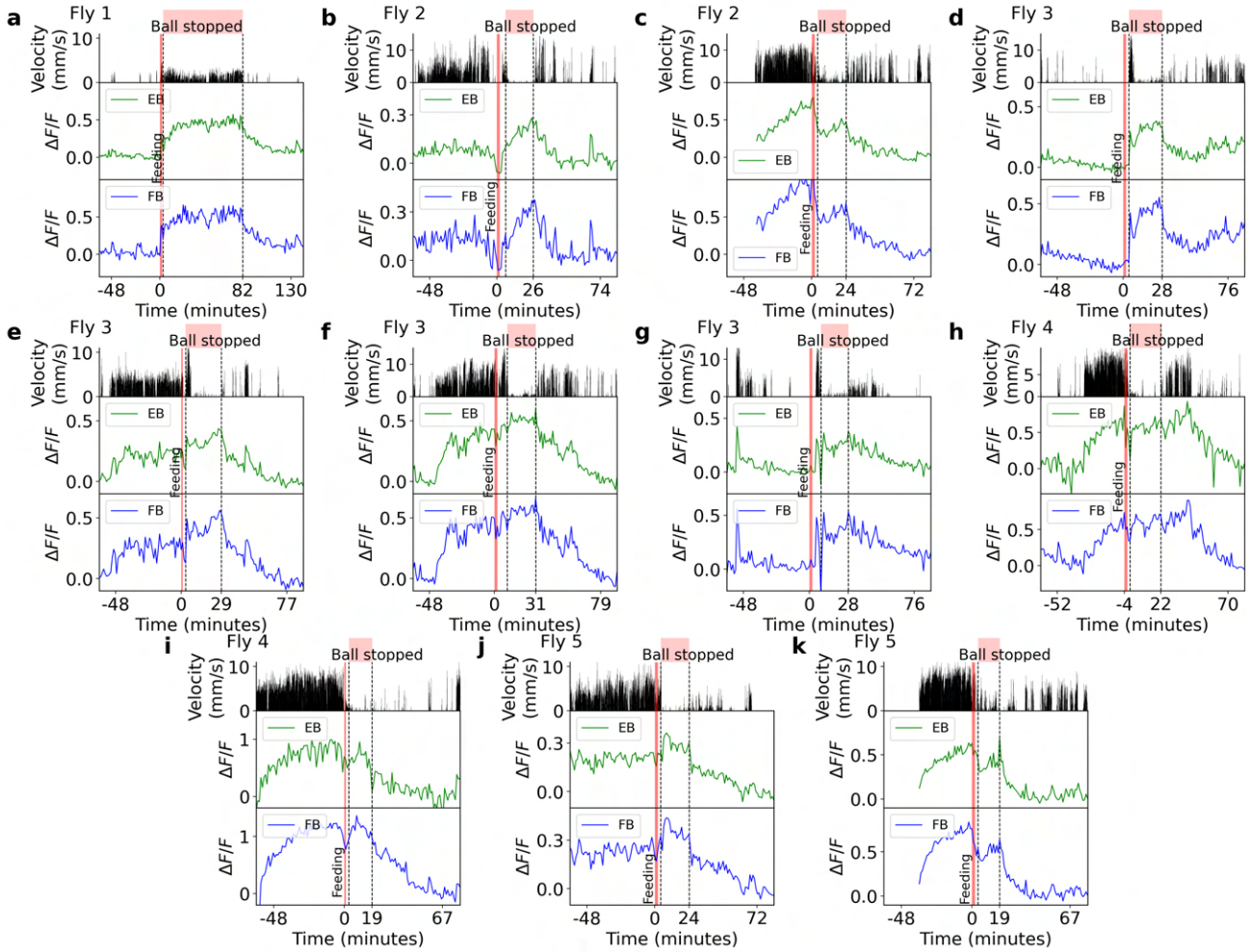

Figure S11. Trials where the ball was blocked after feeding while activity in glia was recorded. **a** First row: time where the ball was stopped (red region). Second row: velocity of the fly. Third and fourth row: Calcium activity of ensheathing glia in the EB (green) and FB (blue). The vertical red line indicates feeding. **b-k** Same as a. Each panel represents a different trial. The fly from which each trial was obtained is shown in the top left corner of each panel.

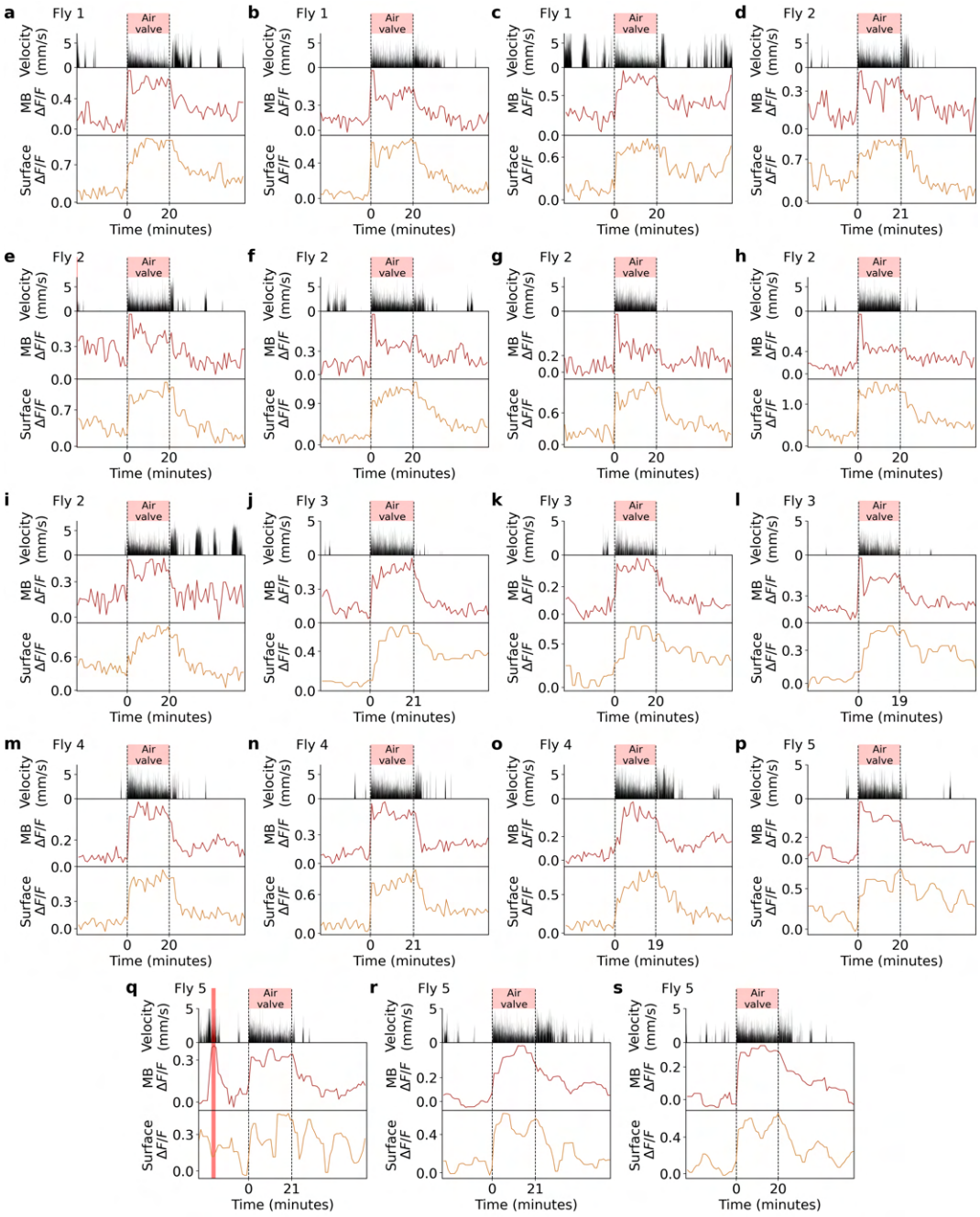

Figure S12. Trials where the air stream supporting the ball was intermittently opened and closed every second to promote walking behavior, while glia in the MB and commissure was recorded. **a** First row: time where the air stream of the ball was intermittently interrupted (red region). Second row: velocity of the fly. Third and fourth row: calcium activity of ensheathing glia in the MB (brown) and commissure (dark orange). Vertical red lines indicates feeding events. **b-s** Same as a. Each panel represents a different trial from a total of 5 flies. The fly from which each trial was obtained is shown in the top left corner of each panel.

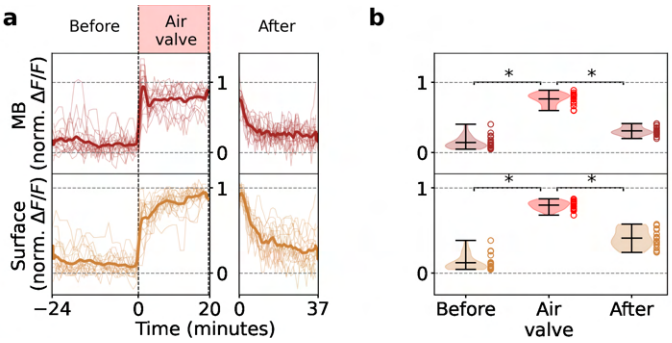

Figure S13. Glia activity in MB and commissure increases with walking behavior. **a** Normalized fluorescence traces from the MB (brown) and commissure (dark orange) from all the trials (thin lines, see Extended Fig. S12) before, during, and after the air valve was used to promote walking. Thick lines indicate the average normalized fluorescence of all trials. **b** Distribution of the mean fluorescence levels of all trials before, during, and after the air valve perturbation. Asterisks indicate statistical significance using t-test ($p < 0.05$).

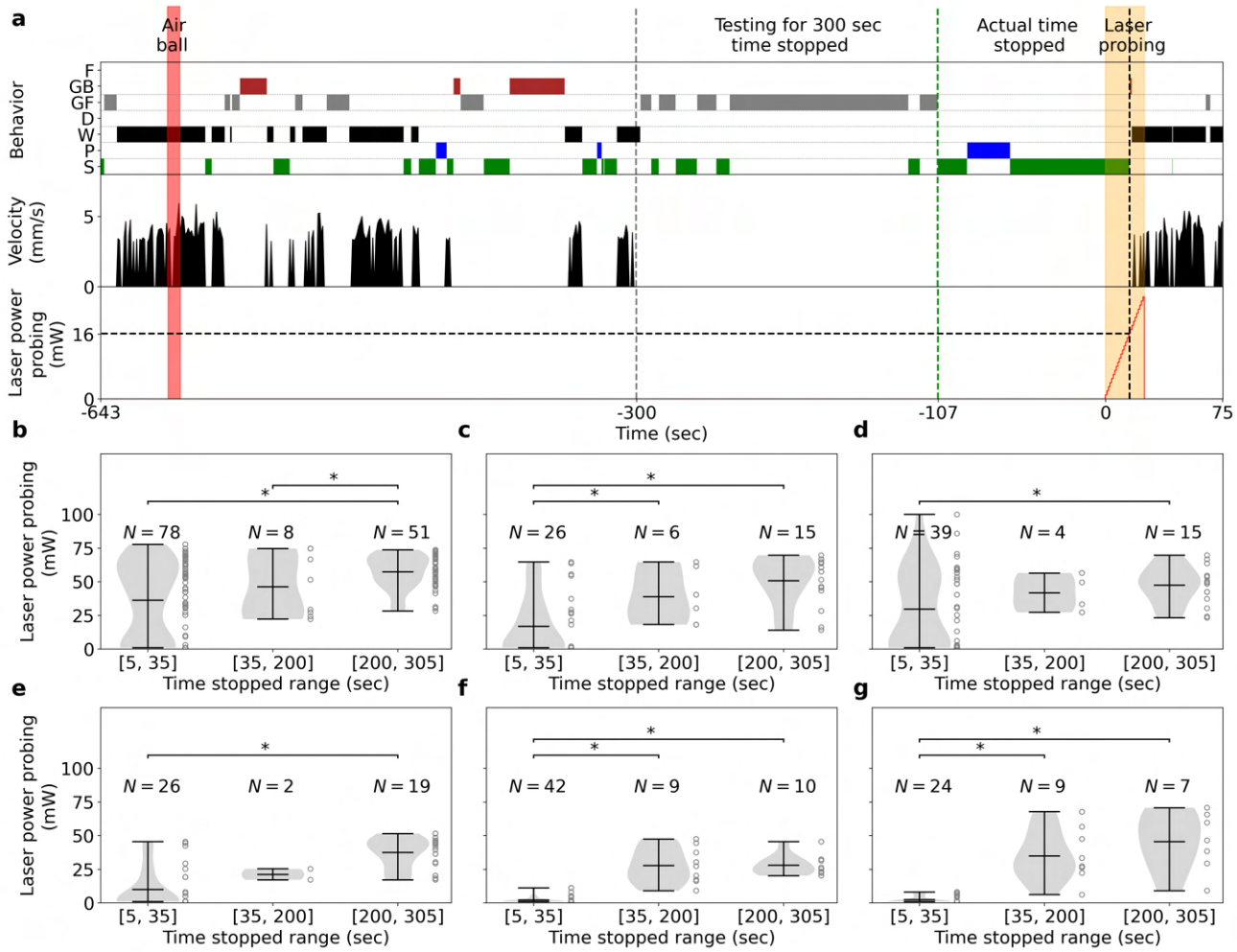

Figure S14. **a** Example of trial protocol for testing arousal threshold after 300 seconds of immobility of a fly on the ball. First, the air ball is switched on and off (red area) to ensure the fly is awake. The fly stops walking for 300 seconds (fly velocity is zero in second row) and the laser (third row) starts probing the arousal threshold of the fly by increasing its power every 0.5 seconds (orange area). The laser is switched off when the fly starts walking again (velocity higher than 0). Post processing: behavior classification (first row) is used to compute the actual time fly was immobile, without grooming (107 seconds in this trial), as well as the actual laser power the fly reacts to by grooming, discomfort, or walking during laser probing (16 mW in this trial). **b,c,d,e,f,g** Distribution of laser powers at which fly wakes up for all trials for different durations of immobility for 6 flies. Asterisks indicate statistical significance using t-test (p-value lower than 0.05).

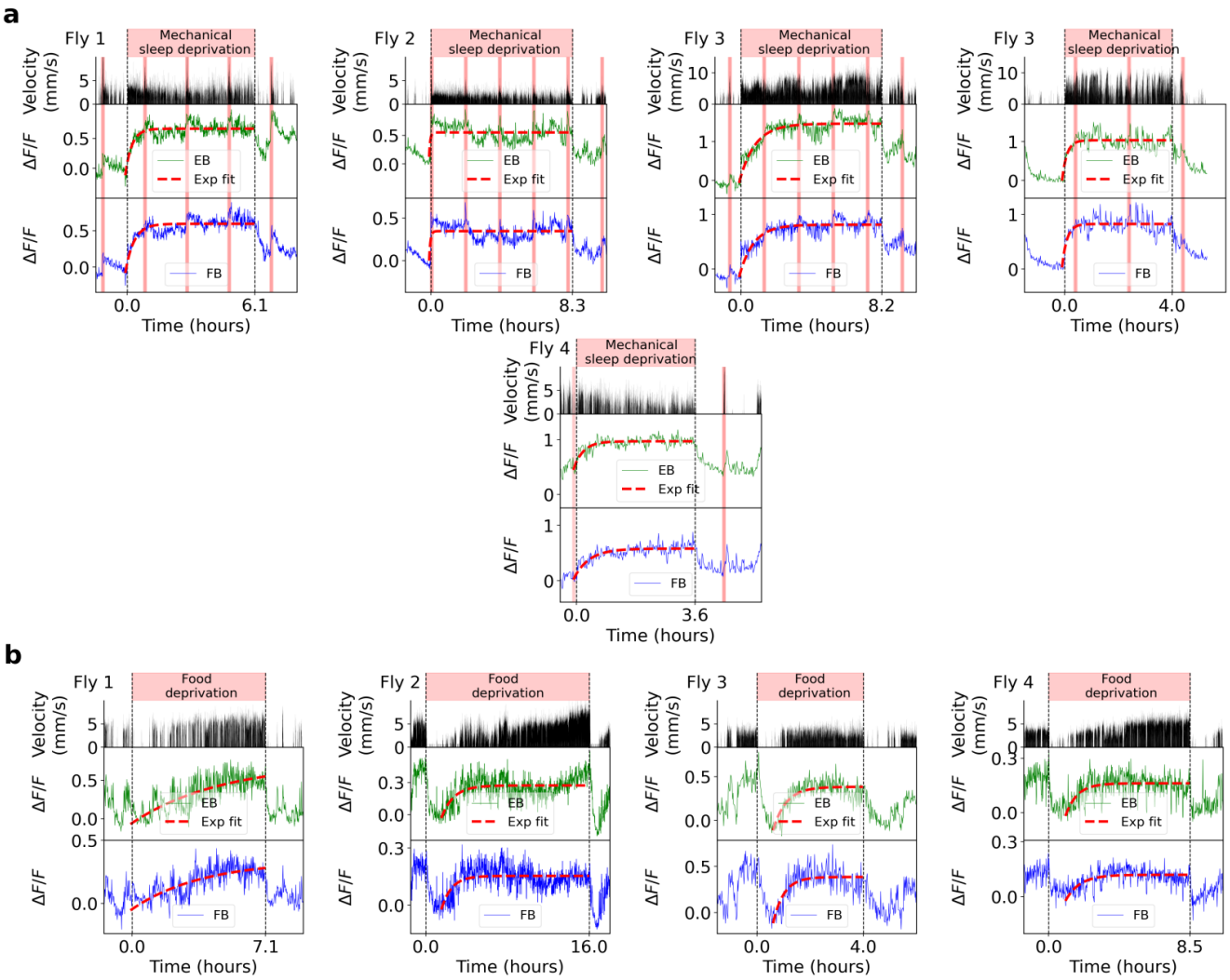

Figure S15. Glia activity during mechanical sleep deprivation (a) and food deprivation (b) in each trial. **a** Each panel shows the velocity over time (second row), and glia activity in EB (third row) and FB (fourth row) during mechanical sleep deprivation (first row) for 5 trials. Vertical red lines indicate feeding events and exponential fits (red) are shown for visualization of saturation levels. The fly from which each trial was obtained is indicated in the top left corner of each panel. **b** Same as a, but during food deprivation, with a different set of flies.

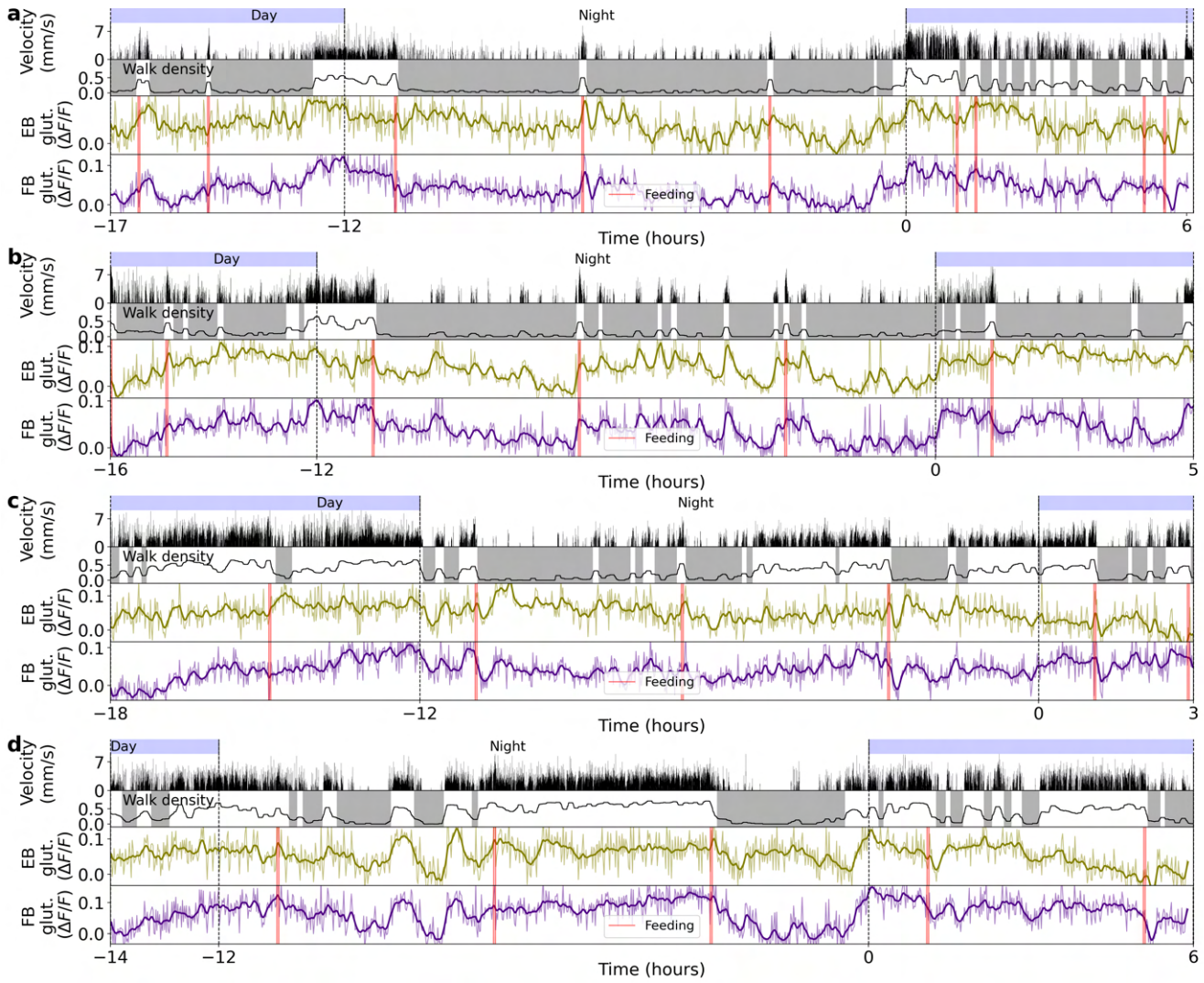

Figure S16. Four different recordings using the glutamate sensor iGluSnFR expressed in ensheathing glia. **a** Top row: day and night cycle in VR. Second row: velocity of the fly in 1 second bins. Third row: walk density (see Methods) and rest (grey region) and active (white region) epochs. Fourth and fifth row: Calcium activity of ensheathing glia in EB (green) and FB (blue). Thick lines indicate a low-pass filter with a 0.1 hours cut-off period. Vertical red lines represent feeding events. **b-d** Same as a. Each panel shows a different fly.

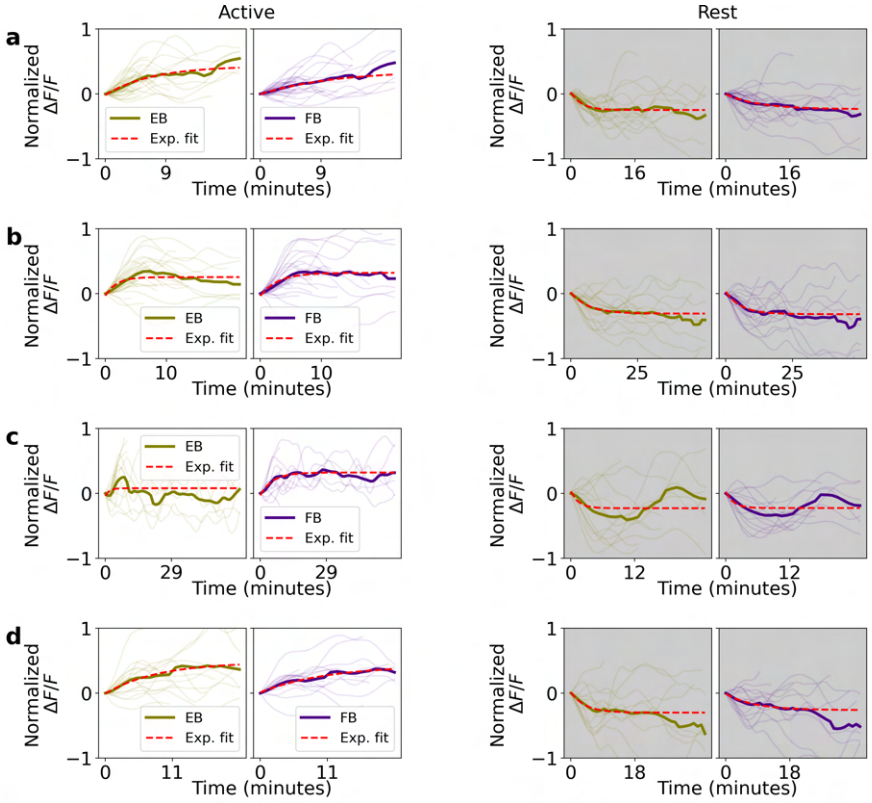

Figure S17. Normalized fluorescence traces recorded with glutamate sensor during active and rest epochs for 4 flies. **a** Left side: single (thin lines) and average (thick lines) normalized fluorescence traces in EB (olive) and FB (indigo) during active epochs. Red lines indicate exponential fit. Right side: same as left side, but during rest epochs. **b-d** Same as a. Each panel is from a different fly.

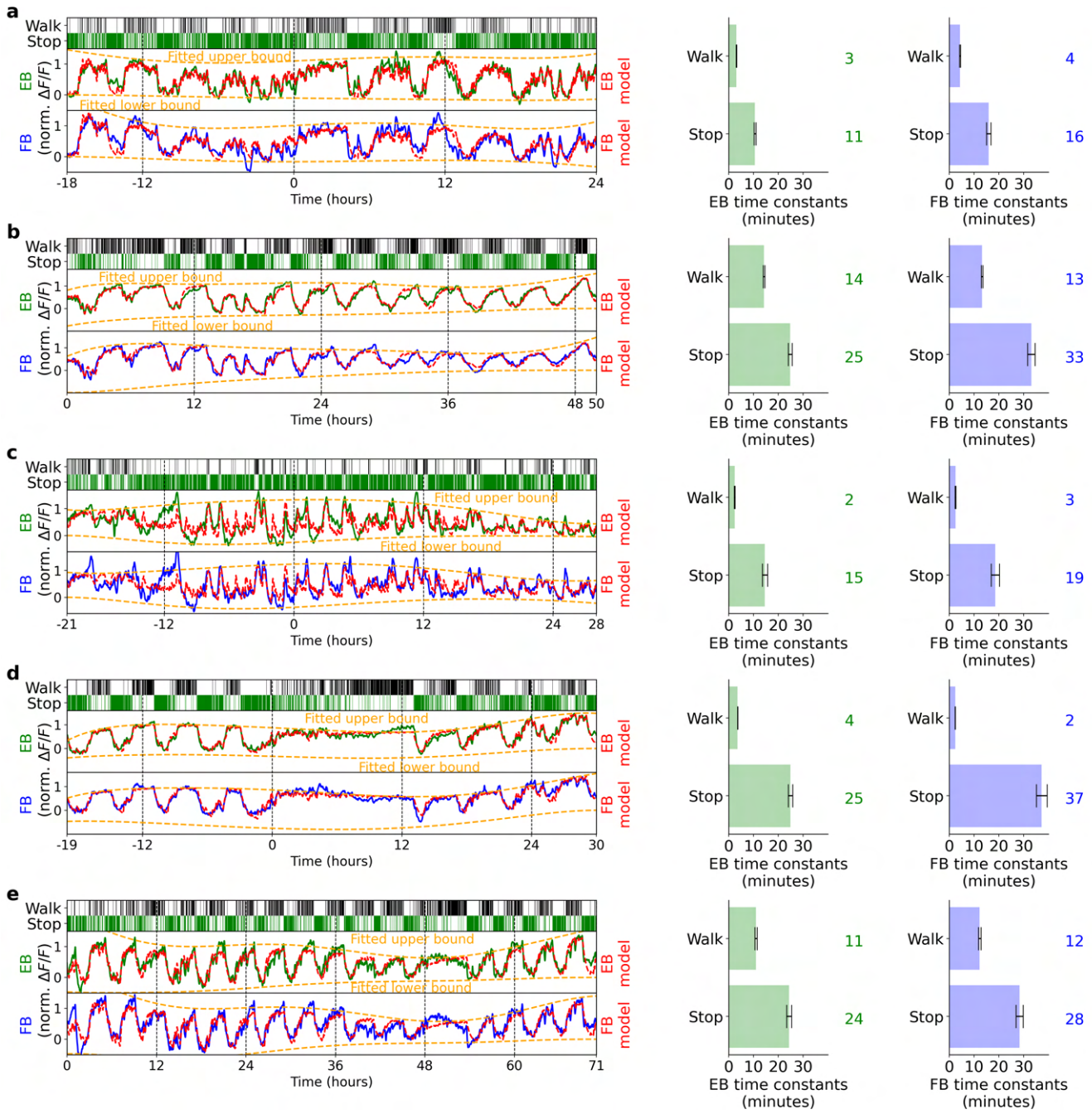

Figure S18. Fitting glia activity in EB and FB with homeostat 2-state model. **a** Left side: top row shows walking and stopping bouts of a fly. Second and third row: Normalized fluorescence in the EB (green) and FB (blue). Red lines show fitted model, while orange lines represent fitted upper and lower bounds of the model. Right side: fitted time constants from EB (green) and FB activity (blue). Grey lines indicate error bars of estimated time constants (see Methods). Green and blue numbers show rounded value of the fitted time constants. **b-e** Same as a. Each panel represents a fitted model for each fly.

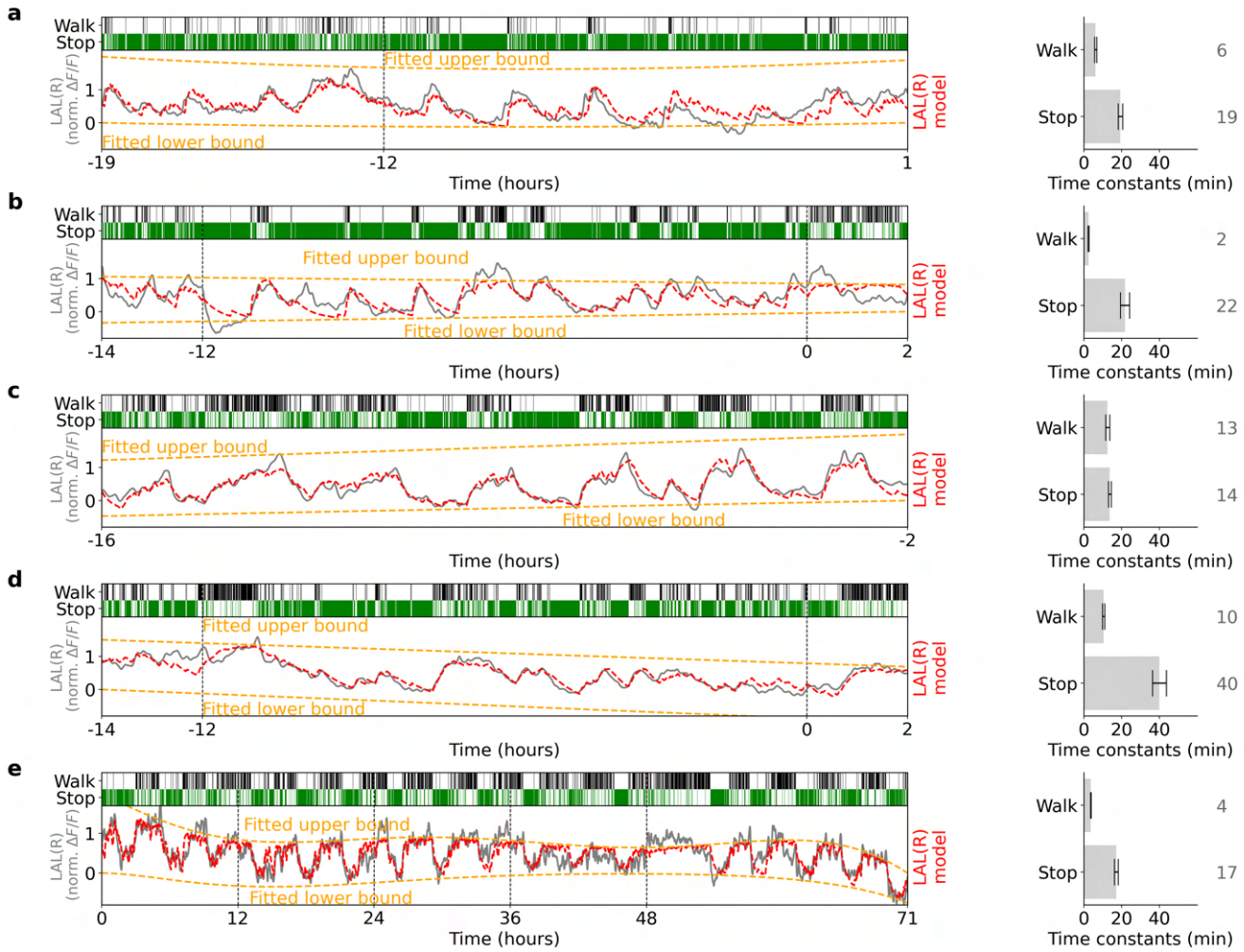

Figure S19. Fitting glia activity in the right LAL with homeostat 2-state model. **a** Left side: top row shows walking and stopping bouts of a fly. Second and third row: Normalized fluorescence in the LAL (grey). Red lines show fitted model, while orange lines represent fitted upper and lower bounds of the model. Right side: fitted time constants in LAL (grey). Grey lines indicate error bars of estimated time constants (see Methods). Grey numbers show rounded value of fitted time constants. **b-e** Same as a. Each panel represents a fitted model for each fly.

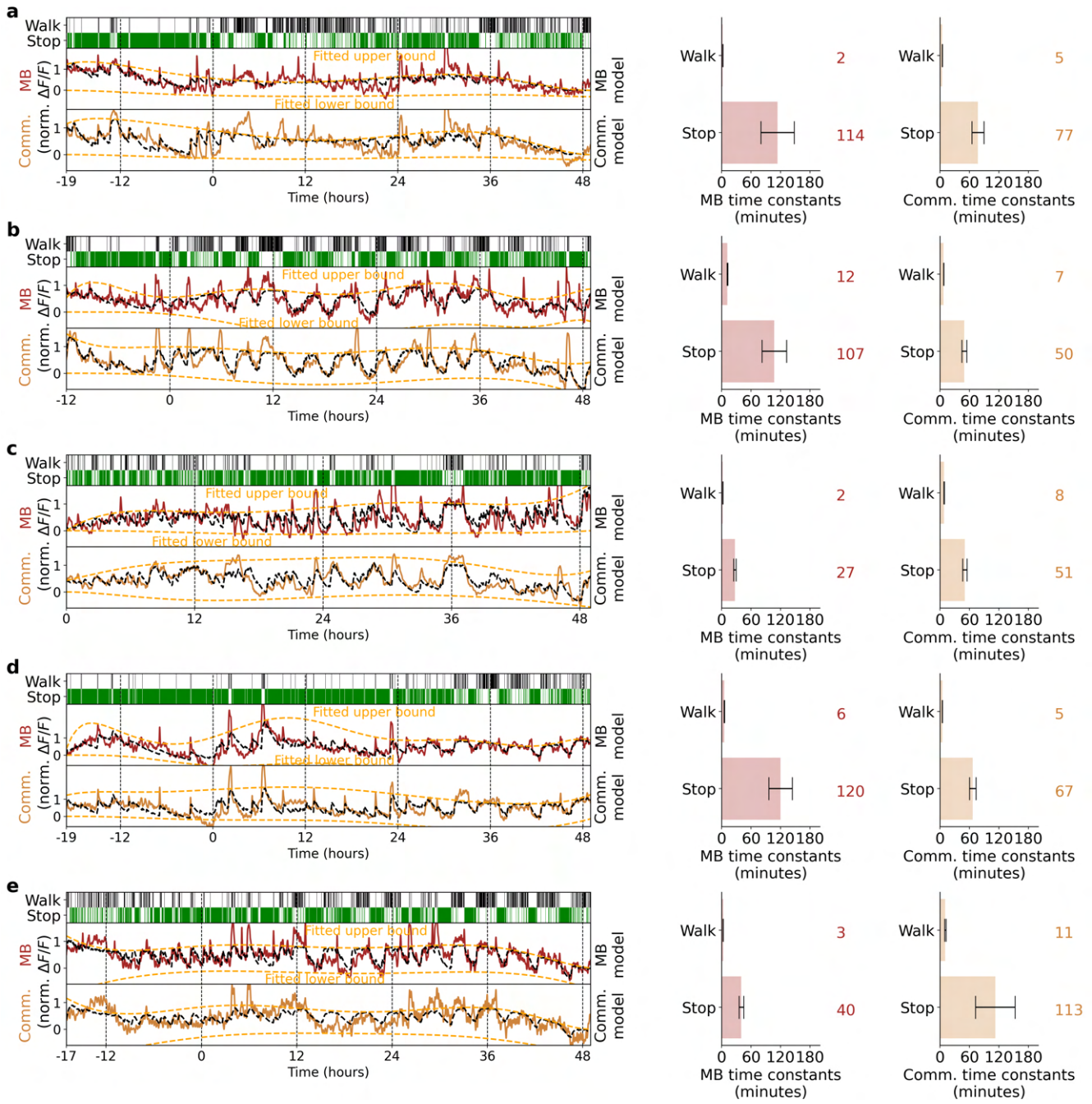

Figure S20. Fitting glia activity in MB and commissure with homeostat 2-state model. **a** Left side: top row shows walking and stopping bouts of a fly. Second and third row: Normalized fluorescence in MB (brown) and commissure (dark orange). Black lines show fitted model, while orange lines represent fitted upper and lower bounds of the model. Right side: fitted time constants in MB (brown) and commissure activity (dark orange). Grey lines indicate error bars of estimated time constants (see Methods). Brown and dark orange numbers show rounded value of the fitted time constants. **b-e** Same as a. Each panel represents a fitted model for each fly.

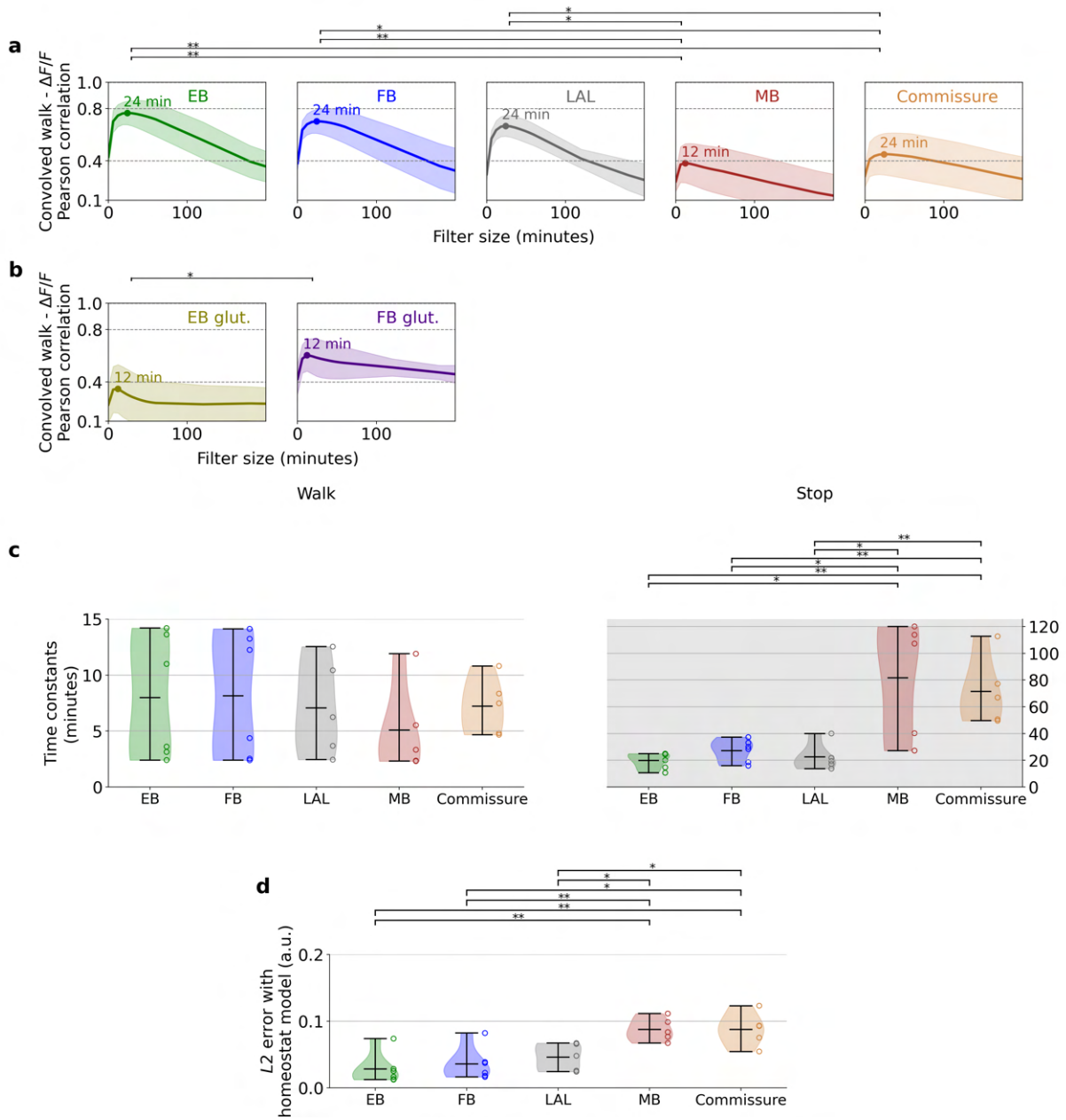

Figure S21. Comparison between glia activity in different neuropils and glutamate activity in the central complex **i** Pearson correlation between 'convolved walk' and glia calcium activity in different neuropils for different filter sizes (x-axis) (see Fig. 5h for concept, and Methods). Thick-colored lines represent average of correlation curves, while light-colored areas represent standard deviation for all flies ($N = 6$ flies for EB and FB, and $N = 5$ flies for LAL, MB, and commissure). Colored numbers indicate filter size at maximum correlation value in minutes. **b** Same as a, but for glutamate activity in the EB and FB ($N = 5$ flies). **c** Distributions of time constants for 'stop' and 'walk' states from model fitting ($N = 6$ flies in EB and FB, and $N = 5$ flies in LAL, MB, and commissure). **d** $L2$ error between normalized fluorescence and the corresponding fitted homeostat 2-state model ($N = 6$ flies in EB and FB, and $N = 5$ flies in LAL, MB, and commissure). Asterisks in each panel represent statistical significance using t-test (one asterisk for p-values < 0.05 and two asterisks for p-values < 0.005).

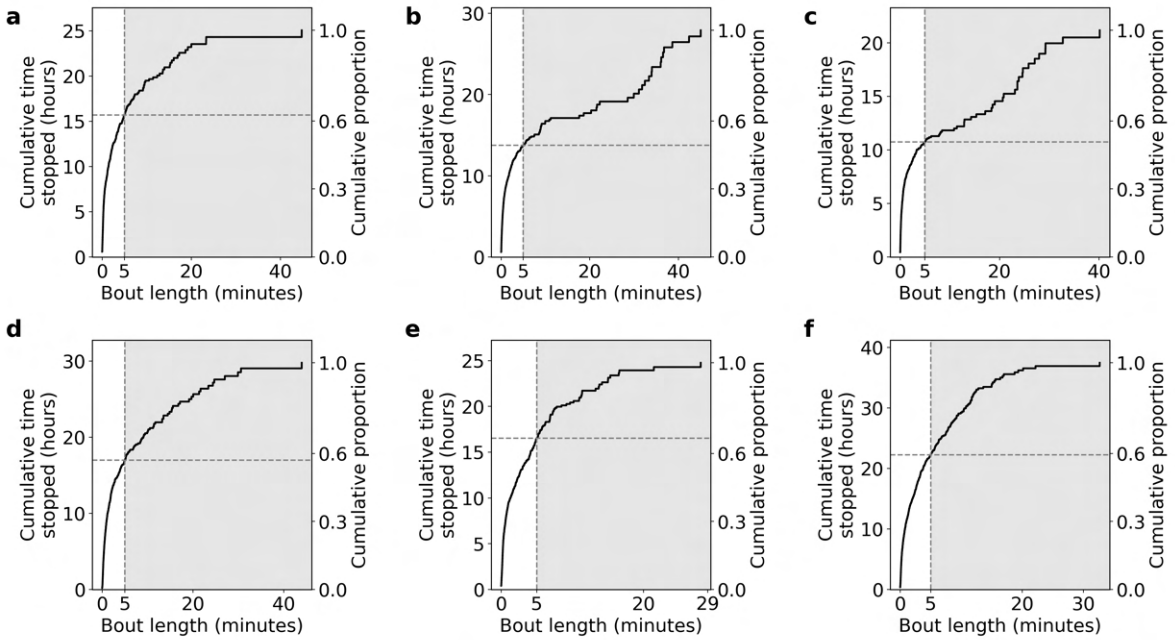

Figure S22. Cumulative time that each fly stops (left y-axis) and corresponding proportion over the total stop time (right y-axis) as a function of the stop duration (**a**-**f** correspond to flies 1-6). Bouts where the fly stops for less than 5 minutes (white background) correspond to around 0.6 of the total stop time across flies.

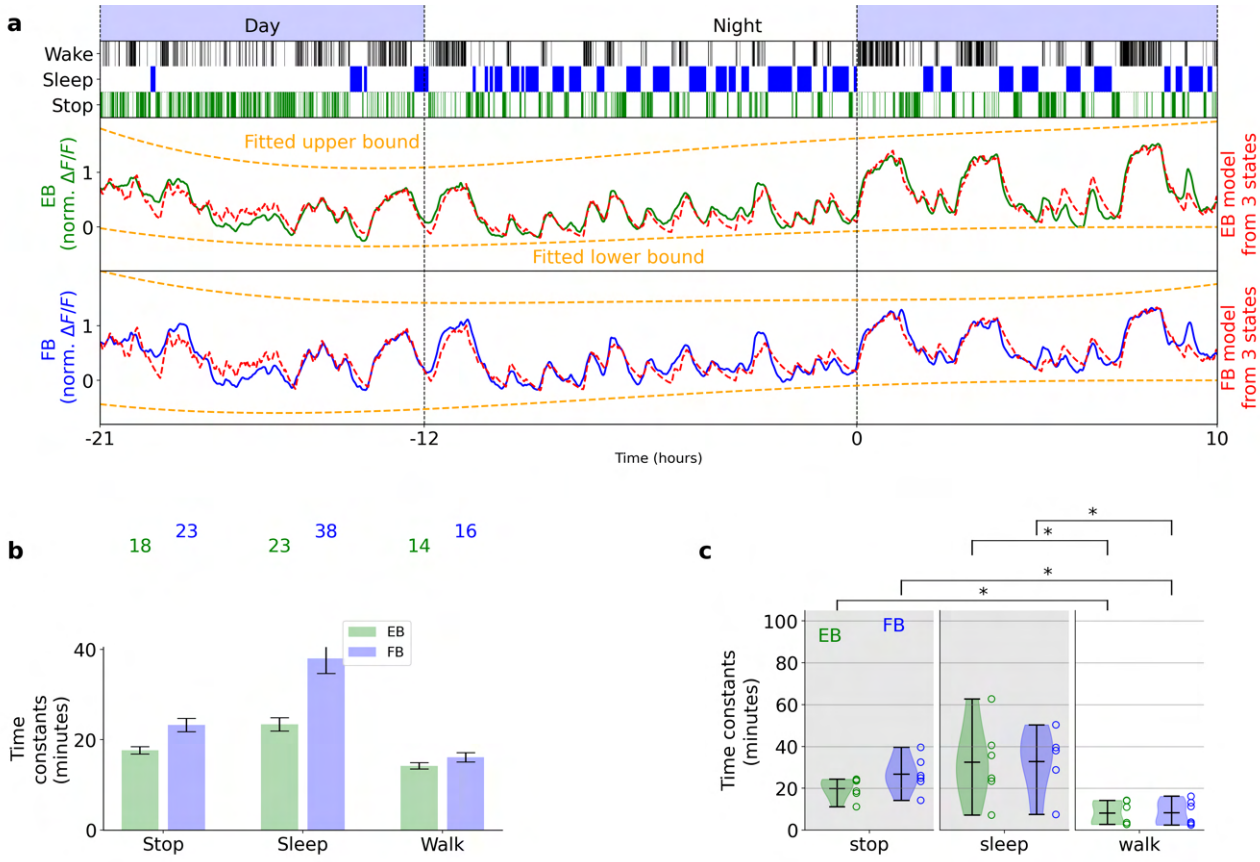

Figure S23. Fitting glia activity with homeostat 3-state model defining a 'sleep' state as epochs where the fly was stopped for more than 5 minutes. **a** First row shows day and night cycle in VR, second row shows behavior of fly 1 extracted from ball velocity. Sleep is defined as epochs where the fly stops walking for at least 5 minutes. The third and fourth rows show fitting of the 3-state model (red line) and corresponding bounds (orange lines) in EB and FB, respectively. **b** Time constants of 3 states resulting from fitting in a for EB (green) and FB (blue). **c** Distribution of time constants for the 3 states for $N = 6$ flies. Asterisks represent statistical significance between states, with p-values lower than 0.05 using t-test.

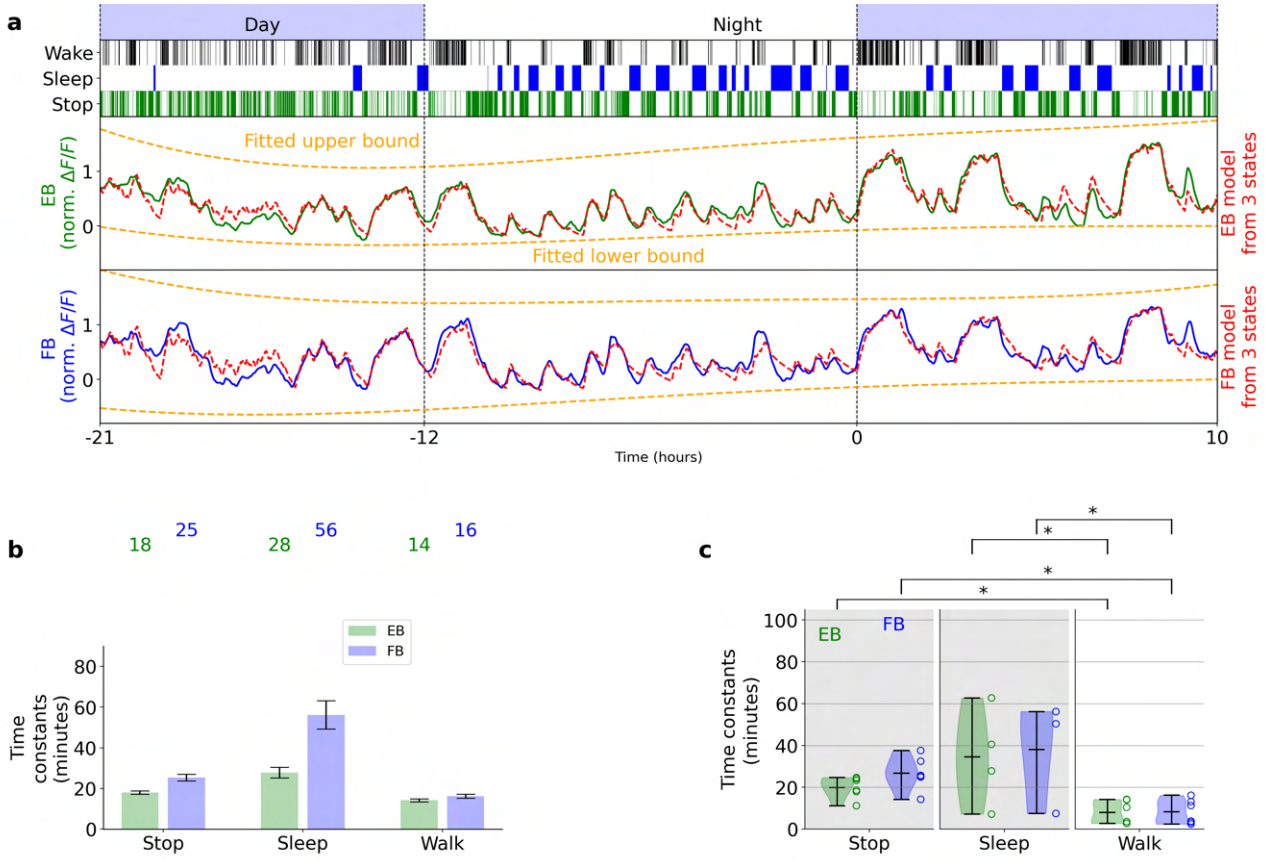

Figure S24. Fitting glia activity with homeostat 3-state model with a 'sleep' state define as only after 5 minutes of immobility. Same as Supplementary Fig Fig. S23.

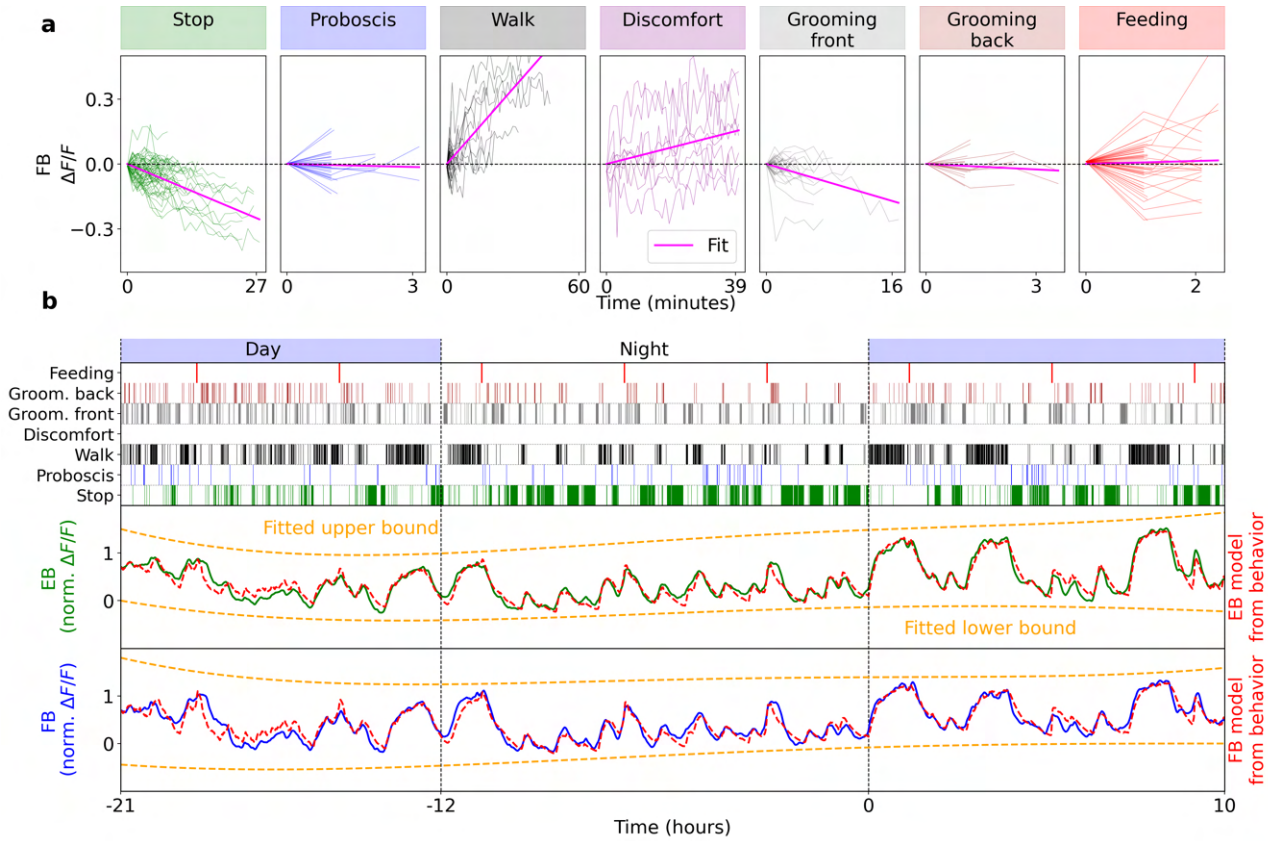

Figure S25. Fitting calcium activity with 7 behavioral states (seven-state model). **a** Determination of sign of weights of each behavior for model fitting. Fluorescence FB traces while fly is performing the respective behavior for at least to consecutive fluorescence recordings (2 minutes, combined across flies, see Methods). Purple shows linear fit, negative slope results in negative weight, and *vice versa*. Flies were often walking fast during feeding, likely resulting in increasing fluorescence. Note that the scale on y-axes differs between plots. **b** Model fitting with 7 states. Top: day-night cycle. Second row: classified fly behavior over time. Third row: band-pass filtered activity of glia in the EB (green line); red line shows model fit, orange lines show fitted correction of fluorescence levels. Fourth row: same as third row for FB.

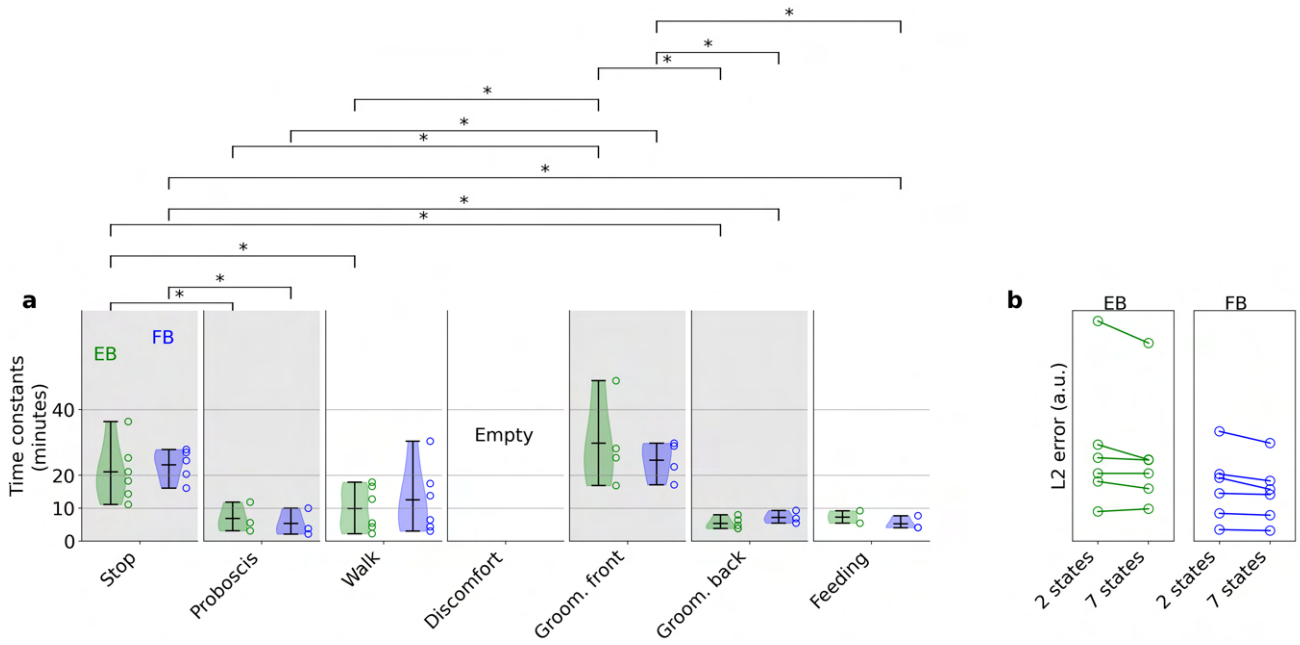

Figure S26. Significance levels for behaviors in 7-state model. Time constants of the 7 classified behaviors fitted in 7-state model for the EB (green) and FB (blue, Fig. S25a). Only time constants with an error of less than 20% were included in the histograms (see Methods). Asterisks include statistical significance between all possible pairs of fitted time constants, based on p-values lower than 0.05 using t-test. **b** Comparison between the 2-state and 7-state models in the EB (left) and FB (right). L2-error between fit and data for $N = 6$ flies.

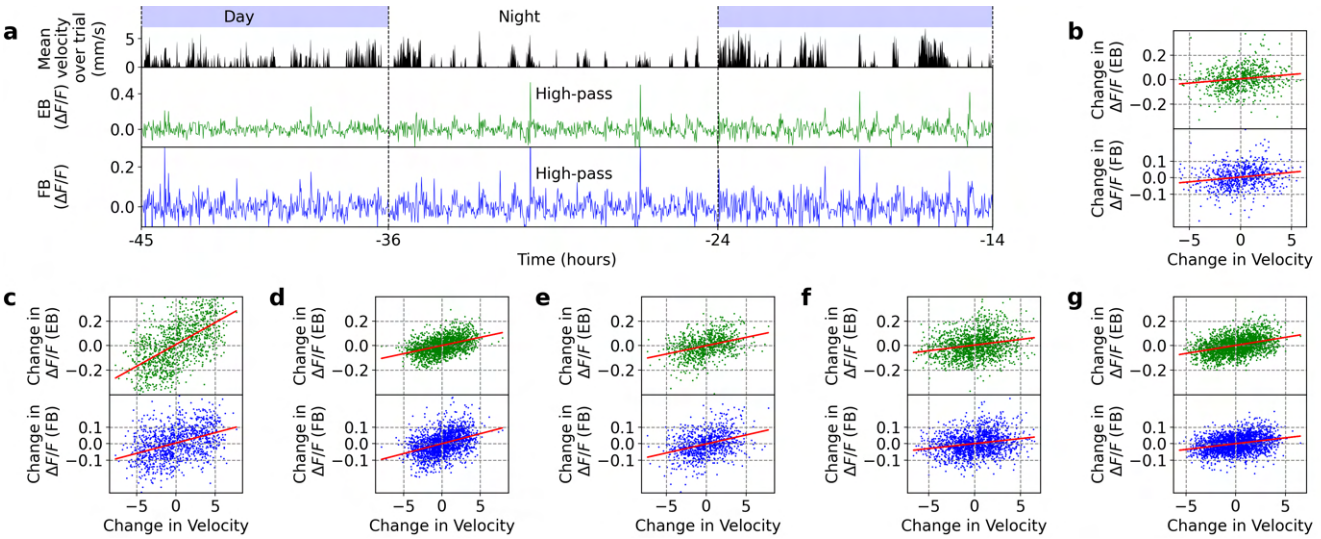

Figure S27. **a** Top row shows day and night cycle in VR over time and second row shows mean velocity during recording epoch (1 second). Second and third row show fluorescence signals in the EB and FB, respectively. Fluorescence was filtered with a high-pass filter for periods higher than 0.5 hours. **b** Correlation between mean velocity over trial and high-pass filtered fluorescence. **c-g** Same as b for 5 more flies.

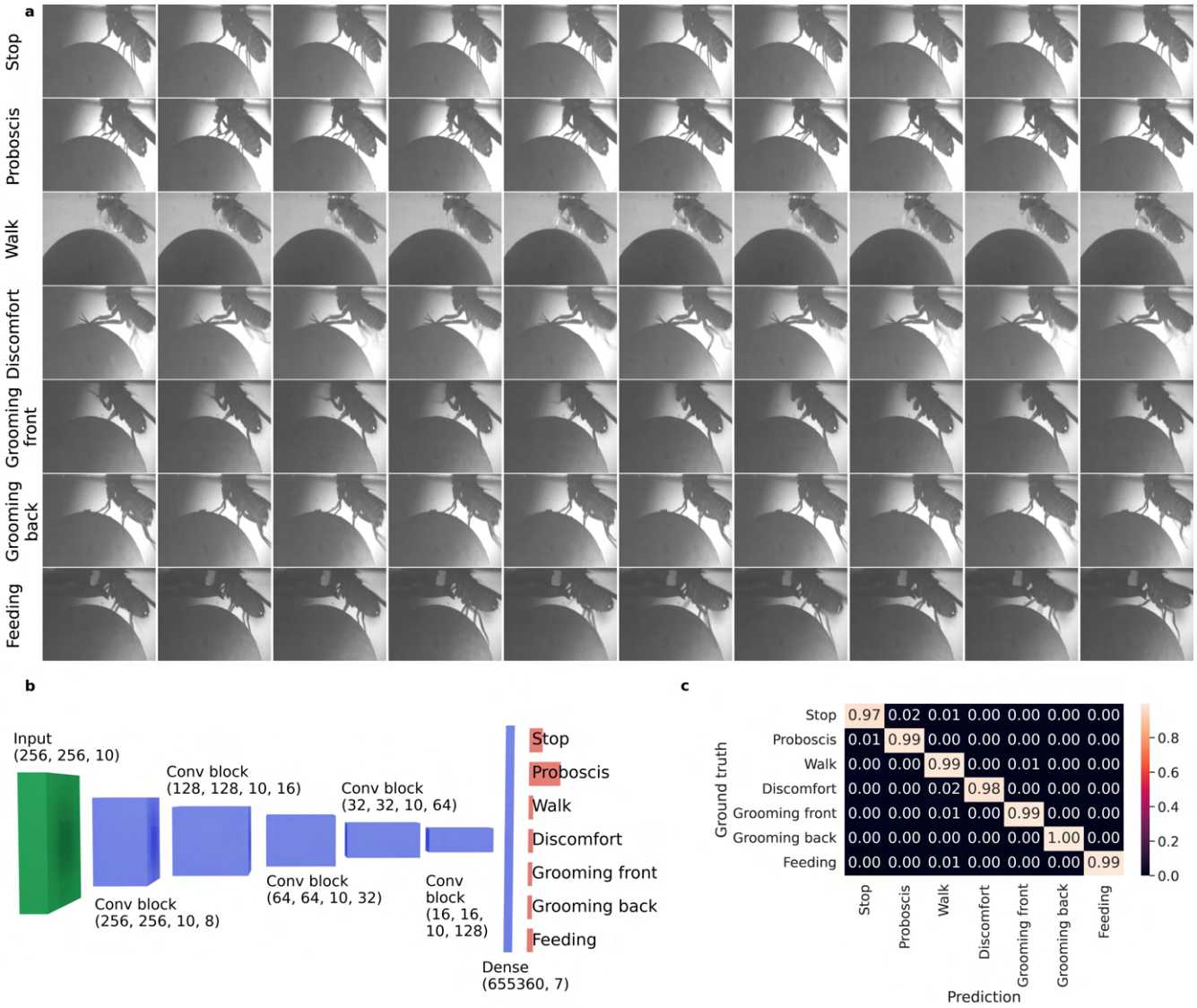

Figure S28. Classification of the behavior of the fly on the ball during long-term imaging. **a** A 3D CNN with 10 consecutive frames with a side view of the fly on the ball is used to classify 7 different behaviors (y-axis). Each row in the plot corresponds to 10 consecutive frames where the fly performs the labeled behavior. **b** Architecture of the 3D CNN. **c** Confusion matrix for each behavior for prediction of the 3D CNN (x-axis) on a test dataset that was manually labeled (ground truth along y-axis).

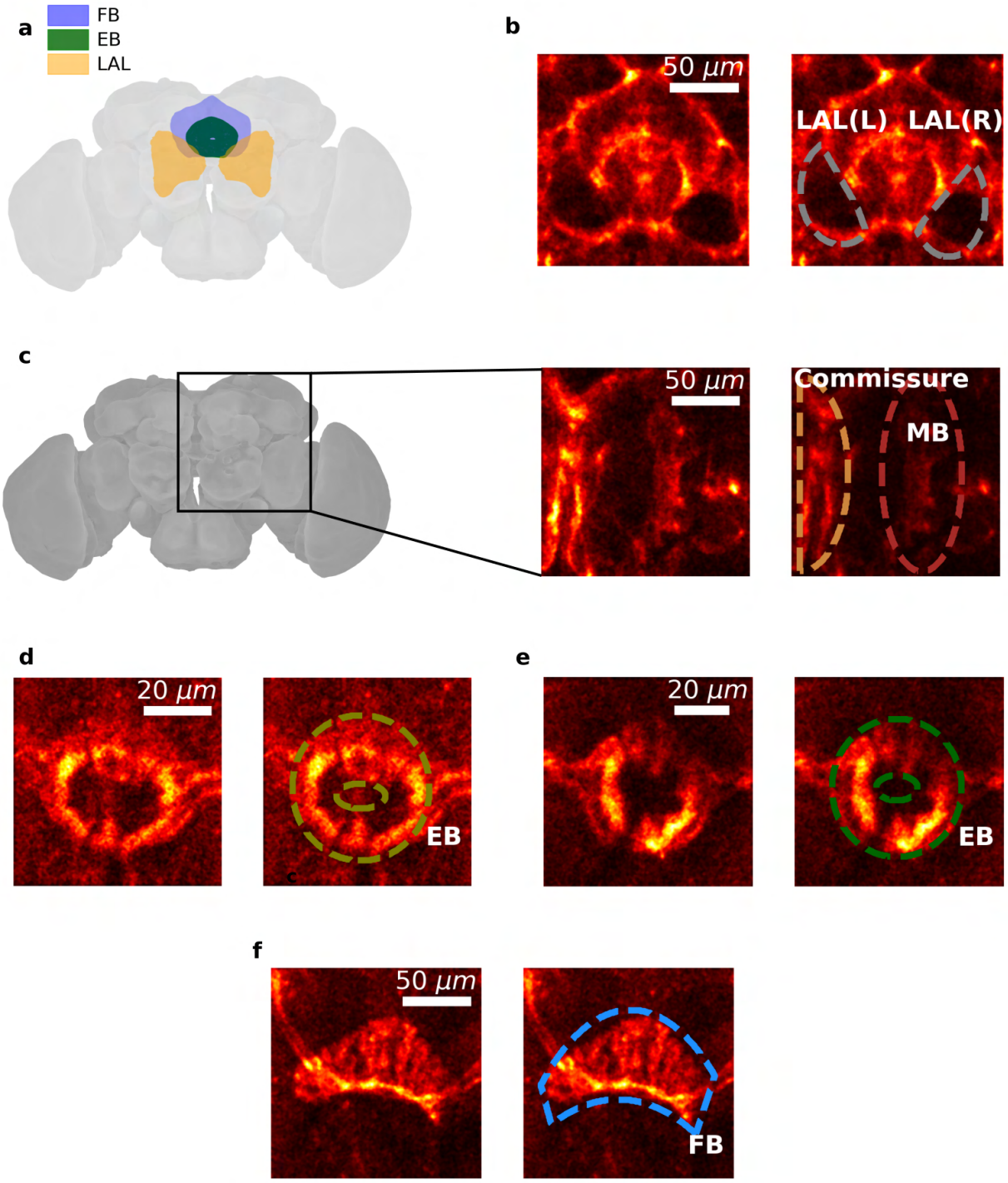

Figure S29. Regions of interests (ROIs) for recordings of ensheathing glia in LAL, MB, and commissure, as well as of R5 and dFB neurons. **a** Schematic of EB, FB, and left and right LAL in the fly brain. **b** On the left, ensheathing glia in the central complex and LAL. On the right, ROI along the right (R) and left (L) LAL **c** On the left, *Drosophila* brain area where ensheathing glia in MB and commissure were recorded (center). On the right, ROI along the MB (brown) and commissure (dark orange). **d** On the left, R5 neurons labeled by 58H05-GAL4. On the right, ROI along the ring-shaped projections of R5 neurons for calculating fluorescence changes. **e** Same as in a, but for R5 neurons labeled by 88F06-GAL4. **f** Same as a and b, but for dFB neurons labeled by 23E10-GAL4.

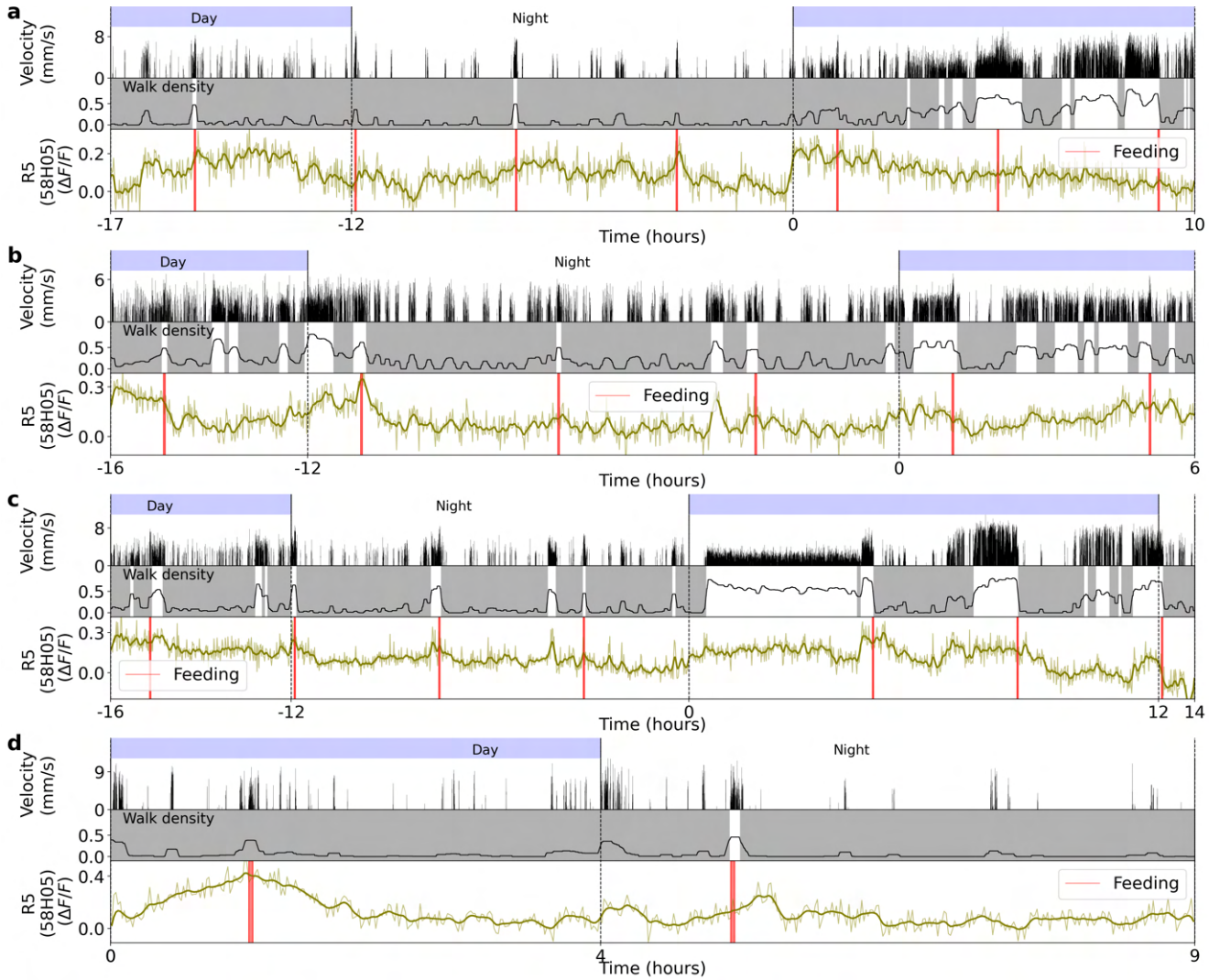

Figure S30. Four different long-term imaging recordings of calcium activity in R5 neurons labeled by GAL4-58H05. **a** Top row: day and night cycle in VR. Second row: velocity of the fly in 1 second bins. Third row: walk density (see Methods) and rest (grey region) and active (white region) epochs. Fourth row: Calcium activity of R5 neurons. The thick line indicates a low-pass filter with a 0.1 hours cut-off period. Vertical red lines represent feeding events. **b-d** Same as a. Each panel shows a different fly.

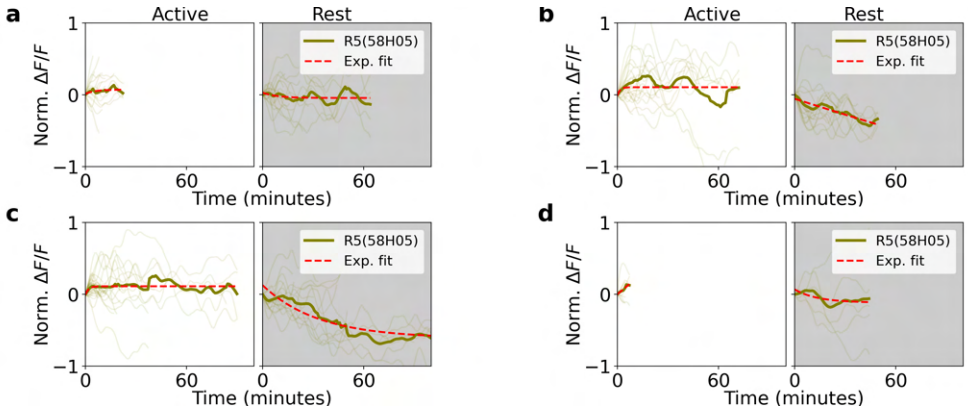

Figure S31. Normalized fluorescence traces during active and rest epochs for four flies in R5 neurons (labeled by GAL4-58H05). **a** Left side: single (thin lines) and average (thick lines) normalized fluorescence traces from activity in R5 neurons during active epochs. Red lines indicate exponential fit. Right side: the same as the left side, but during rest epochs. **b-d** Same as a. Each panel is from a different fly.

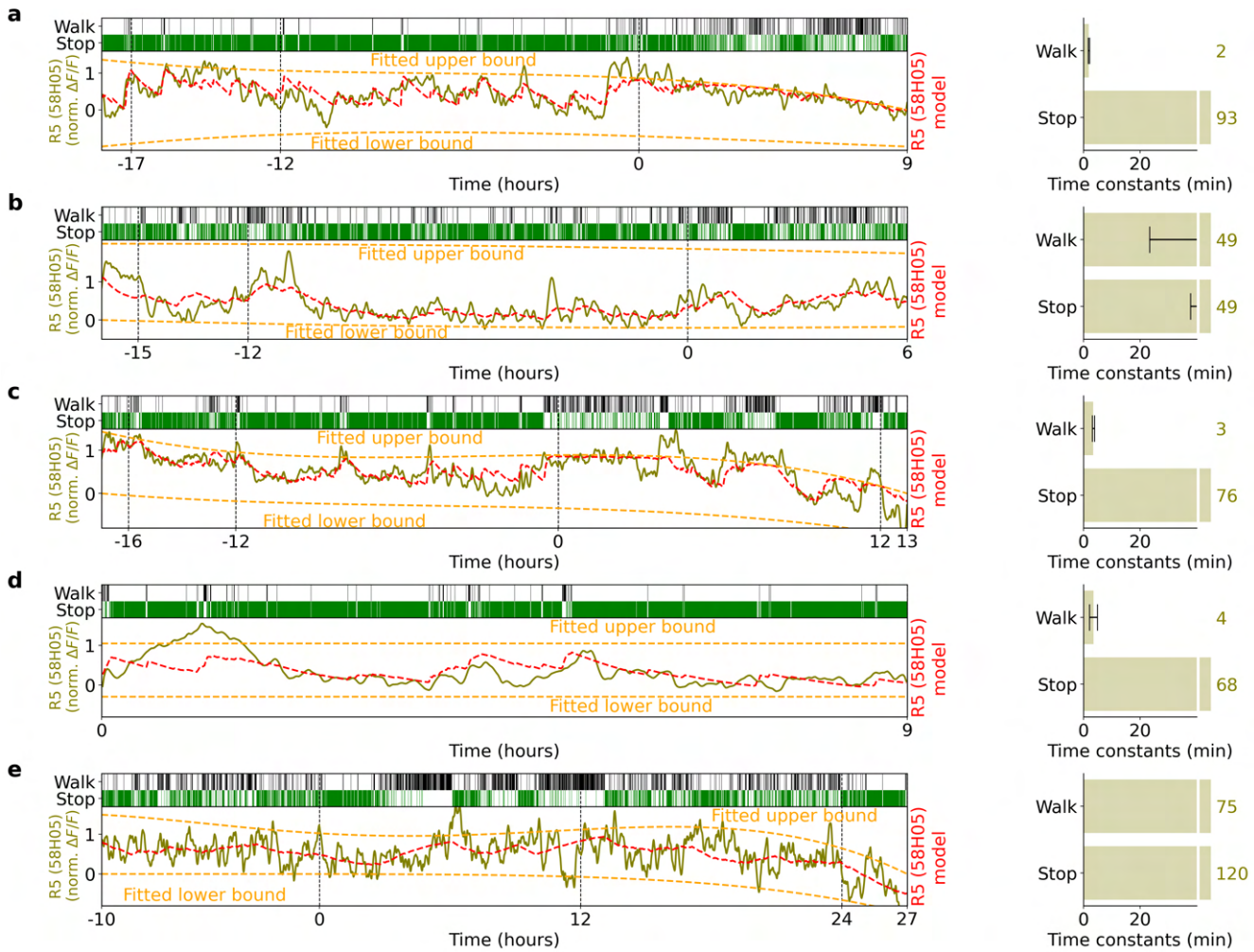

Figure S32. Fitting calcium activity of R5 neurons (labeled by GAL4-58H05) with the homeostat 2-state model. **a** Left side: the top row shows walking and stopping bouts of a fly. Second row: Normalized fluorescence from R5 neurons. Red lines show the fitted model, while orange lines represent the fitted upper and lower bounds of the model. Right side: fitted time constants from the model. Grey lines indicate error bars of the estimated time constants (see Methods), while colored numbers show the rounded value of the fitted time constants. **b-d** Same as a. Each panel represents a fitted model for each fly.

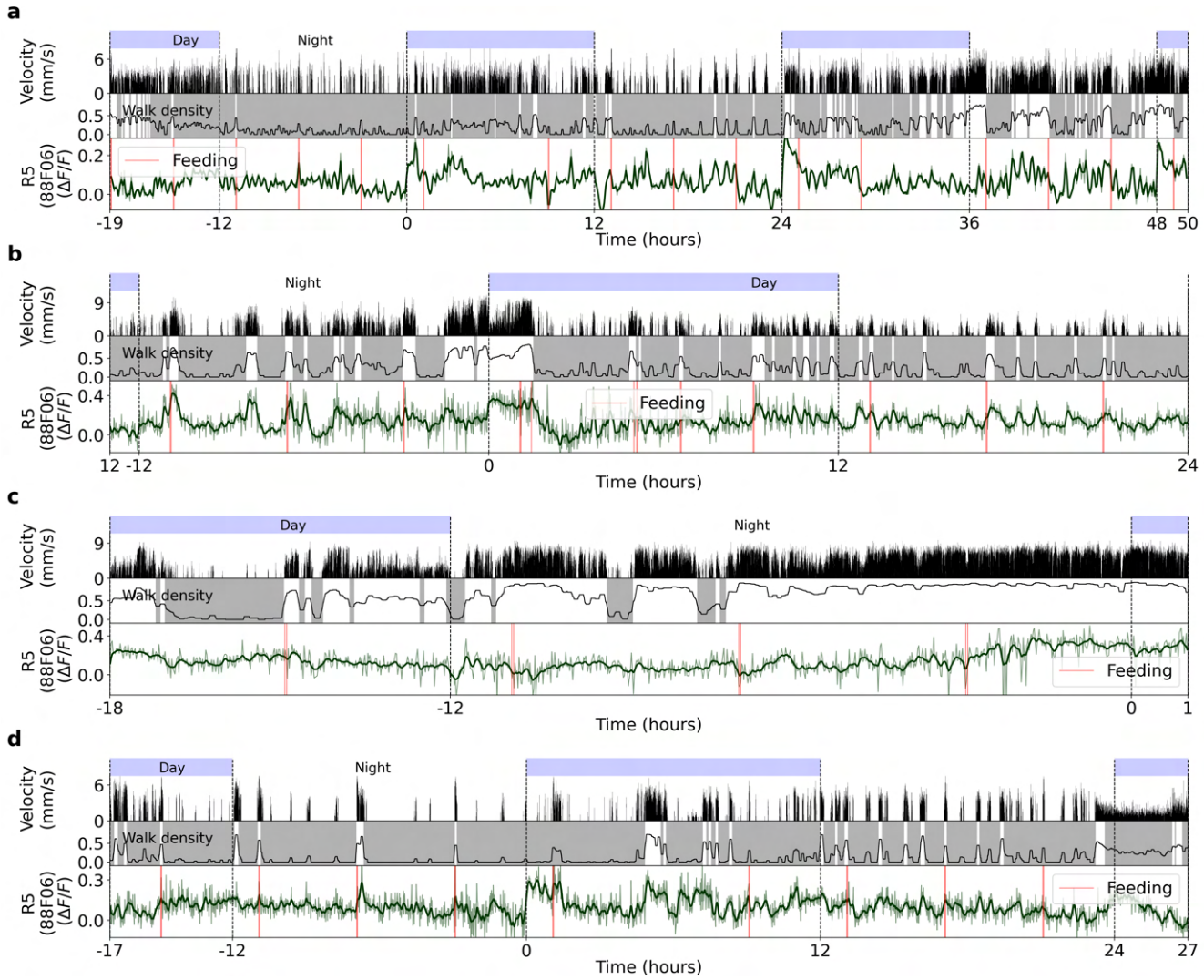

Figure S33. Four different recordings of calcium activity in R5 neurons labeled by GAL4-88F06. **a** Top row: day and night cycle in VR. Second row: velocity of fly in 1 second bins. Third row: walk density (see Methods), rest (grey region) and active (white region) epochs. Fourth row: Calcium activity of R5 neurons. Thick line indicates low-pass filtering with a 0.1 hours cut-off period. Vertical red lines represent feeding events. **b-d** Same as a. Each panel shows a different fly.

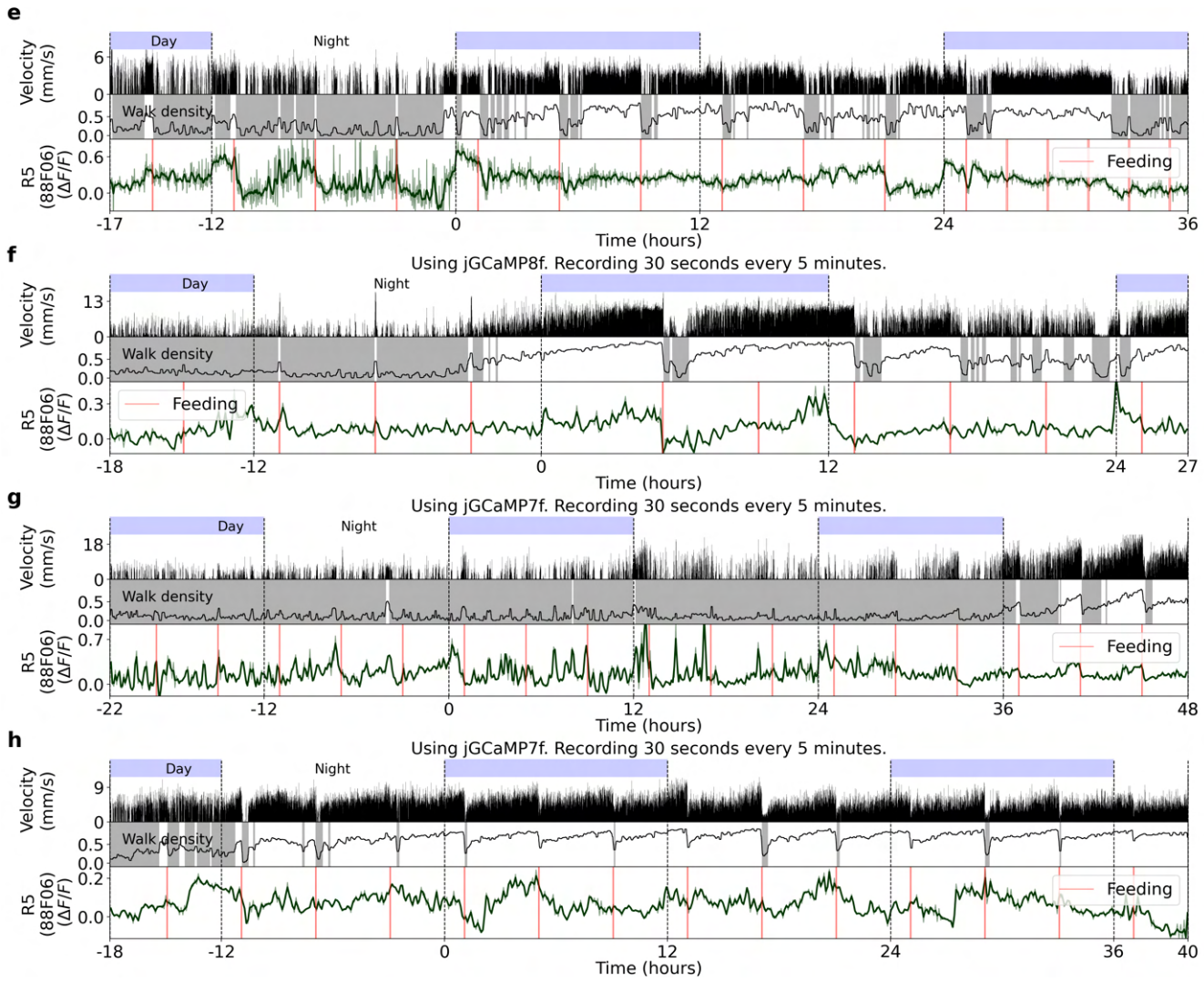

Figure S34. Four more recordings of calcium activity in R5 neurons labeled by GAL4-88F06. Same as Supplementary Fig. S33

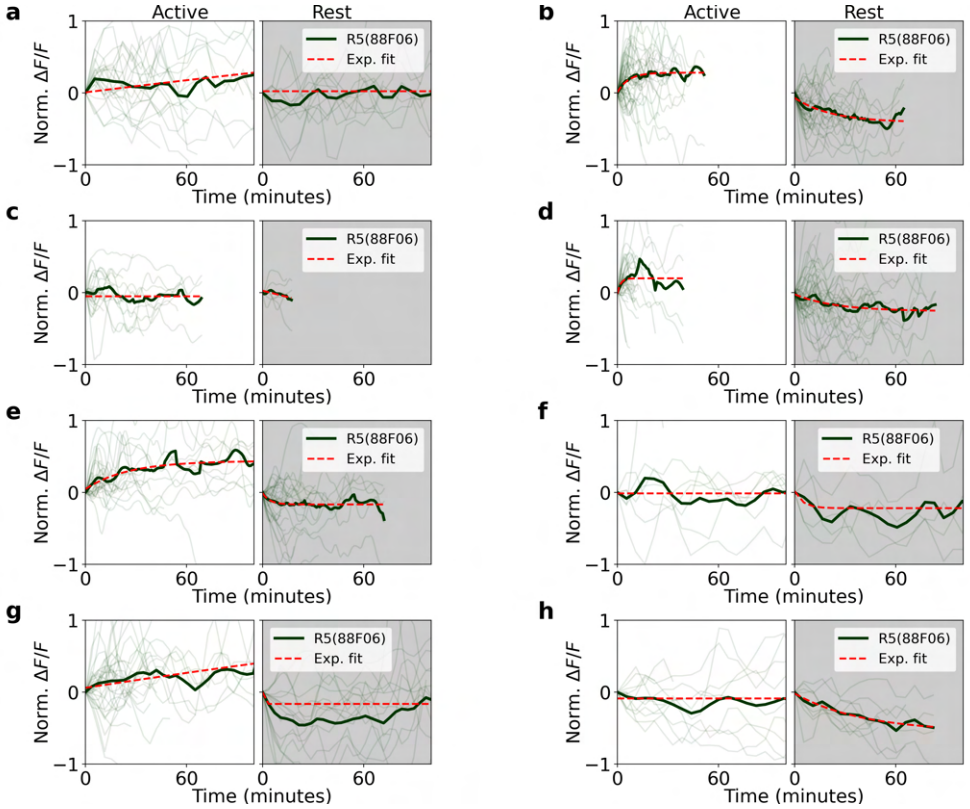

Figure S35. Normalized fluorescence traces during active and rest epochs for eight flies in R5 neurons (labeled by GAL4-88F06). **a** Left side: single (thin lines) and average (thick lines) normalized fluorescence traces of activity in R5 neurons during active epochs. Red lines indicate exponential fit. Right side: the same as left side, but during rest epochs. **b-d** Same as a. Each panel is a different fly.

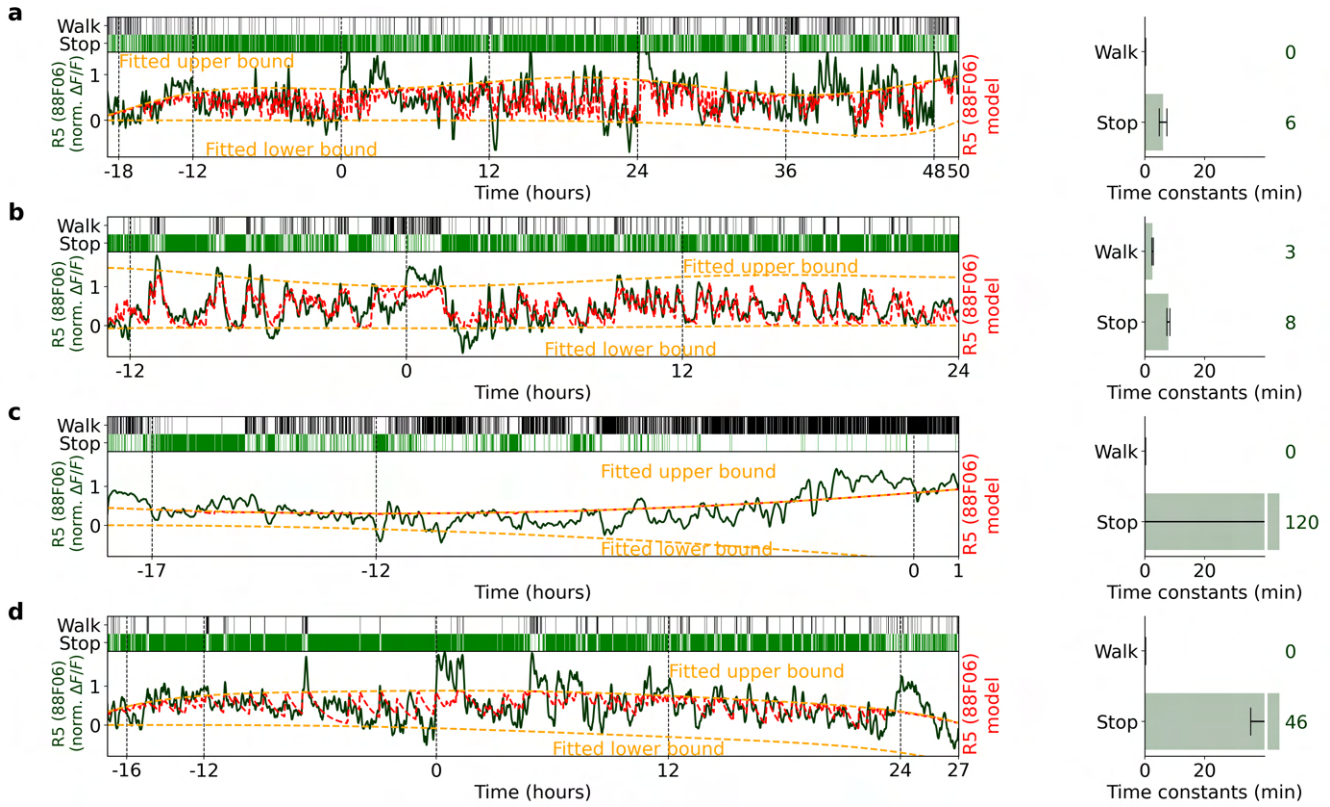

Figure S36. Fitting calcium activity of R5 neurons (labeled by GAL4-88F06) with homeostat 2-state model. **a** Left side: top row shows walking and stopping bouts of a fly. Second row: Normalized fluorescence of R5 neurons. Red lines show the fitted model, while orange lines represent fitted upper and lower bounds of model. Right side: time constants obtained from model fitting. Grey lines indicate error bars of estimated time constants (see Methods), while colored numbers show rounded values of fitted time constants. **b-d** Same as a. Each panel represents a fitted model for each fly.

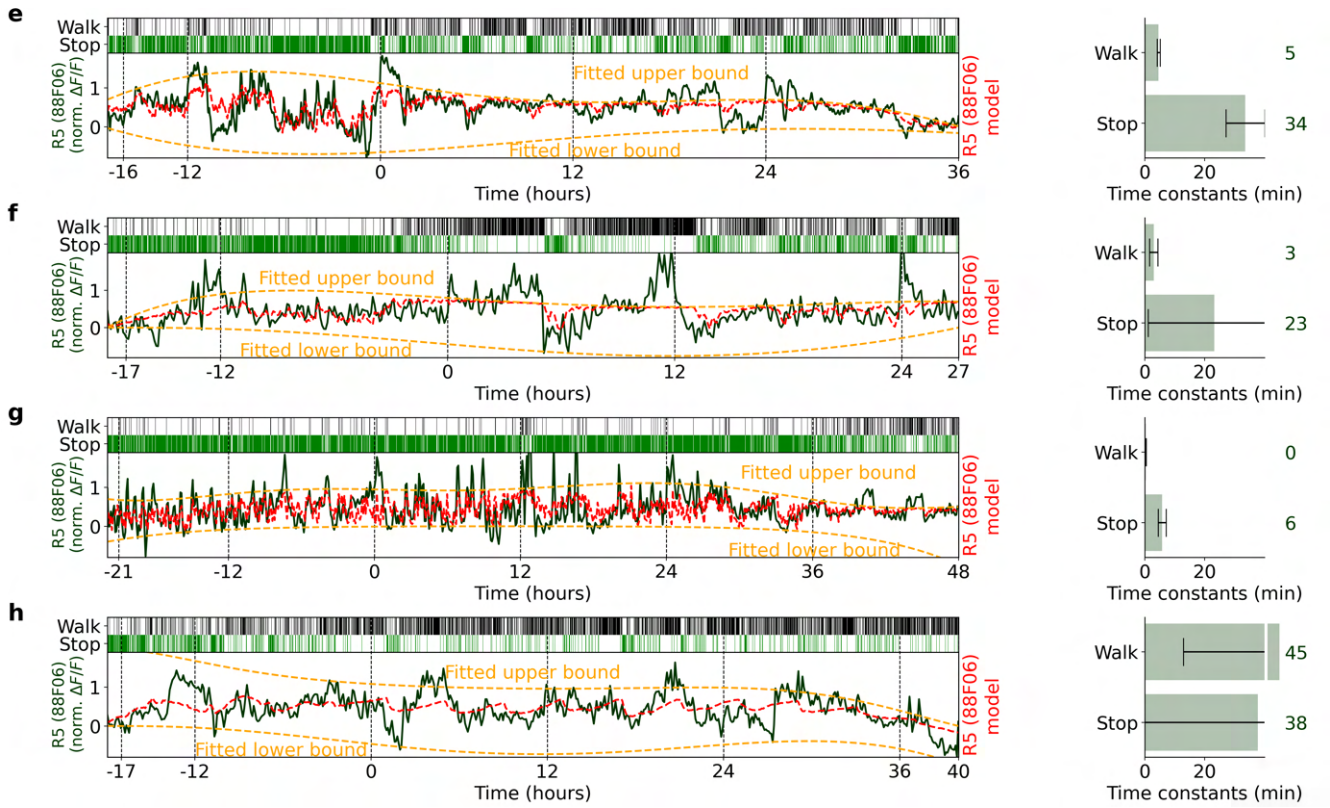

Figure S37. Four more recordings and fits of homeostat 2-state model with calcium activity of R5 neurons (labeled by GAL4-88F06). Same as Supplementary Fig. S36.

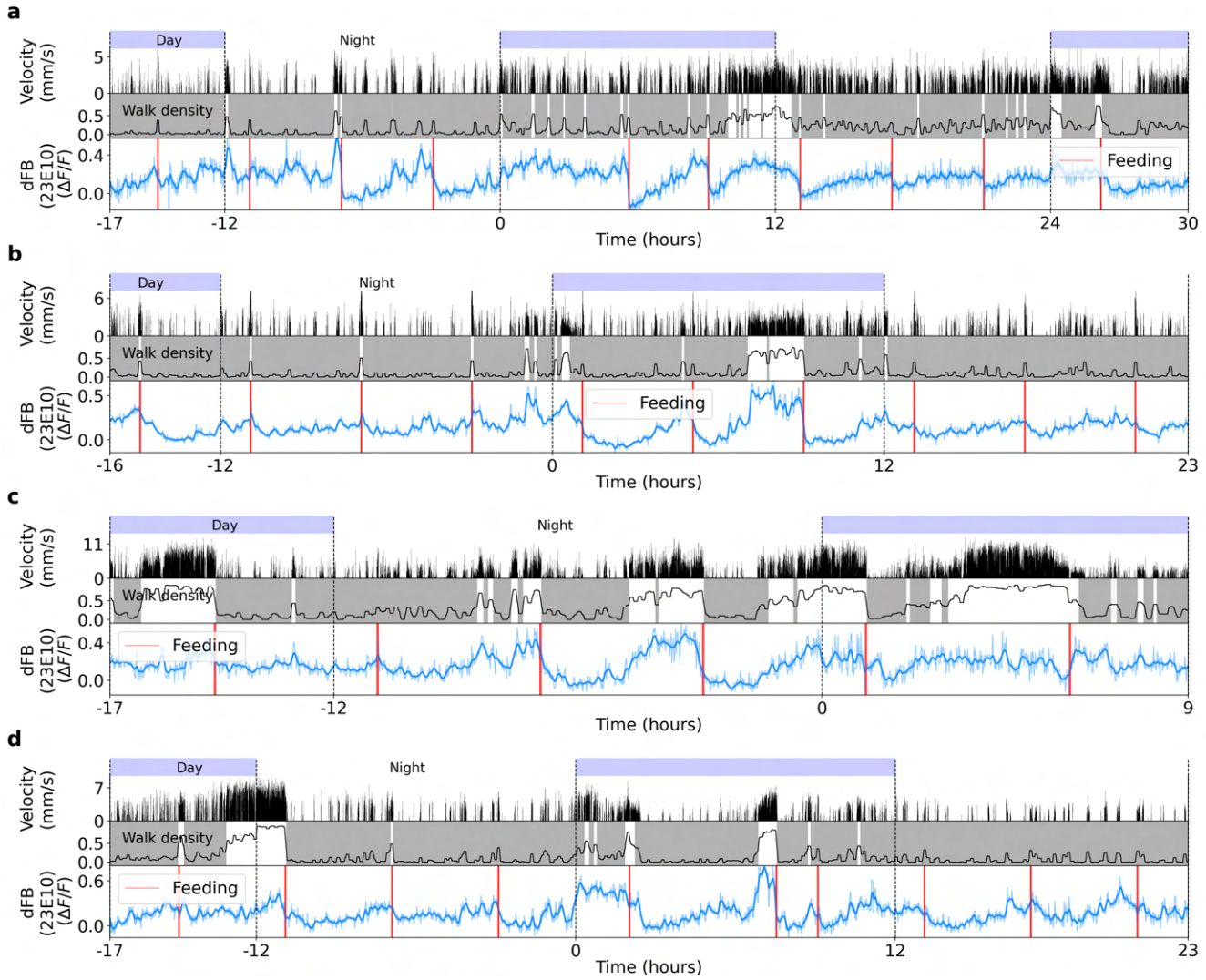

Figure S38. Four different recordings of calcium activity in dFB neurons labeled by GAL4-23E10. **a** Top row: day and night cycle in VR. Second row: velocity of fly in 1 second bins. Third row: walk density (see Methods), rest (grey region), and active (white region) epochs. Fourth row: Calcium activity of dFB neurons. The thick line indicates a low-pass filter with a 0.1 hours cut-off period. Vertical red lines represent feeding events. **b-d** Same as a. Each panel shows a different fly.

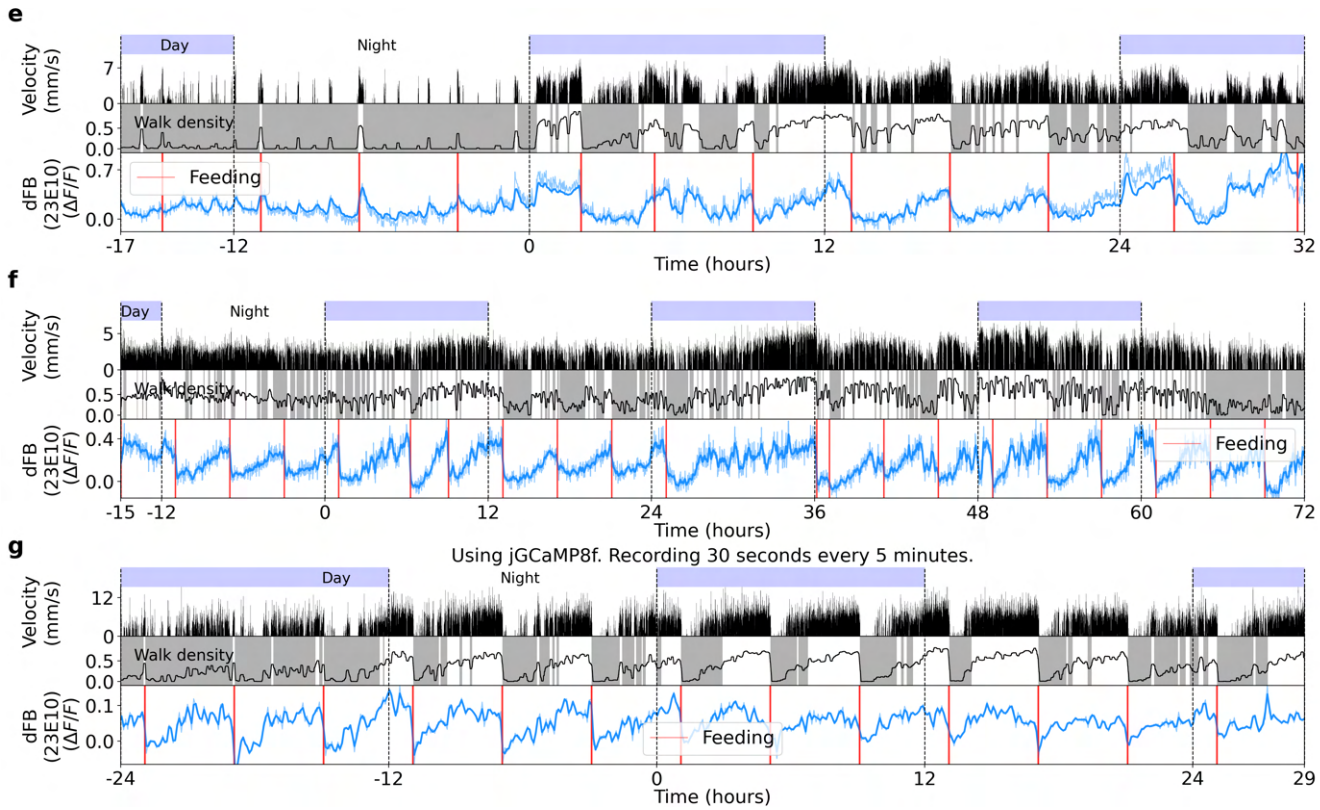

Figure S39. Three recordings of calcium activity in dFB neurons labeled by GAL4-23E10. Same as Supplementary Fig. S38

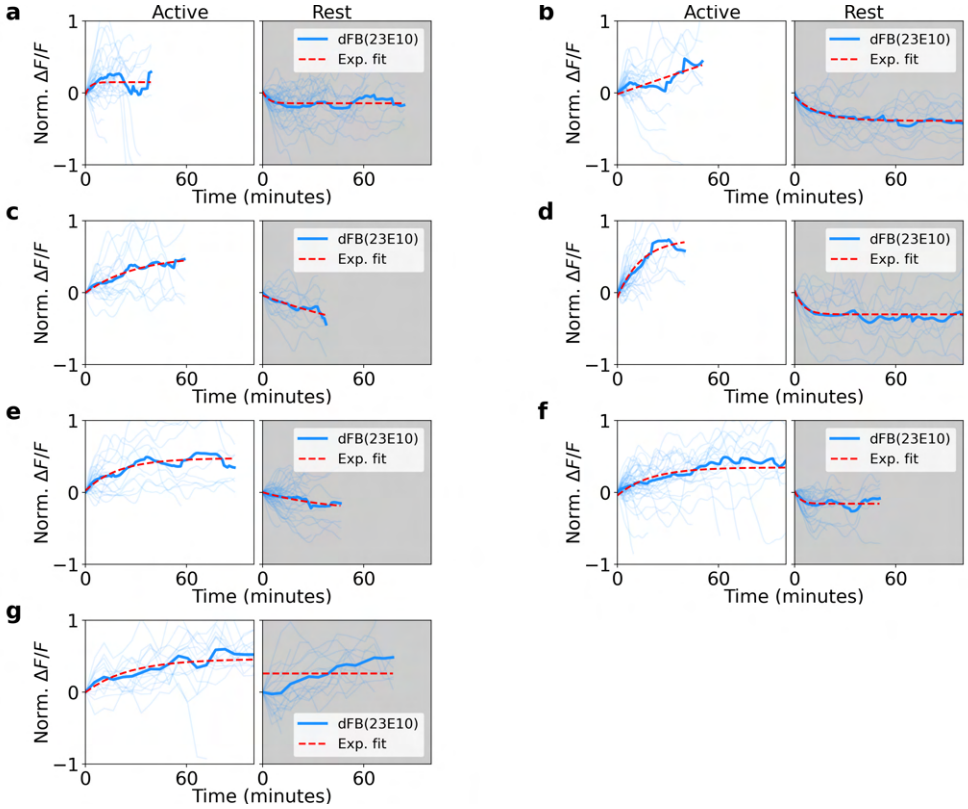

Figure S40. Normalized fluorescence traces during active and rest epochs for seven flies in dFB neurons (labeled by GAL4-23E10). **a** Left side: single (thin lines) and average (thick lines) normalized fluorescence traces of activity in dFB neurons during active epochs. Red lines indicate exponential fit. Right side: same as the left side, but during rest epochs. **b-d** Same as a. Each panel is from a different fly.

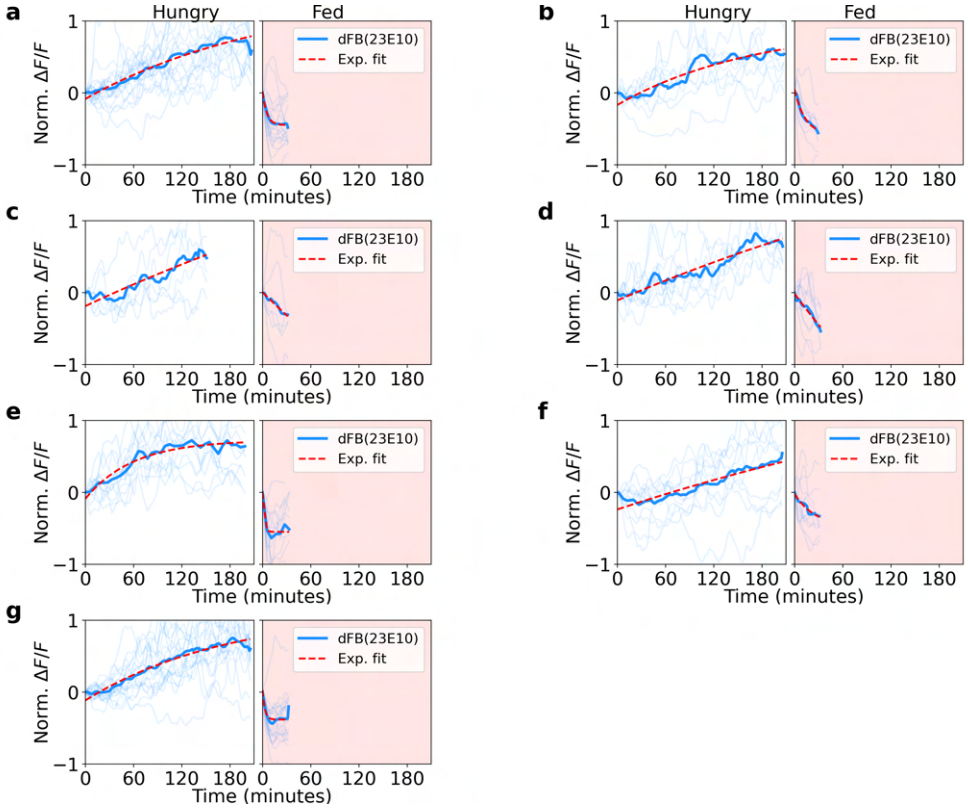

Figure S41. Normalized fluorescence traces during hungry and fed epochs for seven flies in dFB neurons (labeled by GAL4-23E10). **a** Left side: single (thin lines) and average (thick lines) normalized fluorescence traces of activity in dFB neurons during hungry epochs. Red lines indicate exponential fit. Right side: same as the left side, but during fed epochs. **b-d** Same as a. Each panel is from a different fly.

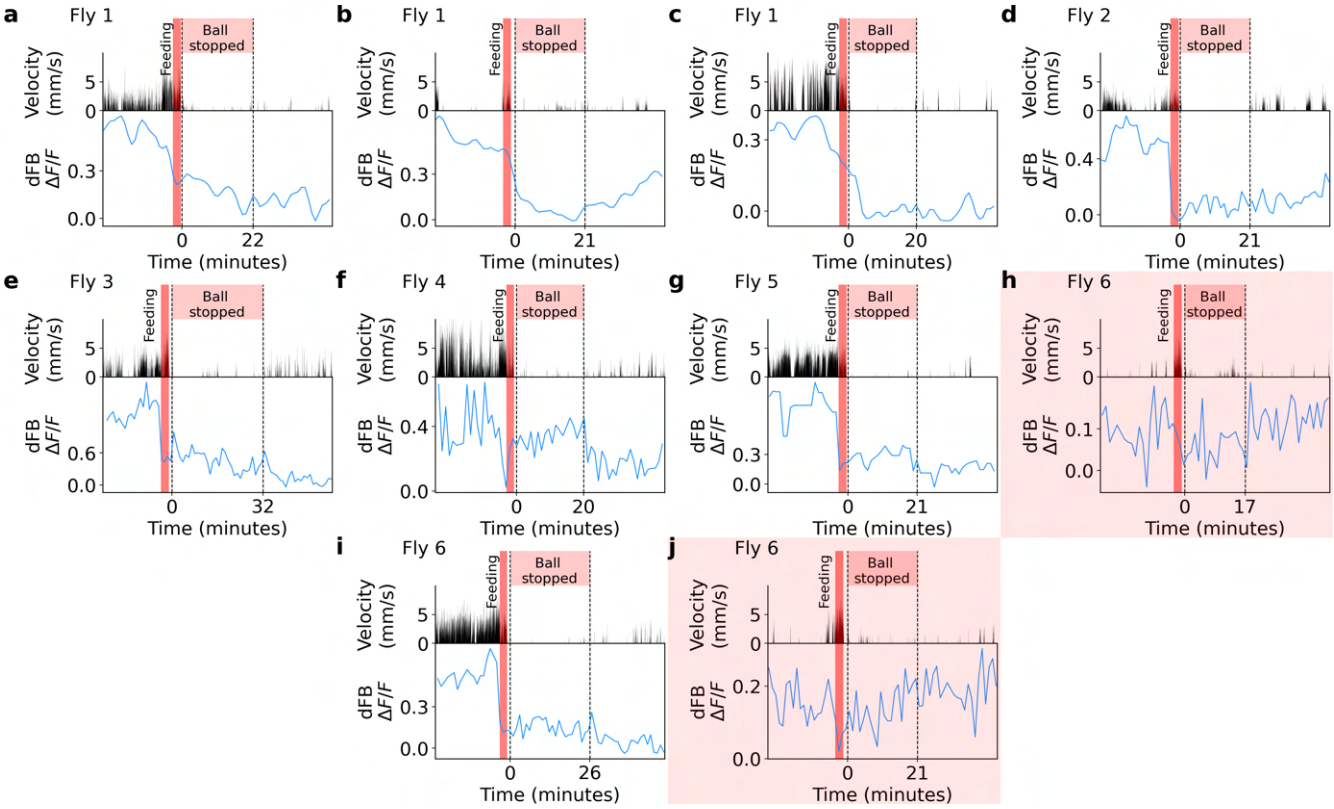

Figure S42. Trials where the ball was blocked after feeding while activity in dFB neurons was recorded. **a** First row: time where the ball was stopped (red region). Second row: velocity of the fly. Third row: Calcium activity dFB neurons. The vertical red line indicates the feeding event before blocking the ball. **b-j** Same as a. Each panel represents a different trial. Trials h and j were not considered for the analysis (highlighted in red) because dFB neurons had low activity levels before feeding. The fly from which each trial was recorded is shown in the top left corner of each panel.

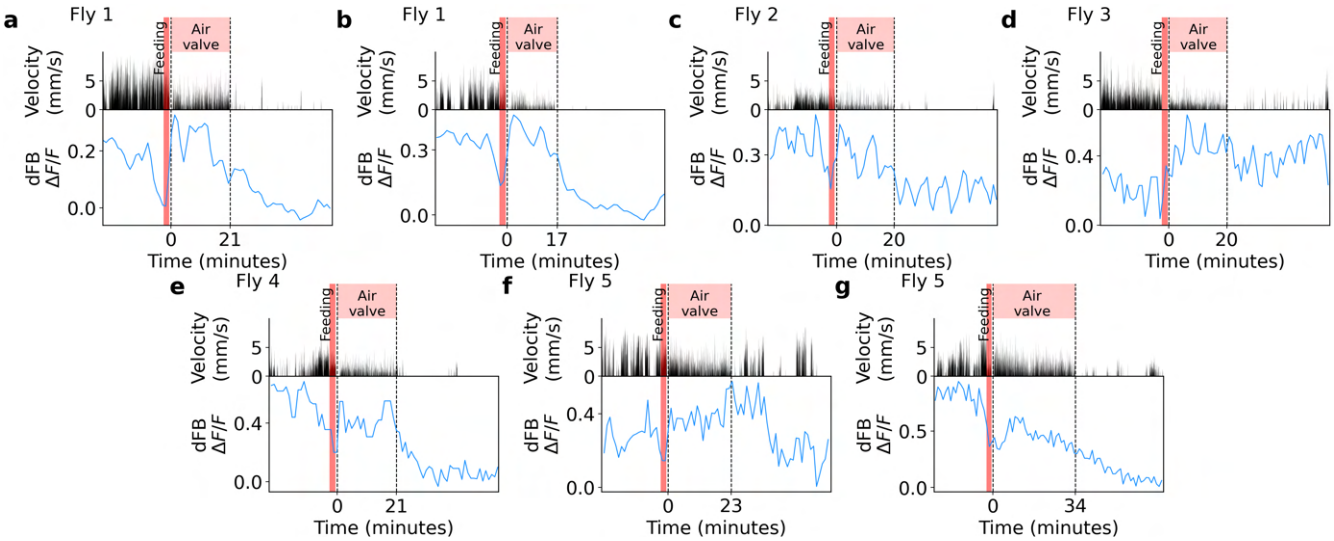

Figure S43. Trials where air supply of the ball was intermittently interrupted to promote walking after feeding, while activity in dFB neurons was recorded. **a** First row: times where the ball was perturbed by the air valve (red region). Second row: velocity of the fly. Third row: Calcium activity in dFB neurons. The vertical red line indicates feeding event before perturbing the ball. **b-g** Same as a. Each panel represents a different trial. The fly from which each trial was recorded is shown in the top left corner of each panel.

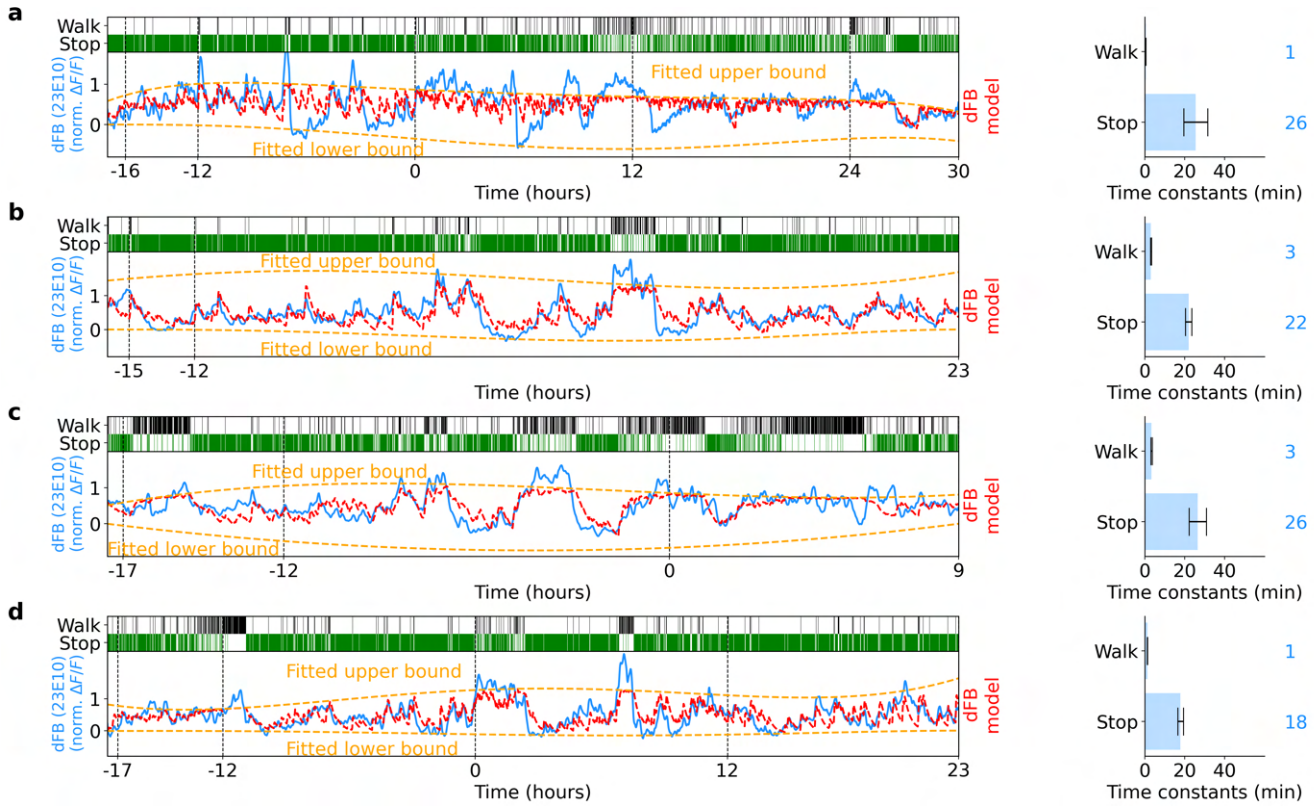

Figure S44. Fitting calcium activity of dFB neurons (labeled by GAL4-23E10) with homeostat 2-state model. **a** Left side: top row shows walk and stop bouts of a fly. Second row: Normalized fluorescence of dFB neurons. Red lines show fitted model, while orange lines represent fitted upper and lower bounds of the model. Right side: fitted model time constants. Grey lines indicate error bars of estimated time constants (see Methods), while colored numbers show the rounded value of the fitted time constants. **b-d** Same as a. Each panel represents a fitted model for each fly.

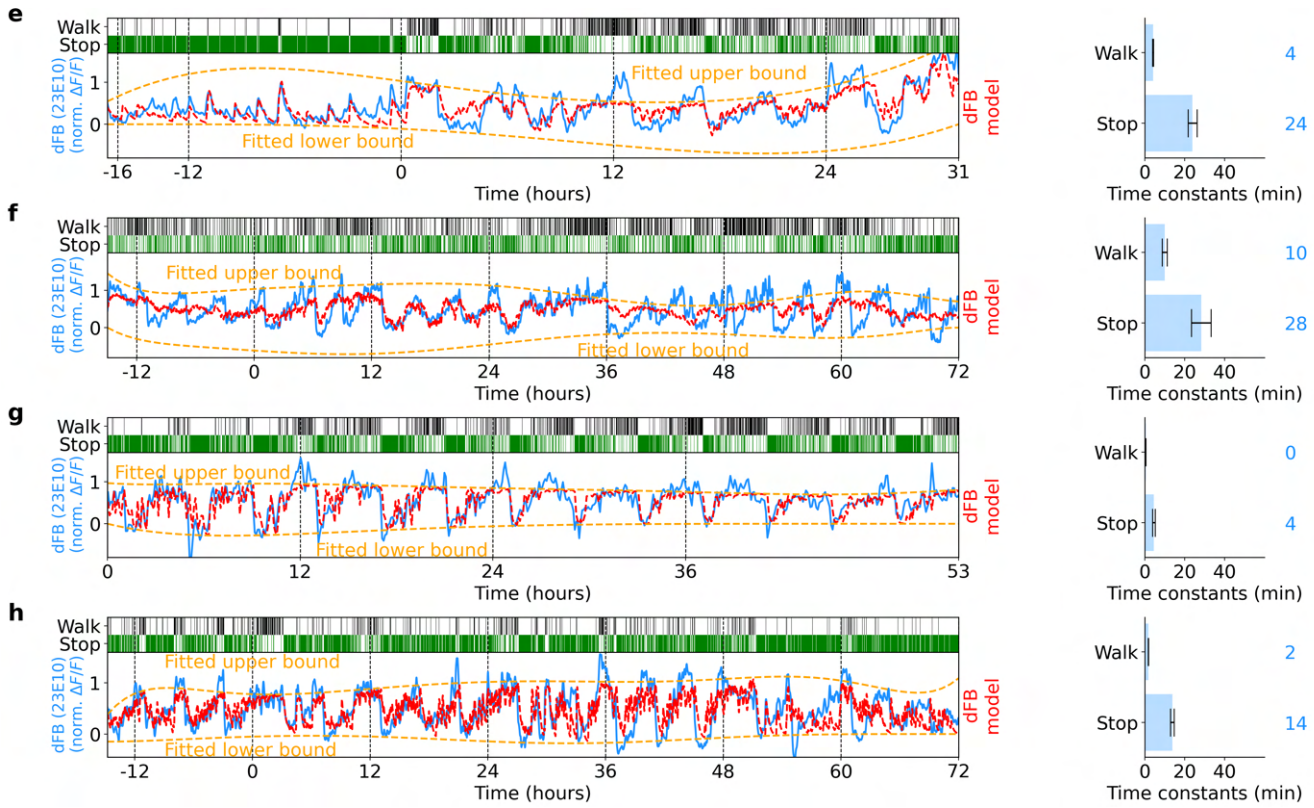

Figure S45. Four more experiments and fits of the homeostat 2-state model with calcium activity of dFB neurons (labeled by GAL4-23E10). Same as Supplementary Fig. S44.

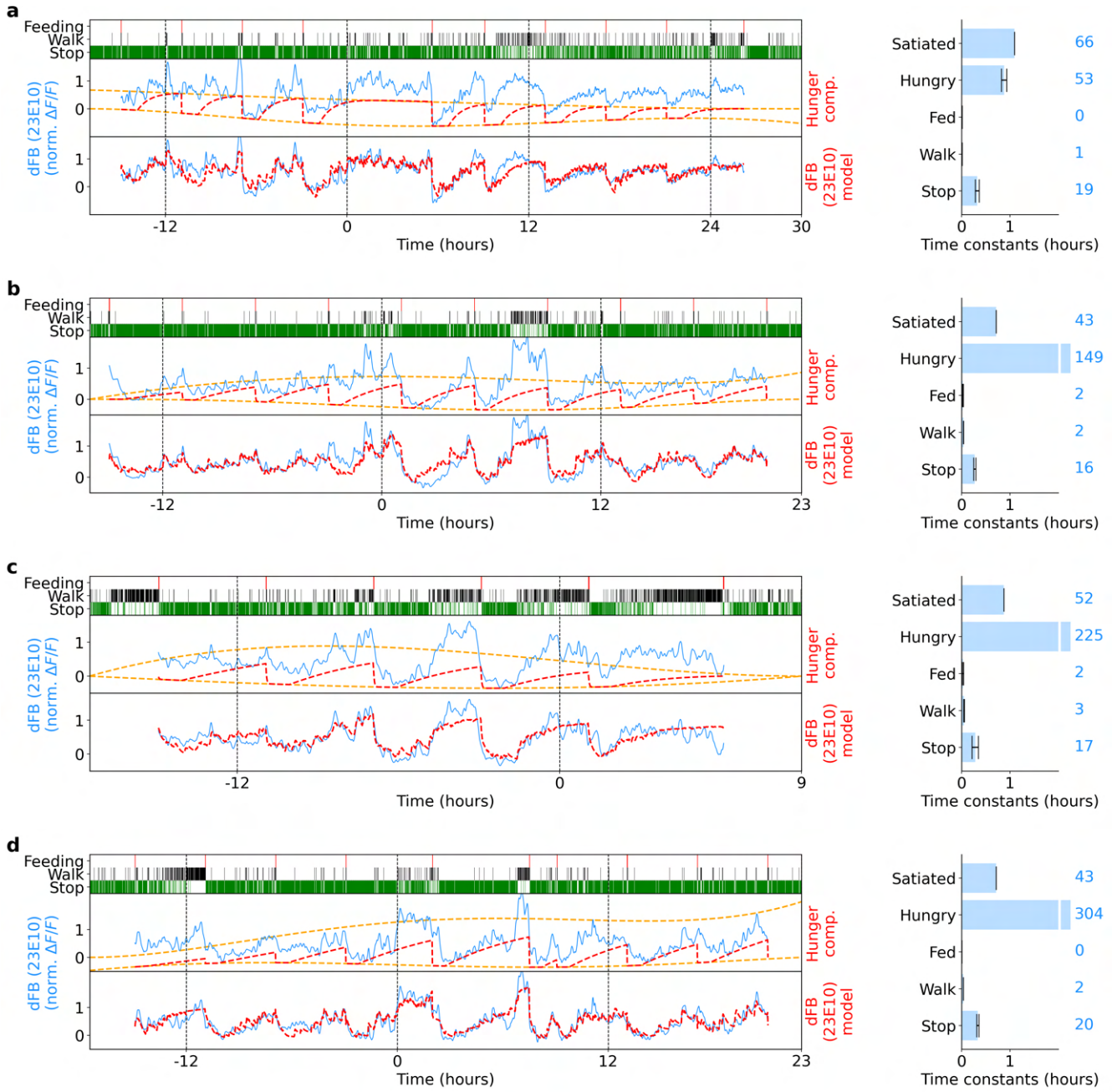

Figure S46. Fitting calcium activity of dFB neurons (labeled by GAL4-23E10) with hunger-walk model. **a** Left side: top row shows feeding events as well as walk and stop bouts of a fly. Second row: normalized fluorescence of dFB neurons in blue. Red line shows hunger component fitted by the model, while orange lines represent fitted upper and lower bounds of the hunger component. Third row: normalized fluorescence of dFB neurons in blue and fitted hunger-walk model in red. Right side: fitted time constants from the model. Grey lines indicate error bars of estimated time constants (see Methods), while colored numbers show their rounded fitted value. **b-d** Same as a. Each panel represents a fitted model for a different fly.

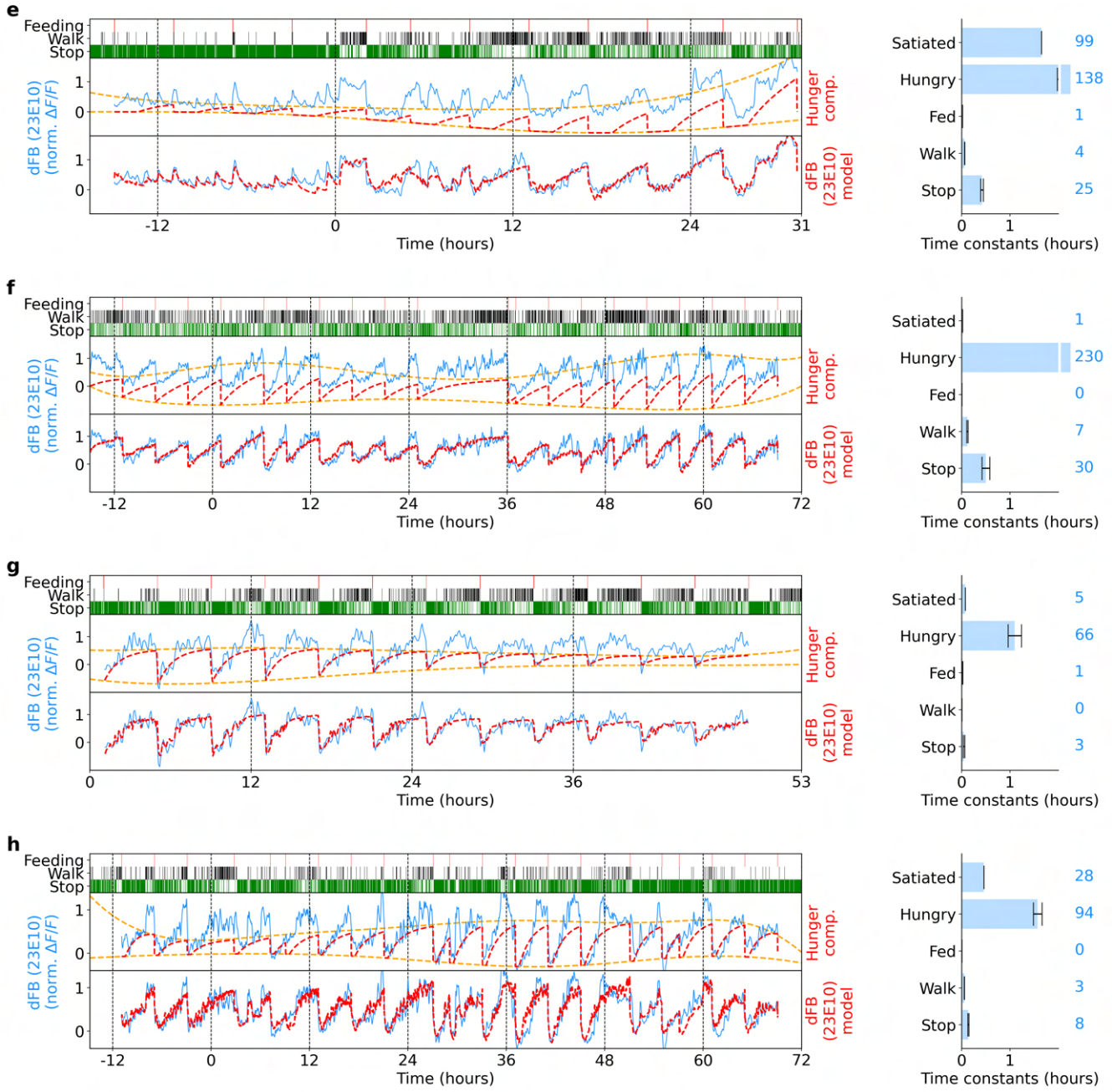

Figure S47. Another four experiments with dFB neurons and fits of hunger-walk model to calcium activity (labeled by GAL4-23E10). Same as Supplementary Fig. S46.

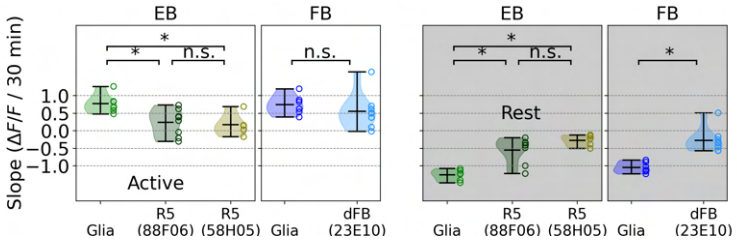

Figure S48. Left side: slope of a linear fit between time that flies spent in active epochs and average fluorescence traces from glia and neurons in EB and FB. Right side: same as left side but during resting epochs.

Supplementary Video S1. Video for experiment of fly 1. Top: time during experiment. Middle, right: raw imaging data (60 frames or 1 second average in epochs of 1 minute). Rotating blue (during the day) or grey (during the night) arch represents stripe orientation in VR with respect to the fly (the fly's head and abdomen are pointing toward the upper and lower axis of the video, respectively). Right: side view of the fly on the ball. Behavior classification is shown in white in the left corner. The bottom panel shows the velocity of the fly (first row), behavior classification (second row), and glia activity in EB (green) and FB (blue) over time. Grey areas in top and bottom rows indicate night (VR display is off). The time of extracted movies in the experiment are shown are indicated by the green bar.

Supplementary Video S2. Same as Supplementary Video S1 for fly 2.

Supplementary Video S3. Same as Supplementary Video S1 for fly 3.

Supplementary Video S4. Same as Supplementary Video S1 for fly 4.

Supplementary Video S5. Same as Supplementary Video S1 for fly 5.

Supplementary Video S6. Same as Supplementary Video S1 for fly 6.

Supplementary Video S7. Classification of fly behavior using the 3D CNN. The video shows different moments where the fly performs different behaviors.

Supplementary Video S8. Example of tracking freely walking flies in optogenetics setup under infrared illumination.